Motion Compensation for Airborne Interferometric Synthetic Aperture Radar

by

DAVID ROBERT STEVENS

B.A.Sc., Engineering Physics, University of British Columbia, 1989

A THESIS SUBMITTED IN PARTIAL FULFILLMENT OF

THE REQUIREMENTS FOR THE DEGREE OF

MASTER OF APPLIED SCIENCE

in

THE FACULTY OF GRADUATE STUDIES

THE DEPARTMENT OF ELECTRICAL ENGINEERING

We accept this thesis as conforming

to the required standard

THE UNIVERSITY OF BRITISH COLUMBIA

March 1994

In presenting this thesis in partial fulfilment of the requirements for an advanced degree at the University of British Columbia, I agree that the Library shall make it freely available for reference and study. I further agree that permission for extensive copying of this thesis for scholarly purposes may be granted by the head of my department or by his or her representatives. It is understood that copying or publication of this thesis for financial gain shall not be allowed without my written permission.

(Signature)

Department of Electrical Engineering

The University of British Columbia
Vancouver, Canada

Date March 3, 1994

DE-6 (2/88)

Abstract

Airborne SAR interferometry has the potential to provide topographic data with a precision of the order of one meter. However, to generate data accurate to this level it is essential to measure and compensate for the antenna baseline motion. Conventional motion compensation techniques and their errors are analyzed and extended to the two channel simultaneous imaging scenario of InSAR. An evaluation of the modelling is made using point target simulation and real motion and InSAR data. Phase compensation of both channels to the same reference track and compensation to two separate tracks are considered. The single track approach allows track segmentation to follow aircraft drifts without causing discontinuities in the differential phase, but is sensitive to range cell migration effects. The dual track approach is not sensitive to this but suffers from discontinuous differential phase at segmentation boundaries, which complicates the phase unwrapping process. A new formulation for each approach is presented that compensates for unknown terrain coupled with low frequency aircraft motion. In addition, a new approach that uses the dual track approach initially and then converts to a single reference track after compression is proposed. This realizes the benefits of both approaches with only a small increase in computation.

Contents

Abstract ii

List of Tables vii

List of Figures viii

Acronyms, Abbreviations and Symbols xi

Acknowledgments xiv

Chapter 1 Introduction 1

1.1 Topographic Mapping With Radar 1

1.2 Topographic Mapping with Interferometric Radar 2

1.2.1 Spaceborne Interferometric SAR 2

1.2.2 Airborne Interferometric SAR 3

1.3 Thesis Outline and Contributions 4

Chapter 2 Airborne InSAR Background 7

2.1 Conventional SAR 7

2.1.1 Conventional Motion Compensation 8

2.2 Outline of Airborne Interferometric SAR 10

2.2.1 Basic Processing Steps 10

2.2.2 Airborne InSAR Motion Compensation 11

Chapter 3 Single Channel Airborne Motion Compensation 14

3.1 Assumptions 14

3.2 Ideal Motion Compensation 15

3.2.1 Point Target Formulation 15

3.3 Non-Ideal Motion Compensation 22
3.3.1 Zero Doppler Pulse Processing 22
3.3.2 Effects of Unknown Terrain 28
3.3.3 Effects of No Motion Compensation Resampling 33
3.3.4 Extension to Clutter Data 34
3.3.5 Effects of Inertial Data Errors 35
3.3.6 Summary of Single Channel Errors and Constraints 40
Chapter 4 Motion Compensation for Interferometry 43
4.1 Assumptions 43
4.2 InSAR Motion Compensation Requirements 44
4.3 Ideal Motion Compensation 47
4.3.1 Dual Reference Track Assuming Ideal Compensation 48
4.4 Non-Ideal Motion Compensation 49
4.4.1 Single Reference Track with Unknown Terrain 50
4.4.2 Dual Reference Track with Unknown Terrain 54
4.4.3 Effects of Unknown Terrain 56
4.4.4 FM Rate Induced Differential Phase Errors 64
4.4.5 RCMC Induced Differential Phase Errors 66
4.4.6 Effects of No Motion Compensation Resampling 68
4.4.7 Effects of Inertial Data Errors 69
4.4.8 Summary of Errors and Constraints for InSAR 70
4.5 Proposed Motion Compensation Approaches 74
4.5.1 Realization of Requirements 74

4.5.2 Combination of Single and Dual Reference Tracks 76

Chapter 5 Evaluation of Non-Ideal InSAR Motion Compensation 79

5.1 Point Target Simulation 79

5.1.1 The Point Target Simulator 79

5.1.2 Modelling of Typical Aircraft Motions 81

5.1.3 Simulation Results of Modelled Motions 81

5.1.4 Simulation Results of Actual Motion Data 87

5.1.5 Discussion of Point Target Results 96

5.2 Processing CCRS InSAR Data 99

5.2.1 Three Hills Data Results 100

5.2.2 Inertial Data Errors 105

Chapter 6 Conclusions 108

6.1 Recommended Approach for CCRS System 110

6.2 Recommended General Approach 111

Chapter 7 Suggestions for Future Work 112

Bibliography 113

Appendix A Effect of Quadratic Phase Errors on Compression 116

Appendix B Single Channel Phase Errors due to Unknown Terrain 119

Appendix C Effect of Linear Phase Errors on Compression 121

Appendix D Directional Random Walk Model 122

Appendix E Inter-channel Azimuth Broadening 125

Appendix F Single Reference Track Phase Errors 127

Appendix G Dual Reference Track Phase Errors 129

Appendix H Unknown Terrain and Translational Motion 132

Appendix I Motion Compensation Resampling 133

Appendix J MATLAB Program Listings 135

List of Tables

Table 1 Typical CCRS Parameters 21

Table 2 Single Channel Phase Errors 41

Table 3 Single Channel Motion Compensation Limitations (CCRS Typical) 42

Table 4 InSAR Motion Compensation Errors and Limitations #1 72

Table 5 InSAR Motion Compensation Errors and Limitations #2 73

Table 6 Comparison of Single and Dual Reference Track Motion Compensation 74

Table 7 Typical Flight Motion for CCRS Convair 580 81

Table 8 Dual Reference Track Motion Compensation with RCMC . . . 83

Table 9 Effects of Angular Acceleration, $a_{roll} = 0.3\ \frac{deg}{s^2}$, $h = 1\ km$, and no antenna pattern 85

List of Figures

Figure 1 Synthetic Aperture Radar Imaging Geometry 8

Figure 2 CCRS InSAR Processing Steps 12

Figure 3 Single Target Motion Compensation Geometry 17

Figure 4 Zero Doppler Applied Motion Compensation Cross-section . . 19

Figure 5 Multiple Target Motion Compensation Geometry 23

Figure 6 Constant Offset Flight Motion 25

Figure 7 Motion Compensation to a Reference Track 29

Figure 8 Flight Profile Without Resampling 34

Figure 9 Flight Profile With Resampling 35

Figure 10 Neglecting Motion Compensation Resampling 36

Figure 11 Cross-section of Neglecting Resampling Geometry 36

Figure 12 Double Reference Track Geometry 49

Figure 13 Single Reference Track Geometry 50

Figure 14 Convair 580 Flight Displacement Data 82

Figure 15 Convair 580 Roll Variation 82

Figure 16 Unknown Terrain with $v_{\perp los} = 0.5\ \frac{m}{s}$, and $R = 10\ km$ 84

Figure 17 Unknown Terrain with $a_{\perp los} = 0.01g$, and $R = 10\ km$ 85

Figure 18 Effect of Sinusoidal Roll on Differential Phase ($0.15\ deg\ peak$, $period = 3\ sec$, $h = 1\ km$, $R = 10\ km$) 86

Figure 19 Effect of Sinusoidal Roll on Height Estimate ($0.15\ deg\ peak$, $period = 3\ sec$, $h = 1\ km$, $R = 10\ km$) 87

Figure 20 Single Track Bias Errors, $R = 10\ km$, and no antenna pattern . 88

Figure 21 Measured Versus Expected Differential Phase Dual Track ($R = 10\ km$, $h = 1\ km$) 89
Figure 22 Height Estimation Errors and Roll ($R = 10\ km$, $h = 1\ km$) . . . 90
Figure 23 Height Estimation Errors ($R = 10\ km$, $h = 1\ km$) 91
Figure 24 Height Estimation Errors ($R = 15\ km$, $h = 1\ km$) 91
Figure 25 Height Estimation Errors ($R = 20\ km$, $h = 1\ km$) 92
Figure 26 Azimuth Broadening with Unknown Terrain ($R = 10\ km$, $h = 1\ km$) 93
Figure 27 Azimuth Broadening with Unknown Terrain ($R = 10\ km$, $h = 500\ m$) 94
Figure 28 Azimuth Shift with Unknown Terrain ($h = 1\ km$) 95
Figure 29 Measured Versus Expected Differential Phase Single Track ($R = 10\ km$, $h = 1\ km$) 96
Figure 30 Height Estimation Errors Single Track no RCMC ($R = 10\ km$, $h = 1\ km$) 97
Figure 31 Differential Phase with Segmented Reference Tracks ($R = 10\ km$, $h = 1\ km$) 98
Figure 32 Height Estimates with Segmented Reference Tracks ($R = 10\ km$, $h = 1\ km$) 98
Figure 33 Square Root of Interferogram Magnitude Image 101
Figure 34 Dual Reference Track Interferogram Phase 102
Figure 35 Dual/Single Reference Track Interferogram Phase 103
Figure 36 Single Reference Track Interferogram Phase 104
Figure 37 Elevation Estimates 105

Figure 38 1:50 000 Contour Map of 3 Hills Area (51°45′ lat. 113°30′ long.), 25 ft contours (82 P/11/12 Energy, Mines, and Resources Canada, 1990) 106

Figure 39 Differential Resampling Geometry 133

Acronyms, Abbreviations and Symbols

RADAR	RAdio Detection And Ranging
SAR	Synthetic Aperture Radar
InSAR	Interferometric Synthetic Aperture Radar
DEM	Digital Elevation Model
CCRS	Canada Centre for Remote Sensing
RCM	Range Cell Migration
RCMC	Range Cell Migration Correction
GPS	Global Positioning System
JPL	Jet Propulsion Laboratory
RVPC	Range Varying Phase Correction
INS	Inertial Navigation System
FM	Frequency Modulation
I	In-phase Channel
Q	Quadrature Channel
PSF	Point Spread Function
PDF	Probability Density Function
FIR	Finite Impulse Response
Channel A	Transmit and Receive Radar Channel
Channel B	Receive Only Radar Channel
RT	Reference Track
ISLR	Integrated Side Lobe Ratio
R	Slant range
V, v	Velocity
t	Azimuth time variable
T	Processed aperture time
λ	Wavelength
PRF	Pulse Repitition Frequency
ϕ	Phase
Φ	Differential phase
d	Displacement from reference track

θ	Off nadir angle
H	Altitude of reference track (channel A)
los	Line of sight component
$\perp los$	Perpendicular to los component
f_o	Range spectral shift
c	Speed of light
F_r	Range sampling rate
BW_r	Range Bandwidth
O_r	Range Oversampling Factor
K	FM rate
Y_a	Altitude of transmit/receive antenna
ΔR_{mf}	Error in range used for matched filter generation
h	Error in assume terrain elevation
ΔP	Azimuth shift in position of compressed peak
a	acceleration
g	acceleration due to gravity
ΔR_{INS}	Inertial Data position error
σ_θ^2	Phase variance of point target peak
σ_ϕ^2	Variance of phase noise
N	Number of independent samples
γ	Inter-channel correlation coefficient
Φ	Differential phase
σ_Φ^2	Variance of differential phase
α_{ab}	Antenna baseline angle
α_{RT}	Reference track baseline angle
b	Antenna baseline separation
b_{RT}	Reference track baseline separation
A_c	Antenna A aperture center position
B_c	Antenna B aperture center position
$E(A)$	Error in applied phase correction for channel A
$E(B)$	Error in applied phase correction for channel B
$\Delta\alpha_{ab}$	Variation of roll angle about mean value
a_{roll}	Angular acceleration of antenna baseline

D	Length of antenna along track
M	Displacement from aperture center
$\Delta\Phi_{bias}$	Differential Phase Bias
Δh_{bias}	Bias error in height estimate
ΔR_{ab}	Inter-channel difference in slant range matched filter errors
Δd	Inter-channel difference in d

Acknowledgments

I would like to extend my sincere thanks to my supervisors Dr. Ian Cumming and Dr. M. Ito for their enthusiastic and instructive supervision and financial support. A special thanks is also extended to Dr. Laurence Gray of CCRS for his many enlightening contributions, discussions, financial support, and for supplying the data used in this work which was prepared by Peter Farris-Manning. In addition, I would like to thank my fellow students Gordon Davidson, Michael Seymour, and Yong Luo for their moral and technical support. I would also like to thank Paul Lim of MacDonald Dettwiler for getting me interested in SAR in the first place. Last but not least, I would like to thank my wife Kathy and my daughter Michelle for their constant support and understanding. Financial support for this project was generously provided by scholarships from the Natural Sciences and Engineering Council, MacDonald Dettwiler, the B.C. Science Council, and UBC. Additional support came from contracts with CCRS. All data used in this study was provided generously by CCRS.

Chapter 1 Introduction

The knowledge of the Earth's topography has been of practical importance for all civilization; initially locally and then gradually to the global scale. For example, the design of an ancient Roman aqueduct would need to consider the local topography in some detail. Until recently, the consolidation of terrain features and topography into a map has been a laborious process of collating and analyzing information from ground surveys. With the advent of the aviation age aerial photographs could be used in a stereoscopic mode to estimate terrain elevation and identify terrain features. Since the introduction of the computer, attempts have been made to automate this arduous process leading to many new techniques of mapping terrain features and topography.

1.1 Topographic Mapping With Radar

One such new technique uses an active microwave sensor (radar) mounted on an airplane or on a satellite. Radar maps are now available in which high-resolution Synthetic Aperture Radar (SAR) images are used to portray the terrain features [1–3]. The radar sensor provides coverage in all weather, and images the terrain in a unique way which has certain advantages to users such as geologists and hydrologists [4]. In addition, this airborne and spaceborne imaging technology has been extended to topographic mapping through the processing of multiple images.

In the initial method of stereo radargrammetry, two passes of airborne SAR data are obtained in an aerial survey, and a correlation process is used to extract terrain height by manipulating the parallax between the two generated images [5]. However, radar speckle noise, caused by coherent scattering effects, and geometric distortion, limit the accuracy of the correlation.

1.2 Topographic Mapping with Interferometric Radar

A new technology, Interferometric SAR (InSAR), is being developed in which elevation data is obtained by processing a pair of stereo images in a unique way [6, 7]. This process utilizes the fact that SAR is a coherent imaging system that is able to produce a complex valued image. If the processing is carefully done, the phase of a given image pixel is a function of the path length travelled by the radar pulse coupled with scene scattering effects. The magnitude of each image pixel is a function of the reflectivity of the corresponding patch in the scene. When the two receiving channels are processed together, interferometric phase patterns are obtained that are caused by the height differences in the imaged terrain. The phase patterns obtained in this "interferogram" are then analyzed by a computer to obtain the elevation of each pixel in the scene by triangulation. The resulting digital elevation model (DEM) can be more accurate than those previously available with SAR.

1.2.1 Spaceborne Interferometric SAR

The spaceborne implementation of this approach combines two SAR images of the same region from two separate satellite passes called satellite InSAR [8]. The spaceborne implementation has certain advantages due to the predictable platform motion and large ground coverage. The disadvantages are:

- The image signal to noise ratio is not very good.
- There may be changes in the ground reflectivity between the particular orbits used, leading to temporal decorrelation between the two images.
- The two images from different orbits must be accurately registered to each other (the orbit positions are difficult to determine accurately).
- The inter-channel baseline separation, which determines the parallax, is a function of the offset between the two orbits and therefore is not easily adjustable.

The baseline separation, or parallax, between the two images, and the radar frequency determine the interferometer's sensitivity to terrain elevation and also determines the amount of baseline speckle noise (decorrelation caused by the parallax). For typical satellite altitudes, radar frequencies, and for adequate terrain elevation sensitivity, the baseline needs to be several hundred meters [9]. It is therefore impractical to produce a DEM from a single pass of a satellite by mounting two typical radar antennas on a single satellite.

Several alternate approaches to obtain single pass InSAR for the satellite case have been proposed. One approach is to use a very short wavelength allowing a much smaller baseline [10], and another is to used a tethered satellite system [11]. With the recent success of the Global Positioning System (GPS) it has been proposed that very accurate satellite interferometry could be done by having two satellites travelling in nearly parallel orbits making simultaneous imagery [12]. By using GPS in a differential mode it should be possible to estimate the relative orbits very accurately. The simultaneous imaging removes the temporal decorrelation inherent to conventional satellite techniques. However, each of these possible improvements to satellite interferometry pose severe technical challenges, and remain impractical for the present time.

1.2.2 Airborne Interferometric SAR

Perhaps the most promising approach to radar topographic mapping in the short term is in using a single flight pass of a dual antenna airborne SAR [7]. The InSAR system uses a conventional SAR for transmitting and receiving the radar signal, but in addition, a second antenna and receiving channel is used to obtain another registered image displaced across track. This single pass approach is possible because the flight altitude is much smaller than that required for the satellite orbit, thus requiring only a several meter baseline. There are several advantages to the airborne approach:

- The altitude of the flight can be adjusted to provide the desired elevation estimation

sensitivity.

- The signal to noise ratio is typically quite large (10–30 dB).
- The inter-channel registration is simpler due to the rigid structure connecting the two antennas.
- There is great flexibility in the direction and number of passes made of a particular region, which can be useful if radar layover and radar shadow are present in rugged terrain regions leading to regions of insufficient sampling of the terrain.
- There is no temporal decorrelation between the two images due to changing ground scattering conditions because the two images are made simultaneously.

The main disadvantage of the airborne approach is that the trajectory of the antennas is subject to perturbations due to air turbulence and aircraft flexure. The effect of undesired aircraft flight motion on the InSAR system is very complex and not well understood.

1.3 Thesis Outline and Contributions

The primary focus of this thesis is to understand the role that motion compensation plays in airborne InSAR. More specifically, we wish to establish the fundamental limitations that motion compensation places on InSAR. It is necessary to first understand the mechanisms involved in conventional airborne SAR before an analysis of interferometric SAR can be made. Given that the purpose of InSAR is to estimate topography, the effect of unknown terrain on motion compensation will be dealt with in some detail. It will be shown that there are fundamental limitations on the accuracy of motion compensation even when the aircraft motion is known precisely. Fortunately, most errors due to motion compensation are similar in both InSAR channels and thus cancel out, leading to small height estimation errors. Some of the residual errors can be minimized by following new approaches, for instance, by combining the best

aspects of two existing methods of motion compensation for InSAR. The thesis report is laid out as follows:

- Chapter 2 will be devoted to the background for airborne InSAR. This will include an overview of Synthetic Aperture Radar (SAR) as well as the basic processing involved in airborne InSAR. The chapter concludes by introducing the issues involved in motion compensation for airborne InSAR.
- Chapter 3 will deal with single channel airborne motion compensation. Initially, ideal motion compensation will be discussed which assumes that all geometric parameters needed for the compensation are known and infinite processing resources are available. Following this, the realistic situation of non-ideal motion compensation will be considered. Several new formulations will be presented such as the coupling effect between the range varying phase correction (RVPC) and range cell migration correction (RCMC), the effects of unknown terrain, and the directional random walk model for phase smoothing of point targets by azimuth compression.
- This single channel analysis is then extended to a comprehensive chapter on motion compensation for interferometry. The bulk of Chapter 4 is original work as little has been published in this area. As in Chapter 3, ideal compensation and non-ideal compensation will be considered. The highlights of the new work include a requirements analysis for InSAR motion compensation, a detailed comparison of the single and dual reference track approaches, closed form solutions for estimating terrain elevation for each approach which removes some terrain induced bias errors, an analysis of differential effects caused by unknown terrain and differential errors caused by the coupling between the range varying phase correction (RVPC) and range cell migration correction (RCMC), and the proposal of a new approach that combines the best aspects of the single and dual track methods.
- The validity of the presented theory and modelling is verified in Chapter 5 by experimen-

tation. An InSAR point target data generator and processor is used with modelled and real aircraft flight motions. Good agreement between the theory and simulation results is demonstrated. Real InSAR data from CCRS is also processed by a basic InSAR processor using the single and dual track approaches. The results illustrate the differences in the effects of the various motion compensation approaches on the differential phase of the interferograms. A slant range topographic map is generated and compared visually with a standard 1:50 000 contour map.

- Chapter 6 presents a summary of the conclusions from this work. This includes recommendations for the CCRS InSAR motion compensation processing as well as a more general approach.
- Chapter 7 lists suggestions for further study such as removing some of the assumptions made in the current work and extending the analysis to other operational scenarios.

Chapter 2 Airborne InSAR Background

In this chapter the general background required to understand airborne InSAR will be presented. This will begin with an overview of conventional SAR followed by the extension to airborne InSAR.

2.1 Conventional SAR

Conventional Synthetic Aperture Radar (SAR) is itself a very interesting and challenging field [13, 3]. For the purposes of interferometry, only topics in conventional SAR that are required to understand the topographic mapping problem will be considered. The basic idea of SAR is that a long antenna is synthesized in the flight direction by transmitting and receiving pulses of microwaves as the much smaller real antenna passes over a region (Figure 1). The backscatter echo from each pulse, incident on a scene patch, is processed coherently to obtain a high resolution reflectivity value in the along flight or "azimuth" direction. In the across track or "range" direction pulse compression techniques are used to obtain good resolution in this coordinate. The range to the target is obtained from the radar timing.

A simplified view of conventional SAR is that the 2–D raw data received in range and azimuth space can be focussed into a reflectivity image by a 2–D linear compression operation. The range coordinate is actually the radar line-of-sight direction and therefore a conversion to "ground" range is necessary for mapping purposes. One complication in the processing comes from the fact that as the synthesized aperture is formed the slant range to the target changes. This causes the echo data from a given target to migrate across range called Range Cell Migration (RCM). In order to perform the compression in the azimuth direction the echo data must be aligned with the flight direction. This operation is called Range Cell Migration Correction (RCMC). For many airborne applications RCMC can be ignored because only the

central part of the aperture is used so the range migration is small. But, when very high resolution in azimuth is required the entire aperture must be processed and often RCMC is necessary. Another complication which is specific to the airborne implementation is the need for motion compensation.

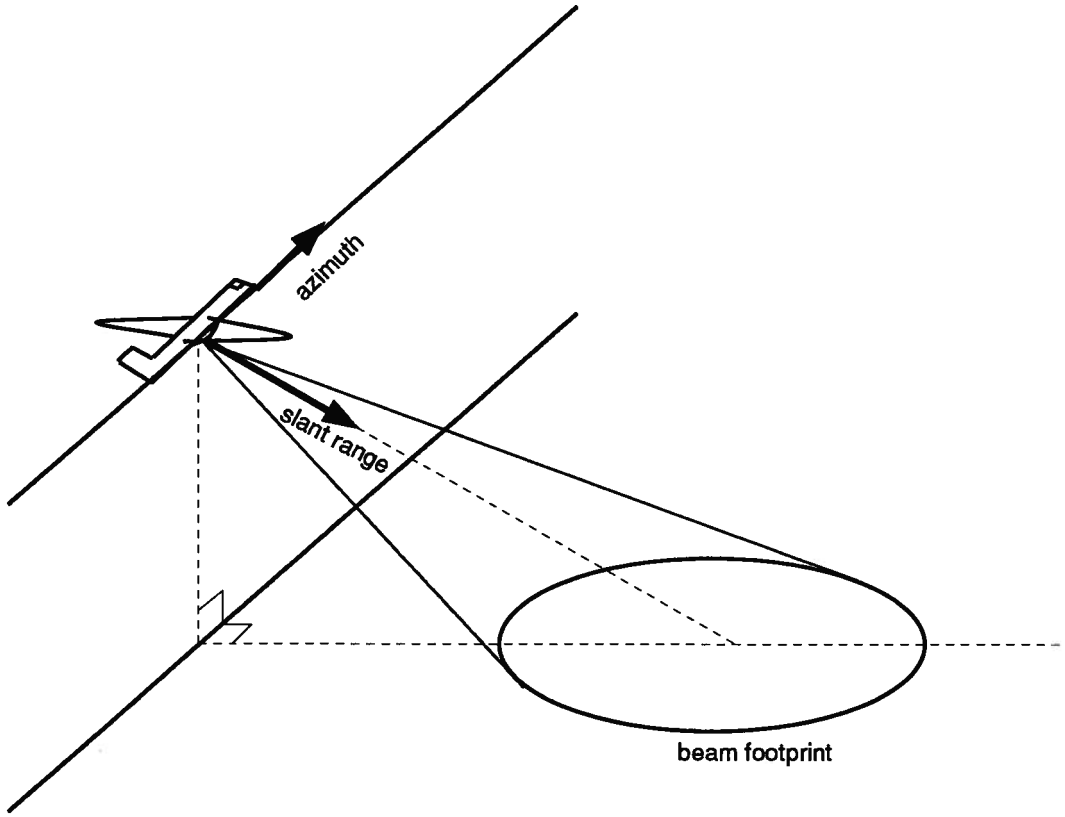

Figure 1 Synthetic Aperture Radar Imaging Geometry

2.1.1 Conventional Motion Compensation

The need for motion compensation to achieve accurate focusing of airborne SAR images has long been understood [14]. Although, efficient approximations to the ideal compensation are still being developed and evaluated. The basic approach involves using the displacement history of the antenna phase center with respect to a selected reference track to calculate a range gate (or time) delay adjustment for each pulse and a slant range dependent phase correction for each

range-compressed pixel. This correction extends along the entire synthesized aperture and is applied to the range compressed data prior to azimuth compression. This can be accomplished in real-time on the aircraft or as a post-flight processing step. The compensated data then emulates the transmission and reception from an antenna travelling in a straight line along the reference track provided the compensation has been successful [15].

Accurate phase correction requires knowledge of the complete geometry of the imaging situation. This requires knowledge of the elevation angle to the scene patch of each range-compressed pixel as well as the precise position of the antenna. Some work has been done on estimating the flight trajectory from analyzing the data post-flight, for example [16], but many approaches rely on Inertial Navigation Systems (INS) to provide the antenna position information [17]. Estimating the elevation angle is a more difficult problem.

Calculation of the elevation angle for each image pixel requires a prior estimate of the terrain height. Without access to a Digital Elevation Model (DEM) of the imaged region, some assumptions or estimates must be made. Typically, the terrain is assumed to be flat at some reference elevation, but the effect of this assumption has not been studied in detail. Most motion compensation error analysis has considered uncompensated motion, such as INS errors and their effect on image focus [17], without addressing the effect of terrain height on motion compensation.

When the residual phase errors after motion compensation, due to INS errors and unknown target elevation, are small, subsequent azimuth compression can be accomplished in a straightforward manner and defocus and image distortion are minimized. As conventional SAR is typically concerned with a magnitude image not the phase, little is known about of the effect of aircraft motion on the image phase. In order to evaluate the importance of various motion compensation errors for terrain mapping an overall understanding of airborne Interferometric SAR processing is required. In addition, it is possible to compensate for some motion

compensation errors at later processing stages.

2.2 Outline of Airborne Interferometric SAR

Airborne InSAR is basically the interferometric processing of two channels of airborne SAR data. The individual channel SAR processing algorithms and subsequent interferometric processing will depend upon the radar hardware used to obtain and possibly process the received data. In this section, the basic processing steps for a typical C-band airborne InSAR system will be discussed followed by an overview of InSAR motion compensation.

2.2.1 Basic Processing Steps

There are many processing steps involved in a typical InSAR system (Figure 2). The steps described below follow those used in the Canada Centre for Remote Sensing (CCRS) InSAR system [18]. Other approaches change the order of some steps and may use alternate algorithms to carry out a particular function.

Before the data is digitized the received echoes are first compressed in the range direction by applying a matched filter operation. This step is often performed in the analog electronics of the receiver system for each of the two channels. The following steps are performed by digital computation within a computer:

- The two channels are digitized and then registered to each other across range to ensure that each corresponding pixel in the two channels are correlated.
- Motion compensation is then applied to both channels.
- The motion compensated range compressed data is then compressed in the azimuth direction by application of a matched filter.
- The interferogram is then formed by applying a complex conjugate multiplication, pixel by pixel, on the two conventional SAR images. The phase of the interferogram is therefore the difference in the phases of the two images and is often called the differential phase.

- The differential phase of the interferogram can be smoothed by sample averaging in the azimuth and range directions to reduce phase noise.
- The modulo 2π differential phase must be unwrapped by adding some multiple of 2π to each sample in order to obtain the absolute differential phase which represents the difference in the path length phase between the two antennas.
- This absolute phase can then be converted into an elevation estimate from the imaging geometry.
- The scene patch location estimate in the SAR reference frame must finally be transformed into a convenient mapping coordinate system.

For airborne InSAR the two steps that pose the greatest challenges are motion compensation and phase unwrapping. The phase unwrapping problem is common to satellite InSAR, as well as other applications in signal and optical processing, and has been studied in detail but a robust solution for InSAR has yet to be found [19–21]. The motion compensation problem will now be considered.

2.2.2 Airborne InSAR Motion Compensation

The InSAR motion compensation situation is more complicated than in conventional SAR because two antennas are involved and terrain height estimation requires high phase accuracy in the processed images. Inter-channel phase bias errors lead directly to biases in the derived terrain model and must therefore be minimized.

Two approaches to InSAR motion compensation have been demonstrated, but neither has been analyzed in detail. The first approach is that adopted by the Jet Propulsion Laboratory (JPL) group. This method involves defining two reference tracks, one for each antenna, and then applying motion compensation for each channel separately [7, 22, 21, 23]. In the JPL case the reference tracks are segmented to keep the displacements small to allow for various

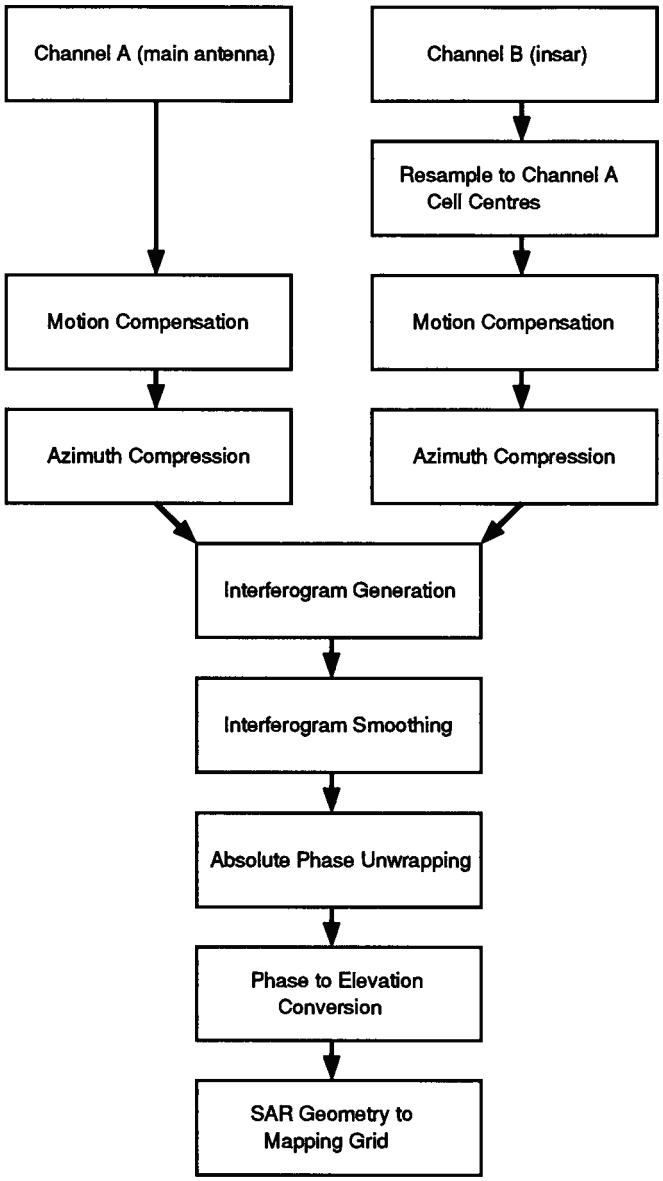

Figure 2 CCRS InSAR Processing Steps

approximations to be made. The absolute phase of each segment is estimated by using the Split-Frequency Approach [21]. In addition, the antenna is not yaw steered so processing to zero Doppler can not be used.

The second approach is used by the Canada Centre for Remote Sensing (CCRS). This method motion compensates both antennas to the same reference track [18]. This approach

basically attempts to undo the relative mapping between the two images caused by the parallax. Any residual mapping is attributed to the unknown terrain effects. The basic processing to date has not used motion compensation resampling and relies upon control points to resolve the absolute phase ambiguity. In addition, the antenna is yaw steered, so zero Doppler processing can be used.

Motion compensation is a complex component of InSAR processing due to the difficulty in predicting the effects of inertial data errors, unknown terrain elevation effects, and possible side-effects from the motion compensation operation. In the next chapter a detailed analysis of single channel motion compensation will be made, specifically considering effects that are important to interferometry. Next, the InSAR motion compensation problem will be defined and studied in detail. The primary errors sources will be identified and new approaches to minimizing their adverse effects will be presented. The developed theory will be verified by simulation of the InSAR imaging and processing situation using modelled and real motion data. A simple combination of the single and dual reference track approaches will be proposed that combines the benefits of both. This new processing approach will be demonstrated by processing actual C-band InSAR data from the CCRS InSAR system.

Chapter 3 Single Channel Airborne Motion Compensation

Motion compensation for single channel SAR systems is a complex problem of attempting to compensate for non-linear motion of the aircraft which occurred during the aperture synthesis. Complete compensation considers the yaw, pitch, roll, and translational motion of the aircraft. In order to focus on particular effects that are important for InSAR a number of reasonable assumptions can be made which will simplify the analysis and allow certain error sources to be isolated.

3.1 Assumptions

The following is a list of the main assumptions made for the subsequent analysis:

1. The antenna is yaw steered to zero Doppler. This means that the antenna is assumed to be pointing perpendicular to the velocity vector of the aircraft.
2. The SAR processing is to zero Doppler.
3. The pitch of the aircraft is fixed.
4. The spacing between transmitted pulses on the ground is kept fixed by adjusting the Pulse Repetition Frequency (PRF) to be proportional to the aircraft velocity.
5. The inertial data will be assumed to be correct, for the most part.
6. The motion compensation to be applied will be post-flight, apart from those mentioned in the above list.
7. Translational motion and aircraft roll must be compensated through motion compensation.

For a typical airborne system, such as the CCRS system, most of these assumptions are reasonable. Errors in the yaw and pitch of the aircraft will lead to radiometric problems but not phase problems if processing is to zero Doppler. The main limiting factor is the assumption

that the inertial data is correct. When inertial data errors occur this can lead to defocussing and mis-registration. These effects have been studied before [24, 15] so will not be considered here except for their effect on the image phase.

With these assumptions in mind the formulation of motion compensation in the ideal case will be investigated. This necessitates the development of the echo response from a point target which depends upon the range history between the antenna and target, called the range equation. Following this, non-ideal compensation will be investigated considering such issues as the effect of unknown terrain.

3.2 Ideal Motion Compensation

The ideal case of motion compensation assumes that all the necessary geometrical information is available for compensation and that there are no processing restrictions. The necessary compensation can be analyzed by considering how the echo from a point target (or impulse reflectivity) in the scene is affected by non-linear flight motion. The required compensation will be described followed by an analysis of an unavoidable side-effect of the phase correction operation.

3.2.1 Point Target Formulation

The point target formulation considers motion compensation to correctly image a single point scatterer in a perfectly absorbing background. The radar transmits a linear FM chirp and the receiver compresses the echo using a matched filter. The time delay of the range compressed sinc-like point spread function (PSF) depends upon the two-way distance the pulse travelled to the point target [3]. This is called the range equation.

The Range Equation

The ideal range equation is obtained for a straight flight and a flat earth (Figure 3):

$$R(t) = \sqrt{R_o^2 + v^2 t^2} \tag{3.1}$$

where R_o is the slant range of closest approach, v is the aircraft ground velocity, and t is time. The phase of the range compressed point spread function for each pulse is [3]:

$$\phi(t) = -\frac{4\pi R(t)}{\lambda} \tag{3.2}$$

where λ is the carrier wavelength and the phase component due to delays in the radar system have been removed. The target energy in azimuth can be compressed by using this phase history to form a matched filter. The slant range R can be expanded in a binomial series to 4th order in t:

$$R(t) \approx R_o + \frac{v^2 t^2}{2R_o} - \frac{v^4 t^4}{8R_o^3} \tag{3.3}$$

Therefore, the instantaneous Doppler frequency as a function of time is:

$$f_D = \frac{1}{2\pi}\frac{\partial \phi}{\partial t} \approx -\frac{2v^2 t}{\lambda R_o} + \frac{v^4 t^3}{\lambda R_o^3} \tag{3.4}$$

It is clear that the position of the range compressed PSF will vary along the aperture, called range migration (RCM), according to the range equation. Range cell migration correction (RCMC) must be performed in order to extract the correct energy. A phase correction is not applied to compensate for this because it is this Doppler phase history that is required in order to compress the energy in azimuth. For instance, the quadratic term in the range equation produces the linear FM part of the Doppler history. When the flight is non-linear the range equation becomes more complicated.

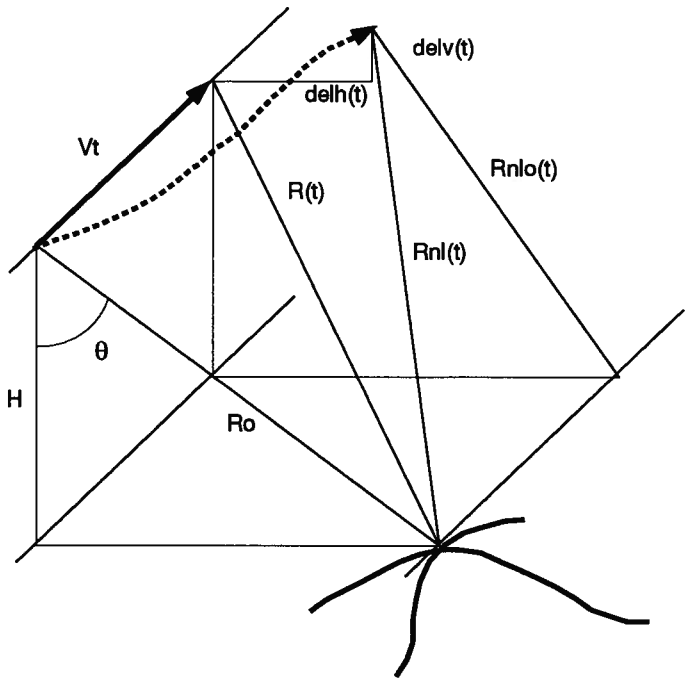

Figure 3 Single Target Motion Compensation Geometry

Non-linear Flight Motion

When the flight is non-linear the expression for R has a component that represents the displacement of the antenna from the nominal linear track along the direction of the antenna to the target. It will be assumed that the along track velocity is constant:

$$R_{nl}(t) = \sqrt{R_{nlo}^2(t) + v^2t^2} \tag{3.5}$$

where

$$R_{nlo}(t) = fn(\theta, H, R_o, delh(t), delv(t)) \tag{3.6}$$

is the projected distance in the plane of the particular pulse and is a function of many parameters. When processing a single target only, there are two options:

1. Form a matched filter using $R_{nl}(t)$ and process. This involves resampling the range data to follow the target energy as it migrates due to $R_{nl}(t)$. The matched filter will not be a linear FM chirp.

2. Modify the received data to appear as though the flight were linear, then compress using normal matched filtering and normal RCMC.

In the second approach, the following calculation is required:

$$\begin{aligned}\Delta R_e(t) &= R_{nl}(t) - R(t) \\ &\approx R_{nlo}(t) + \frac{v^2t^2}{2R_{nlo}(t)} - \left(R_o + \frac{v^2t^2}{2R_o}\right)\end{aligned} \tag{3.7}$$

The following phase correction can then be applied:

$$\Delta\phi_e(t) = \frac{4\pi\Delta R_e(t)}{\lambda} \tag{3.8}$$

as well as a resampling operation to extract the correct target energy along the aperture [15]. The resampling operation is referred to as the motion compensation resampling operation.

Typically, the range compressed data is at baseband and processing after motion compensation is based on this assumption. It will now be shown how the required phase correction, which varies across range, can invalidate this assumption even when the phase history along azimuth has been adequately corrected [21].

Range Varying Phase Correction (RVPC)

An approximation can be made to the phase correction applied at the zero Doppler pulse (Equation 3.8) by defining (Figure 4):

$$\begin{aligned}d(t) &= \sqrt{delv(t)^2 + delh(t)^2} \\ \alpha(t) &= atan2(delh(t), delv(t))\end{aligned} \tag{3.9}$$

By assuming parallel rays this yields:

$$R_{nlo}(t) - R_o \approx d(t)\cos\left(\alpha(t) + \theta\right) \tag{3.10}$$

giving a phase correction of [21]:

$$\Delta\phi(t) \approx \frac{4\pi}{\lambda}d(t)\cos\left(\alpha(t) + \theta\right) \tag{3.11}$$

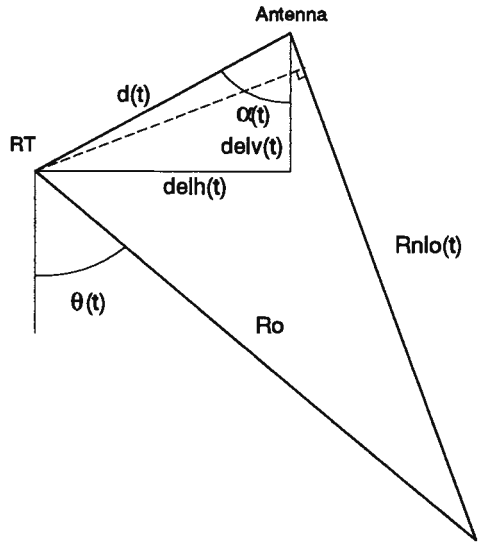

Figure 4 Zero Doppler Applied Motion Compensation Cross-section

where

$$\theta = \cos^{-1}\left(\frac{H}{R_{ao}}\right) \tag{3.12}$$

and H is defined in Figure 3.

For a given pulse the phase correction varies as a function of the off-nadir angle (θ) to the target. Differentiating Equation 3.11 yields:

$$\frac{\partial \Delta\phi(t)}{\partial \theta} \approx -\frac{4\pi}{\lambda} d(t) \sin\left(\alpha(t) + \theta\right) \tag{3.13}$$

A change of variables using:

$$R\cos\theta = H \tag{3.14}$$

and

$$\frac{\partial \theta}{\partial R} = \frac{1}{R\tan\theta} \tag{3.15}$$

yields

$$\frac{\partial \Delta\phi(t)}{\partial R} \approx -\frac{4\pi}{\lambda} \frac{d(t)\sin\left(\alpha(t) + \theta\right)}{R\tan\theta} \tag{3.16}$$

This describes the range varying phase correction (RVPC) which has been noted before [21].

This range varying phase correction, which is locally linear, will alter the range spectra which can invalidate the baseband assumption that is usually made by subsequent processing steps. By using the following Fourier Transform property an estimate of the resulting range spectral shift can be made:

$$\begin{aligned} \mathcal{F}\{g(t)\} &= \widetilde{g}(f) \\ \mathcal{F}\left\{g(t)e^{-j2\pi f_o t}\right\} &= \widetilde{g}(f+f_o) \end{aligned} \tag{3.17}$$

The magnitude of the frequency shift can be calculated from the range time varying phase correction, yielding:

$$|f_o| = \frac{c}{2}\frac{1}{2\pi}\frac{4\pi|d_{\perp los}|}{\lambda R \tan\theta} \ (Hz) \tag{3.18}$$

If the baseband assumption is to be valid all subsequent processing must have transfer functions with a constant spectral response as well as a sufficiently large range oversampling factor. The limit on the oversampling factor becomes:

$$\frac{BW_r}{2} + |f_o| < \frac{F_r}{2} \tag{3.19}$$

where BW_r is the bandwidth of the range chirp and F_r is the range sampling rate. This simplifies to:

$$1 + \frac{2f_o}{BW_r} < O_r \tag{3.20}$$

or

$$1 + \frac{2\,c\,|d_{\perp los}|}{\lambda R \tan\theta BW_r} < O_r \tag{3.21}$$

where $O_r = \frac{F_r}{BW_r}$ is the oversampling factor. For typical CCRS parameters (Table 1):

$$1 + 0.032|d_{\perp los}| < O_r \tag{3.22}$$

This provides a limit to the allowed displacement from the reference track. Given that the phase modulation varies non-linearly across range, significant distortions to the range spectra can occur even if the oversampling factor is sufficient.

Table 1 Typical CCRS Parameters

Parameter	Typical Value
Wavelength λ	56.56 mm
Altitude H	6 km
Baseline length b	2.8 m
Baseline angle α_{ab}	40 degrees
Slant range R_{ao}	10 km
Pulse Repetition Frequency PRF	337 Hz
Processed Aperture T	3 sec $\sim$ 2.23 degrees
Range Bandwidth BW_r	25 MHz
Range Sampling Rate F_r	37.5 MHz
Velocity v	130 m/s

One example of subsequent processing that is sensitive to the spectral shift is RCMC, which is normally accomplished by baseband interpolation. Normal baseband interpolation (I and Q channels interpolated separately with a baseband kernel) can be performed provided the range oversampling factor is large enough and the spectrum of the interpolation kernel if flat and real valued. When the shift becomes large non-baseband interpolation is required. Given that the shift is range dependent this implies performing interpolation with a range varying kernel which is undesirable.

Since the range varying phase correction depends upon the displacement from the reference track, the magnitude of the range spectral shift can be minimized by segmenting the reference track to follow the aircraft drifts. The consequence of this is that the data becomes discontinuous along azimuth across the boundaries. Alternately, one might expect that a real-time range gate delay adjustment can be used (if available in the hardware) to maintain a constant swath center position. This will help the alignment of the target energy along azimuth but does not help the range varying phase correction. The range gate delay adjustment does not change the phase of the echo energy from a given ground scatterer.

It is important to note that because the displacement from the reference track varies along track the motion compensation required at each pixel of the raw data depends upon the location of each target on the ground. This means that in order to perform ideal compensation the entire aperture for each target on the ground must be processed uniquely and separately. This leads to prohibitively large computational loads. For this reason non-ideal approximate motion compensation approaches are usually used. The errors resulting from this will now be analyzed.

3.3 Non-Ideal Motion Compensation

Typical of most engineering problems is the trade-off between the quality of the result and the resources and time required to generate the result. Given an unlimited amount of time and computer resources and complete knowledge of the geometry of the situation, ideal motion compensation could be used. In reality, much more efficient and therefore approximate solutions are required. This leads to the zero Doppler pulse processing approach that handles multiple targets at once.

3.3.1 Zero Doppler Pulse Processing

A second point target will now be added to the previous single target ideal motion compensation approach to examine how multiple targets can be processed simultaneously.

Multiple Point Targets

By considering Figure 5 it is clear that there are different phase corrections to be applied for a given range cell of a given pulse depending upon which target you are correcting for, even if the targets are at the same elevation. As the echoes from each target are overlapped along the aperture, only one correction can be applied for the pulse at this range bin if the targets are processed together. The only way to process each target correctly is to process the aperture separately for each target. But, this is inefficient and is often not necessary. Therefore, one can use $R_{nlo}(t)$ for each target [25]. In other words, the center of aperture (or zero Doppler) pulse

is corrected properly for each target but the correction has a small error across its aperture for each target. This can be called zero Doppler pulse processing.

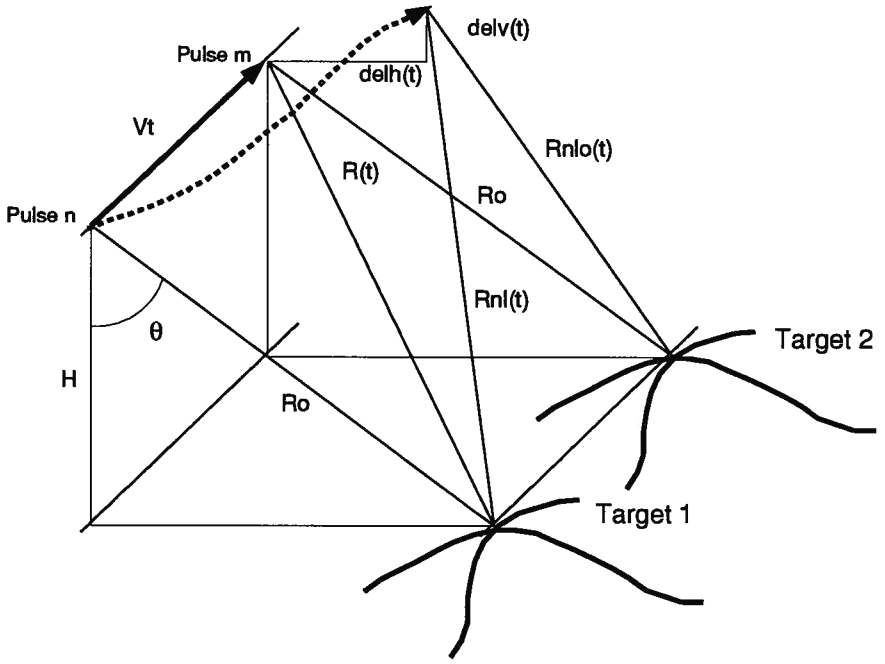

Figure 5 Multiple Target Motion Compensation Geometry

The slant range correction for zero Doppler pulse processing is:

$$\Delta R(t) = R_{nlo}(t) - R_o \tag{3.23}$$

yielding a phase correction of:

$$\Delta\phi(t) = \frac{4\pi\Delta R(t)}{\lambda} \tag{3.24}$$

In order to extract the correct target energy the range data must be interpolated to obtain $R_{nlo}(t)$ instead of the normal sampling range of R_o.

An analysis of the error in the applied motion compensation as the pulse position varies from the zero Doppler pulse can be made. The difference between the desired phase correction for target 1 at a given pulse $\Delta\phi_e(t)$ and the phase correction actually applied at the slant range

where the echo energy resides $\Delta\phi(t)$ is:

$$\begin{aligned}\Delta\phi_e(t) - \Delta\phi(t) &\approx \frac{4\pi}{\lambda}\left(\frac{v^2t^2}{2R_{nlo}(t)} - \frac{v^2t^2}{2R_o}\right) \\ &\approx \frac{2\pi v^2t^2}{\lambda}\left(\frac{R_o - R_{nlo}(t)}{R_o^2}\right)\end{aligned} \tag{3.25}$$

By incorporating the parallel ray approximation one gets:

$$\begin{aligned}\Delta\phi_{err}(t) &\approx -\frac{2\pi}{\lambda}\frac{v^2t^2d(t)\cos\left(\alpha(t)+\theta(t)\right)}{R_o^2} \\ &\approx -\frac{2\pi}{\lambda}\frac{v^2t^2d_{los}(t)}{R_o^2}\end{aligned} \tag{3.26}$$

where d_{los} is the projected line-of-sight displacement. Another way to view this effect is to consider this error as a mismatch between the FM rates of the corrected data and the matched filter. This approach is described below.

FM Rate Errors

Motion compensation has attempted to modify the data to appear as thought it was generated from an ideal trajectory. One important case to consider is when the flight is parallel but offset from the reference track and the terrain is flat (Figure 6). For this case there is a constant phase correction applied along the aperture for each azimuth line. The consequence of this is that the FM rate of the data is unchanged. If the motion compensation had been able to consider the RCM along the aperture for a single target (ideal compensation) then the FM rate would have been changed. It is therefore important to use an FM rate for the matched filter that matches the data, not the reference track. If there is a difference between the effective slant range of the data and that of the matched filter it is easy to calculate the phase error resulting from the different FM rates. The FM rate is:

$$K = \frac{2v^2}{\lambda R} \tag{3.27}$$

so, the phase error is therefore:

$$\Delta\phi_{err} = \pi\Delta Kt^2 = \frac{2\pi v^2t^2}{\lambda}\left(\frac{1}{R_1} - \frac{1}{R_2}\right) \approx \frac{2\pi v^2t^2}{\lambda}\frac{\Delta R_{mf}}{R^2} \tag{3.28}$$

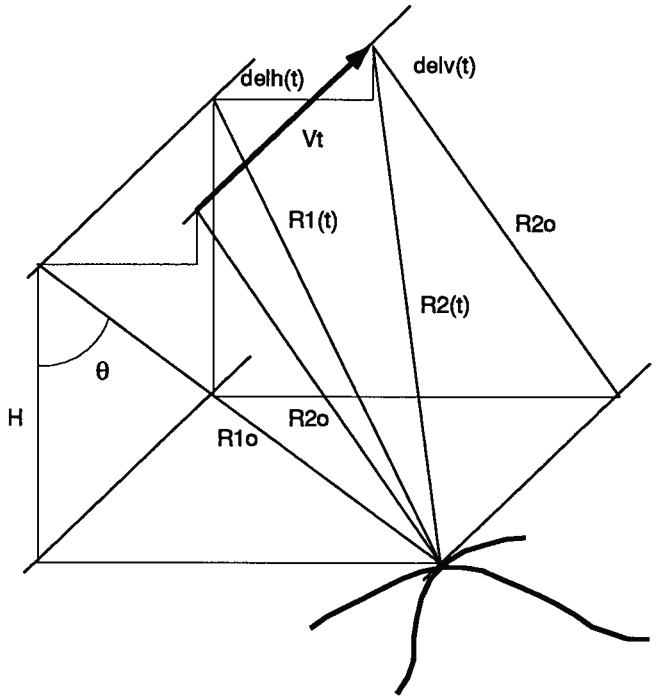

Figure 6 Constant Offset Flight Motion

Notice that this error is of the same form as the multiple target scenario. The effect of this inherent problem in non-ideal motion compensation can be reduced by adjusting the matched filter to match the data from the true antenna position rather than from the reference track. Given that this adaptive matched filter will vary along the aperture as the antenna deviates from the reference track, it will be necessary to define a nominal filter if compression is implemented using fast convolution [26]. The residual phase error will be due to an effective difference in the slant range used to generate the matched filter ΔR_{mf}.

In Appendix A the effect of quadratic phase errors on the phase and shape of the compressed peak has been analyzed. It was found that for quadratic phase errors of less than about π at the edge of the processed band, the peak phase error was about one third of what was applied. This is in agreement with results from [27]. From simulation it was found that if the applied quadratic phase error is less than about $\pi/2$ then the broadening is less than about 5% and the sidelobe level increases about 4 dB. This is in agreement with results from [24]. Ignoring the peak phase errors for the moment, a limit on the allowable quadratic phase errors can be made to

keep the peak deformation reasonable. For instance, one could (somewhat arbitrarily) say that the phase error must not vary more than $\frac{\pi}{2}$ over the aperture. Therefore, from Equation 3.28:

$$\frac{\pi}{2} > \frac{2\pi}{\lambda}\frac{v^2 \Delta R_{mf}}{R^2}\left(\frac{T}{2}\right)^2 \tag{3.29}$$

and

$$\Delta R_{mf} < \frac{\lambda R^2}{v^2 T^2} \ (m) \tag{3.30}$$

where ΔR_{mf} is the displacement of the true antenna position from the one used to generate the matched filter and T is the duration of the processed aperture. For typical CCRS parameters (Table 1) this corresponds to a maximum displacement of 37 m between the antenna and the reference track. This is not normally a problem for the single channel case.

Effects of Range Cell Migration Correction (RCMC)

Another consequence of zero Doppler pulse processing is the coupling effect between the range varying phase correction (RVPC) and RCMC [21]. Consider again the case of a trajectory which is offset but parallel to the reference track (Figure 6). RCMC extracts the target energy following the range migration. Due to the zero Doppler pulse processing and the RVPC the effective phase correction that is applied for a given target varies along the aperture. The constant component is the zero Doppler phase correction and the varying component is equal to the product of the slope of the RVPC and the range cell migration (RCM):

$$\begin{aligned}
\Delta\phi_{app}(t) &\approx -\frac{4\pi}{\lambda}(R_{1o} - R_{2o}) + \frac{\partial \Delta\phi(t)}{\partial R}\Delta R_{RCM}(t) \\
&\approx \frac{4\pi}{\lambda} d(t)\cos\left(\alpha(t)+\theta\right) - \left(\frac{4\pi}{\lambda}\frac{d(t)\sin\left(\alpha(t)+\theta\right)}{R\tan\theta}\right)\left(\frac{v^2 t^2}{2R}\right) \\
&\approx \frac{4\pi}{\lambda} d(t)\cos\left(\alpha(t)+\theta\right) - \frac{2\pi}{\lambda}\frac{d(t)\sin\left(\alpha(t)+\theta\right)v^2 t^2}{R^2\tan\theta}
\end{aligned} \tag{3.31}$$

There are two possible ideal cases to compare this result with. The first is if the data is expected to be perfectly corrected to the reference track such that the reference track is used

to define the FM rate of the matched filter. In this case, the ideal applied phase correction would be:

$$\begin{aligned}\Delta\phi_{ideal1}(t) &= -\frac{4\pi}{\lambda}(R_1(t) - R_2(t)) \\ &\approx -\frac{4\pi}{\lambda}\left((R_{1o} - R_{2o}) + \frac{v^2t^2}{2}\left(\frac{1}{R_{1o}} - \frac{1}{R_{2o}}\right)\right) \\ &\approx \frac{4\pi}{\lambda}d(t)\cos(\alpha(t)+\theta) - \frac{2\pi}{\lambda}\frac{d(t)\cos(\alpha(t)+\theta)v^2t^2}{R^2}\end{aligned} \tag{3.32}$$

Therefore, the resulting quadratic phase error along the aperture, by using

$$\sin(a-b) = \sin a\cos b - \cos a\sin b \tag{3.33}$$

is:

$$\begin{aligned}\Delta\phi_{err1} &\approx -\frac{2\pi v^2t^2d(t)}{\lambda R^2}\left(\cos(\alpha(t)+\theta) - \frac{\sin(\alpha(t)+\theta)}{\tan\theta}\right) \\ &\approx \frac{2\pi v^2t^2d(t)}{\lambda R^2}\frac{\sin\alpha(t)}{\sin\theta}\end{aligned} \tag{3.34}$$

The alternative is to assume that effectively a constant phase correction has been applied along the aperture that has not altered the FM rate. In this case, the filter is matched to the original position of the antennas. The ideal correction for this approach is:

$$\Delta\phi_{ideal2}(t) = -\frac{4\pi}{\lambda}(R_{1o} - R_{2o}) \tag{3.35}$$

Therefore, the resulting quadratic phase error along the aperture is:

$$\Delta\phi_{err2} \approx \frac{\partial\Delta\phi(t)}{\partial t}\Delta R(t) \approx -\frac{2\pi v^2t^2d(t)}{\lambda R^2}\left(\frac{\sin(\alpha(t)+\theta)}{\tan\theta}\right) \tag{3.36}$$

This quadratic phase error is slightly smaller, on average, than the previous one, therefore, the antenna positions should be used to define the filters.

If a peak error is estimated using the perpendicular to the line-of-sight displacement component, one obtains:

$$\Delta\phi_{err} \approx -\frac{2\pi v^2t^2d_{\perp los}}{\lambda R^2\tan\theta} \tag{3.37}$$

Furthermore, if a limit of $\pi/2$ is placed on the quadratic phase error, the maximum allowed displacement from the reference track is:

$$d_{\perp los} < \frac{\lambda R^2 \tan\theta}{4v^2t^2} \ (m) \tag{3.38}$$

For typical CCRS parameters (Table 1) this yields:

$$d_{\perp los} < 49 \ m \tag{3.39}$$

The easiest way to reduce this effect is to segment the reference track to follow the antenna along track so that the displacement is small enough to produce insignificant range varying spectral shifts. But, this leads to discontinuous phase data.

3.3.2 Effects of Unknown Terrain

Another important source of error is the unknown terrain elevation. When the elevation of the scene patch (or point target) is unknown it is impossible to correctly calculate the slant range shift that occurred [15]. An approximation is to resample to the $R_{nlo}(t)$ points and apply the phase correction assuming flat terrain at the reference level (Figure 7). It should be noted that the resampling will only extract the correct part of the echo when the target is actually at the reference level.

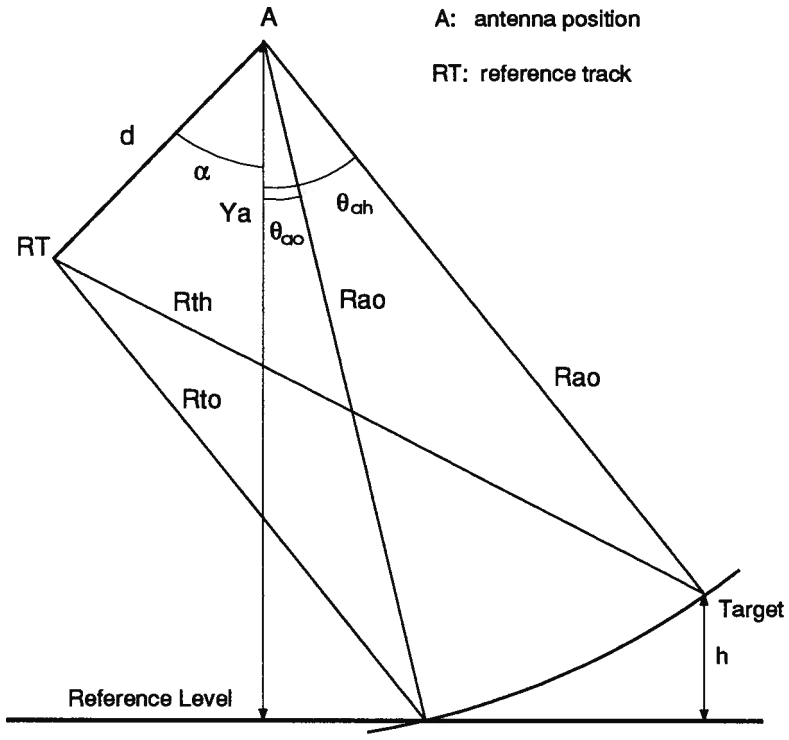

Figure 7 Motion Compensation to a Reference Track

The applied phase correction assuming flat terrain at the reference level is:

$$\phi_{mc}(applied) = -\frac{4\pi}{\lambda}(R_{to} - R_{ao}) \tag{3.40}$$

for the zero Doppler pulse of a particular target. The proper correction is:

$$\phi_{mc}(ideal) = -\frac{4\pi}{\lambda}(R_{th} - R_{ao}) \tag{3.41}$$

The error in the applied phase correction is therefore:

$$\Delta\phi_{err} = \phi_{mc}(applied) - \phi_{mc}(ideal) = -\frac{4\pi}{\lambda}(R_{to} - R_{th}) \tag{3.42}$$

When the slant range distances are expanded in a binomial series and parallel rays are assumed, one obtains (Appendix B):

$$\Delta\phi_{err}(t) \approx \frac{4\pi h d_{\perp los}(t)}{\lambda R_{ao} \sin\theta(t)} \tag{3.43}$$

where $\theta(t)$ is the assumed angle to the target which will vary according to the geometry, and

$$d_{\perp los}(t) = d(t)\sin\left(\alpha(t) + \theta(t) + \frac{\Delta\theta(t)}{2}\right) \tag{3.44}$$

is the component of the displacement that is perpendicular to the line-of-sight direction, and $\Delta\theta(t) = \theta_{ah} - \theta_{ao}$ is the error in the assumed angle to the target.

It is clear that as the flight deviation varies with time ($d(t)$ and $\alpha(t)$ change) and so will the error in the applied phase correction. If the displacement has a constant offset term with a smaller time varying term the constant term will produce a phase bias along the aperture which will be unaltered by the compression operation.

The form of the phase error is very nearly the same as the form of the flight motion. For instance, a linear deviation from the reference track along the aperture leads to approximately a linear phase error. The same is true for quadratic and higher order motions. This can be seen by noting that the sine term will be approximately linear in $\alpha(t)$ provided the variation is small. When the angular variation is large $d(t)$ must be small (close to the reference track) resulting in a very small non-linear component. One can therefore proceed to analyze the effect of linear and higher order cross-track flight motions by examining the effects on compression of linear and higher order phase errors along the aperture. This has been described in detail in Appendix A and C.

Cross-track Velocity

Appendix C examines the effect of linear phase errors on the compression of a linear FM pulse. It was found that the peak is shifted in position, identical in shape, and has a phase error at the compressed peak. More specifically, a linear phase error $\frac{\partial\phi}{\partial t} = \pi L$ produces a shift in the compressed peak position of:

$$\Delta P = -\frac{L}{2K} = -\frac{\lambda R}{4\pi v^2}\frac{\partial\phi}{\partial t} \quad (sec.) \tag{3.45}$$

where K is the FM rate. The corresponding phase error at the peak is:

$$\phi_{err} = \frac{\pi L^2}{4K} = \frac{\lambda R_o}{8\pi v^2}\left(\frac{\partial \phi}{\partial t}\right)^2 \tag{3.46}$$

This shift and phase error can be put in terms of changes to the motion compensation phase errors along the aperture:

$$\frac{\partial \phi}{\partial t} \approx \frac{\partial \Delta\phi_{err}}{\partial t} \approx \frac{4\pi h}{\lambda R \sin\theta}\,\frac{\partial d_{\perp los}(t)}{\partial t} \tag{3.47}$$

The derivatives involving the off-nadir angle are ignored as they do not contribute appreciably. The unknown parameter required to predict the shift is the target elevation (or equivalently the correct off-nadir angle). If an estimate of this were available one could predict the shift and correct for it. The same is true of the phase error at the peak. The resulting shift is:

$$\Delta P \approx -\frac{h}{v^2 \sin\theta}\frac{\partial d_{\perp los}}{\partial t}\ \ (sec.) \tag{3.48}$$

If this is limited to less than one sample then:

$$\frac{\partial d_{\perp los}}{\partial t} < \frac{v^2 \sin\theta}{hPRF} \tag{3.49}$$

where PRF is the Pulse Repetition Frequency. For typical CCRS parameters (Table 1) this yields:

$$\frac{\partial d_{\perp los}}{\partial t} < \frac{40}{h}\,\frac{m}{s} \tag{3.50}$$

When the phase error at the peak is evaluated one obtains:

$$\Delta\phi_{peak} \approx \frac{2\pi h^2}{\lambda R v^2 \sin^2\theta}\left(\frac{\partial d_{\perp los}}{\partial t}\right)^2 \tag{3.51}$$

The limits on the phase error of the compressed data depends upon the use for the data. For interferometry this effect is negligible.

Cross-track Acceleration

It is difficult to predict analytically the effect of non-linear phase errors on the compressed peak PSF. In Appendix A an approximate analysis is given for the effect of quadratic phase errors on the phase and shape of the compressed peak. This corresponds to uniform translational acceleration coupled with unknown terrain. Ignoring the peak phase errors for the moment one can place a limit on the allowable quadratic phase errors to keep the peak deformation reasonable (to be less than $\frac{\pi}{2}$ over the aperture). It is desirable to extend this limit to represent maximum flight motions given a particular imaging situation.

It is shown in Appendix B that the largest variation in the phase error occurs for motion perpendicular to the line-of-sight of the radar. This is interesting as the phase of the received signal is sensitive to displacements in the line-of-sight direction. But, for terrain induced phase errors of concern is the variation of this error as a function of flight motion. The approximate maximum phase error from Equation 3.43 is:

$$\Delta\phi_{err_{max}} \approx \frac{4\pi\ h\ \Delta d_{\perp los_{max}}}{\lambda R_{ao} \sin\theta} \tag{3.52}$$

where $\Delta d_{\perp los_{max}}$ is the maximum flight motion displacement perpendicular to the line-of-sight. If one limits this motion to be such that the motion compensation phase variation over the aperture is less than $\frac{\pi}{2}$ from uniform acceleration, this yields:

$$\Delta d = \frac{1}{2} a_{\perp los} \left(\frac{T}{2}\right)^2 = \frac{1}{8} a_{\perp los} T^2 \tag{3.53}$$

The resulting upper limit on uniform acceleration is:

$$a_{\perp los} < \frac{\lambda R_{ao} \sin\theta}{h\ T^2} \quad \left(\frac{m}{s^2}\right) \tag{3.54}$$

For typical CCRS parameters (Table 1) this is:

$$a_{\perp los} < \frac{5\ g}{h} \quad \left(\frac{m}{s^2}\right) \tag{3.55}$$

where g is the acceleration due to gravity.

3.3.3 Effects of No Motion Compensation Resampling

Up to this point in the analysis the range gate delay adjustment of the echo energy, which is the motion compensation resampling operation, has been mostly ignored. SAR processing is most sensitive to phase but still relies on the signal strength. Some simplifications to the phase processing result if the range gate delay adjustment is ignored because the slant range sample spacing is constant. The effect of this is now considered.

If resampling had not been done and the processing had simply sampled the range data at fixed slant range values and phase compensated these samples then the effect of turbulent flight is to produce some uncompensated range cell migration (RCM). Uncompensated RCM leads to broadening in both the range and azimuth directions. Figures 8 and 9 show flight profiles for the two cases of resampling and no resampling, indicating from where on flat terrain the samples would be taken. Figure 10 shows an example of the no-resampling case.

The error in the sampled slant range for a particular pulse from Figure 10 is:

$$\Delta R(t) = R_s - R_o \tag{3.56}$$

One can approximate the difference in the slant range values by considering Figure 11. The difference is approximately the projected line-of-sight displacement from the center of aperture position (A_c):

$$R_s - R_o \approx x(t) \sin \xi(t) \triangleq M_{los}(t) \tag{3.57}$$

Given that typical flight motion over an aperture is small compared with the slant range resolution, this effect is not expected to produce significant broadening. This will be confirmed by simulation in Chapter 5.

An alternative to motion compensation resampling is to have a real-time range gate delay adjustment which maintains a constant ground range at the swath center. This range gate

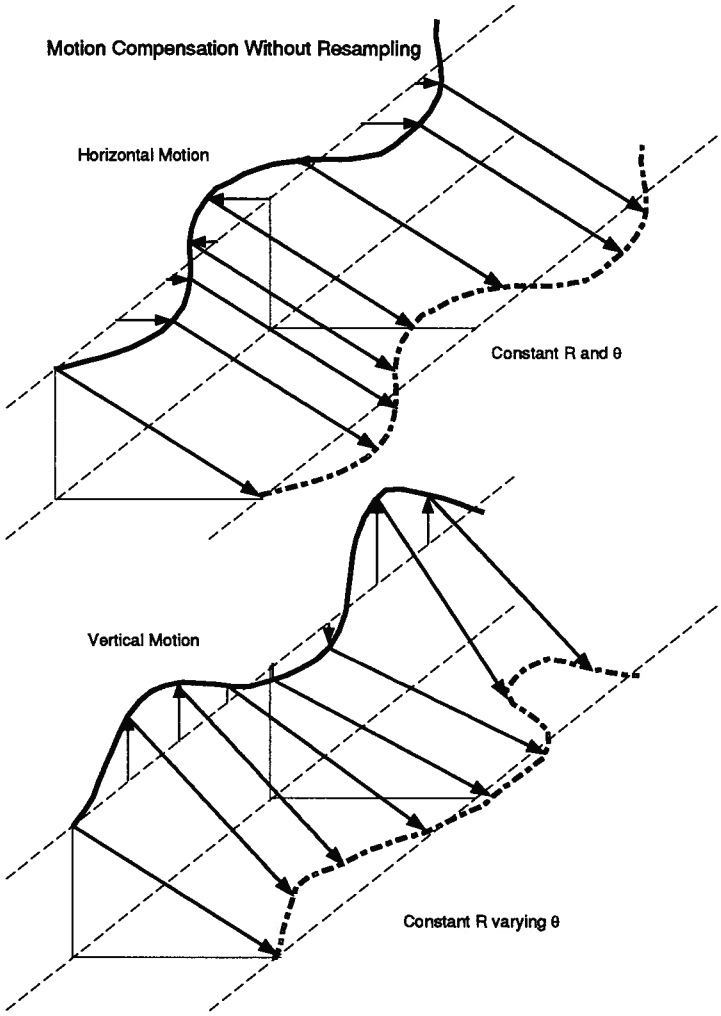

Figure 8 Flight Profile Without Resampling

delay adjustment alters the start time of the echo receive window. This will provide a rough compensation for aircraft drift but only correctly compensates for one slant range (assuming the terrain assumption is correct as well).

3.3.4 Extension to Clutter Data

So far the analysis has considered the effect of motion compensation errors on point targets. Since typical imaged terrain has many contributing scatterers per resolution cell one must extend the results to consider this. Given that the aircraft flight motions are essentially constant during the time corresponding to a single resolution cell (of order 30 *ms*) it is reasonable to expect that all contributing scatterers for a given sample value are affected by the motion in an identical

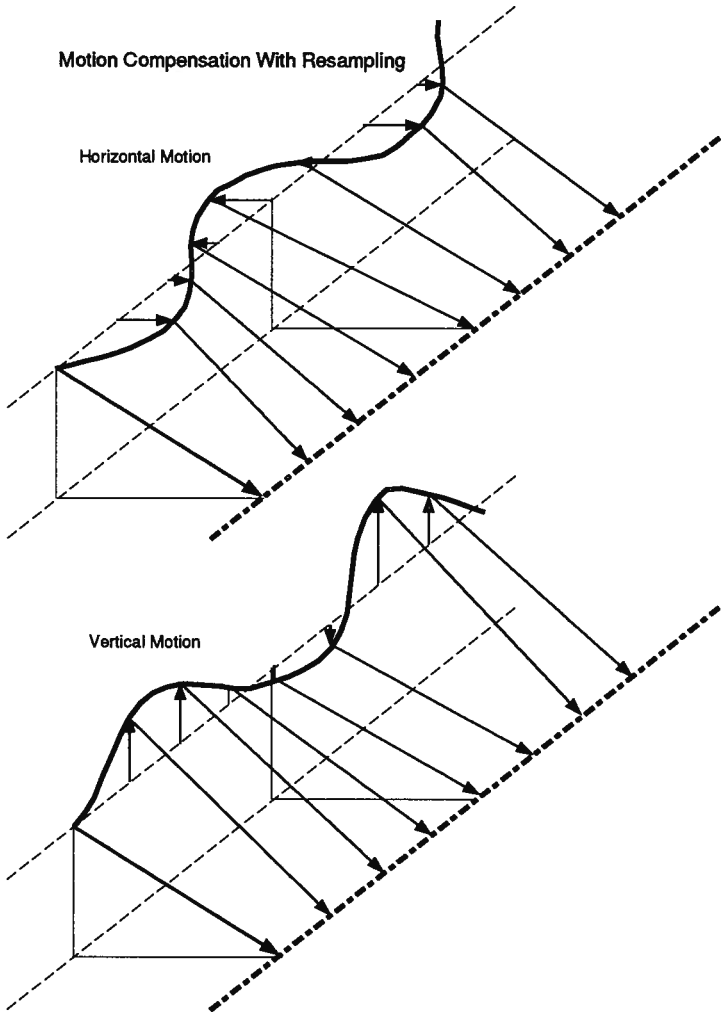

Figure 9 Flight Profile With Resampling

way. For instance, all the point spread functions corresponding to the contributing scatterers will be broadened or shifted by the same amount because each scatterer will experience the same phase error along the aperture. This means that all scatterers will be altered by the same amount leading to an altered clutter value.

3.3.5 Effects of Inertial Data Errors

In the preceding analysis the position of the antennas was assumed to be correct. In reality, there will be errors in the inertial data. Inertial data errors basically fall into two categories: high frequency errors and low frequency drifts. The high frequency errors have periods that

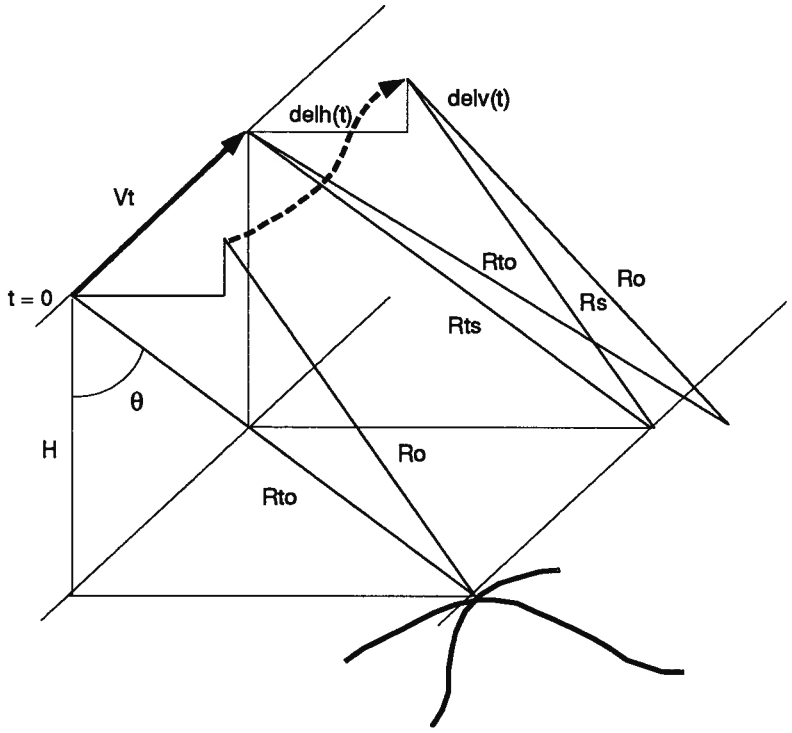

Figure 10 Neglecting Motion Compensation Resampling

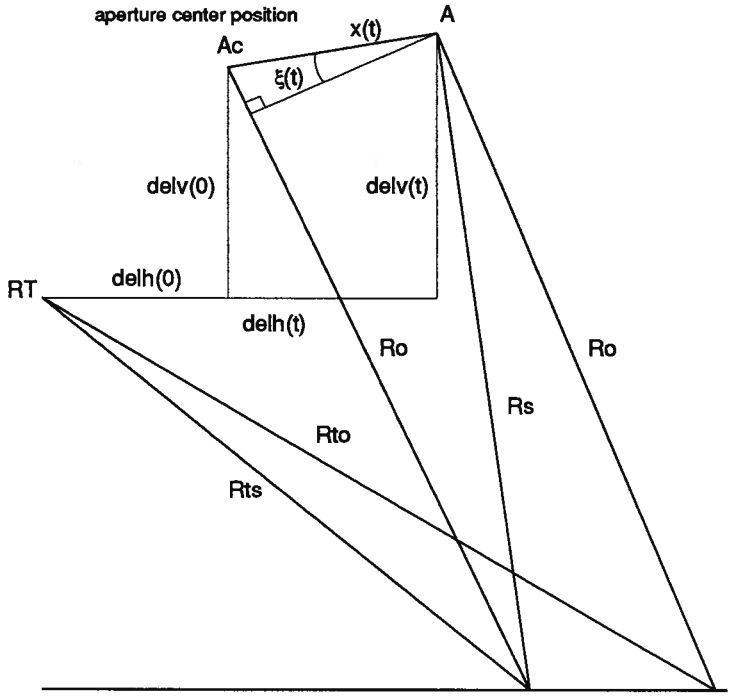

Figure 11 Cross-section of Neglecting Resampling Geometry

are short compared to the processed aperture. The low frequency drifts have periods that are long compared with the processed aperture.

The low frequency drifts will yield effectively constant antenna position errors during an aperture synthesis. These errors will behave much like the errors due to the unknown terrain and will depend upon the motion during the aperture. For instance, a roll bias will behave very similarly to an error in the assumed target elevation because it is basically a rotation error in the geometry. Most biases, such as a roll bias, are small and should not have a significant impact at the motion compensation stage. Some work has been done to determine upper bounds on inertial data errors for a specific system by simulation [17]. In addition, a more general rule has been proposed that for a maximum broadening of 10% the phase errors must be less than $\pi/2$ when the period is greater than the processed aperture [24]. In terms of INS errors this corresponds to about 7 *mm* for the CCRS C-band system.

The high frequency errors translate into small high frequency errors in the antenna position estimates, which in turn become high frequency phase correction errors along the aperture. Limits on the allowable high frequency phase errors in terms of the impulse response of the system have been analyzed [24, 28]. To maintain an Integrated Side Lobe Ratio (ISLR) of at least –20 dB, one standard deviation of the high frequency phase error must be less than about 6 degrees. In terms of INS errors this corresponds to about 0.5 *mm* for the CCRS C-band system. A preliminary investigation into the effect on the resulting phase of the impulse response has been made [29]. This will be extended further in the following section.

Directional Random Walk for Point Targets

The effect of high frequency (or random) phase errors on the phase of the azimuth compression result can be modelled. Azimuth compression can be thought of as the repeated summation of complex samples. When there are errors in the phases this will lead to peak deformation and phase distortion. To simplify the problem, consider only the resultant of the summation that yields the complex peak value. Furthermore, assume that the expected phase

of the compressed peak is zero. Each sample that contributes to this summation is the result of the complex multiplication of the data sample with an estimate of the complex conjugate of that sample. The matched filter attempts to remove any imaginary component in the data sample leaving a purely real result. When there is no noise and the filter is perfectly matched then the peak value will be purely real valued because every vector summed will be directed along the positive real axis in the complex plane. When noise is present or the filter is not correctly matched in phase, the contributing sample will have an imaginary component. The complex peak value can be modelled as the result of what could be called a directional random walk. Each sample in the summation can be thought of as taking a step in the complex plane in the general direction of the positive real axis but with a small random direction error.

The statistics of the complex summation result for the case of communication theory problems has been studied [30]. The summation can be characterized by:

$$Re^{j\theta} = X + jY = \sum_{i=1}^{N} A_i e^{j\phi_i} \tag{3.58}$$

where each contribution $A_i e^{j\phi_i}$ is independent and the expectation of Y is zero (expect zero phase). The A_i's can be regarded as the modulated scattering strength along azimuth including any compression windowing. The calculation of phase variance at the peak is carried out in Appendix D for Gaussian phase noise. The variance to be solved is:

$$\sigma_\theta^2 = \frac{< \left(X - \bar{X}\right)^2 >}{\bar{X}^2} = \frac{< Y^2 >}{\bar{X}^2} \tag{3.59}$$

The resulting phase variance using integrals from [31] is:

$$\sigma_\theta^2 = \frac{\left(1 - e^{-2\sigma_\phi^2}\right)}{2\, e^{-\sigma_\phi^2}} \frac{\sum_{i=1}^{N} A_i^2}{\left\{\sum_{i=1}^{N} A_i\right\}^2} \tag{3.60}$$

where σ_ϕ^2 is the variance of the Gaussian phase noise and the A_i's represent the compression weighting. When there is uniform weighting this reduces to:

$$\sigma_\theta^2 = \frac{\left(1 - e^{-2\sigma_\phi^2}\right)}{2N\, e^{-\sigma_\phi^2}} \tag{3.61}$$

The validity of this model to describe the phase smoothing ability of compression of a point target was verified using simulation with typical parameters for SAR. The simulation results agreed to very high precision with the theory. The intuitive explanation for the significant smoothing observed ($\sim \frac{1}{2N}$) is that the compression operation has little effect on the distribution of the phase noise within the data but collapses most of the signal energy into a small region. The phase noise at the compressed peak is very small due to the significant increase in the signal to noise ratio at that point.

INS Errors for Clutter Data

When the resulting phase errors for the clutter data case is considered very different results are obtained. Previous work [29] and repeated simulations and real data processing in the current work have demonstrated that random phase errors are not smoothed when the signal is clutter data. The real data experiments added random phase noise to uncompressed SAR data and compared the focussed results with the noiseless compressed image. There was no evidence of smoothing. The resulting phase errors depended upon the specific processing conditions, such as the processed beamwidth. The intuitive understanding of this is that the clutter to noise ratio at a particular pixel is unchanged by compression. The individual point target responses are focussed but the overall signal strength at any one point is, on average, unchanged. This means that high frequency phase errors are transferred to the compressed image result without the effect of smoothing.

3.3.6 Summary of Single Channel Errors and Constraints

In ideal motion compensation all the required geometric parameters are known and there is no restrictions placed on the processing. This leads to accurate compensation except that the range varying phase correction induces a range spectral shift. This can be minimized by keeping the reference track close to the antenna position by segmenting the track.

In realistic processing situations non-ideal motion compensation must be used. In this scenario multiple targets must be processed together and certain important information, such as the terrain elevation, is not known. This leads to various errors (Table 2). Given the assumptions made at the beginning of the chapter the following tables summarize the phase errors occurring in single channel non-ideal motion compensation and the limitations these errors place on the imaging configuration and flight motion. The zero Doppler pulse processing leads to phase errors along the uncompressed azimuth data due to multiple target processing, possible FM rate errors, and the coupling between the range varying phase correction and RCMC. Given that the target elevation is not typically known, assuming flat terrain also leads to phase errors along the aperture. Inertial data errors translate into phase correction errors along the aperture proportional to the error in the antenna position. This leads to peak deformation and phase errors.

Table 3 indicates how these errors translate into limitations on the allowed flight motion for a given imaging configuration. Specific numbers are included for the nominal CCRS case.

- Errors in the slant range value used to generate the matched filters will cause peak broadening.
- The coupling between the range varying phase correction (RVPC) and RCMC produces peak broadening that depends upon the displacement from the reference track perpendicular to the line-of-sight direction.

Table 2 Single Channel Phase Errors

Physical Effect	Phase Error Along Aperture
Multiple Target Consideration	$\Delta\phi_{err}(t) \approx \frac{2\pi v^2 t^2 d_{los}(t)}{\lambda R^2}$
FM Rate Errors	$\Delta\phi_{err}(t) \approx \frac{2\pi v^2 t^2 \Delta R_{mf}}{\lambda R^2}$
Range Cell Migration Correction	$\Delta\phi_{err}(t) \approx \frac{2\pi v^2 t^2 d_{\perp los}(t)}{\lambda R^2 \tan\theta}$
Unknown Terrain Elevation	$\Delta\phi_{err}(t) \approx \frac{4\pi\ h\ d_{\perp los}(t)}{\lambda R \sin\theta}$
Inertial Data Errors	$\Delta\phi_{err}(t) \approx \frac{4\pi}{\lambda}\Delta R_{INS}(t)$

- The range varying phase correction (RVPC) causes a non-linear range spectral shift which depends upon the displacement from the reference track perpendicular to the line-of-sight direction. This can be an important factor when subsequent processing is considered.
- The effect of unknown terrain is to produce peak broadening for acceleration perpendicular to the line-of-sight direction and a peak shift for velocity perpendicular to the line-of-sight direction.
- The effect of inertial data errors is to produce peak broadening and phase errors. For high frequency errors there is significant smoothing for point targets but not for clutter data.

In addition, neglecting to resample for motion compensation will lead to some PSF deformation.

Table 3 Single Channel Motion Compensation Limitations (CCRS Typical)

Physical Effect	Limitation
FM Rate Errors	5% broadening: $\Delta R_{mf} < \frac{\lambda R^2}{v^2 T^2}$ $< 37\ m$
Range Cell Migration Correction	5% broadening: $d_{\perp los} < \frac{\lambda R^2 \tan\theta}{v^2 T^2}$ $< 49\ m$
Displacement Offset (range varying phase correction)	Range Oversampling Factor O_r: $1 + \frac{2c\lvert d_{\perp los}\rvert}{\lambda R \tan\theta B W_r} < O_r$ $1 + 1.032\ \lvert d_{\perp los}\rvert < O_r$
Unknown Terrain Elevation	5% broadening: $a_{\perp los} < \frac{\lambda R \sin\theta}{h T^2}$ $< \frac{5\ g}{h}\ \frac{m}{s^2}$
	one sample shift: $\frac{\partial d_{\perp los}}{\partial t} < \frac{v^2 \sin\theta}{h P R F}$ $< \frac{40}{h}\ \frac{m}{s}$
Inertial Data Errors	High Frequency INS Errors Clutter Data: no smoothing Point Target: $\sigma_\theta^2 = \frac{\left(1 - e^{-2\sigma_\phi^2}\right)}{2N\ e^{-\sigma_\phi^2}}$

Chapter 4 Motion Compensation for Interferometry

Now that the foundations of motion compensation for a single channel SAR have been formed, it is now possible to consider the specific problem of motion compensation for InSAR. This chapter will begin by defining the assumptions made and the requirements of motion compensation for InSAR. Following this, ideal motion compensation will be investigated and the corresponding interpretation of the differential phase of the interferogram. The required interpretation for non-ideal motion compensation will then be analyzed for the case of single and dual reference tracks. Finally, InSAR errors resulting from non-ideal compensation will be investigated by extending the preceding single channel error analysis to the two channel case under the same assumptions.

4.1 Assumptions

The assumptions made are the same as those presented in the previous chapter, namely:

1. Both antennas are yaw steered to zero Doppler. This means that both antennas are assumed to be pointing perpendicular to the velocity vector of the aircraft.
2. The SAR processing is to zero Doppler for both channels.
3. The pitch of the aircraft is fixed.
4. The spacing between transmitted pulses on the ground is kept fixed by adjusting the Pulse Repetition Frequency (PRF) to be proportional to the aircraft velocity.
5. The inertial data will be assumed to be correct, for the most part.
6. The motion compensation to be applied will be post-flight, apart from those mentioned in the above list.
7. Translational motion and aircraft roll must be compensated through motion compensation.

These basic assumptions are consistent with the CCRS Convair 580 InSAR system [18], and the Environmental Research Institute of Michigan (ERIM) IFSARE system in strip-map mode [32].

4.2 InSAR Motion Compensation Requirements

SAR Interferometry is concerned with extracting the phase difference between two processed images, pixel by pixel, in order to estimate the terrain elevation. InSAR is no longer concerned with the "focus" of the image in terms of its radiometric appearance, but rather how the focus affects the estimate of the phase, and in turn the estimate of elevation. This requires viewing the motion compensation and azimuth compression stages of conventional airborne SAR in a different way.

For example, InSAR is not affected by large phase bias errors that exist in each channel provided they are common to both and thus cancel out in the differential phase. As the two antennas are rigidly connected on the aircraft, much of the motion experienced by each channel will be common to both. Therefore, phase errors resulting from the common flight motion may not degrade the interferometer. What affects the height estimate is differential phase biases and differential phase variances, which translate into height estimate biases and height estimate variances.

In a recent paper by Bamler and Just [27], a frequency domain analysis was conducted to evaluate the effect on the differential phase of differences in the transfer functions between channels. For distributed homogenous targets the signals for the two channels can be characterized by:

$$S_1 = R_1 e^{j\theta_1} \tag{4.1}$$

$$S_2 = R_2 e^{j\theta_2} \tag{4.2}$$

where each is a circular Gaussian random variable [10]. The expected differential phase bias was shown to be the phase of the inter-channel correlation coefficient [27]:

$$\Phi_{bias} = arg\,(\gamma) \tag{4.3}$$

$$\gamma = \frac{< S_1 S_2^* >}{\sqrt{< S_1 S_1^* >< S_2 S_2^* >}} = \frac{\int_{-\infty}^{\infty} H_A(f) H_B^*(f) df}{\sqrt{\int_{-\infty}^{\infty} |H_A(f)|^2 |H_B(f)|^2 df}} \tag{4.4}$$

where $< >$ is the expectation operator, and $H_A(f)$ is the transfer function of channel A, and $H_B(f)$ is the transfer function of channel B. The probability density function of the differential phase can be shown to be (page 46 of [33]):

$$p(\Phi) = \frac{1-\gamma^2}{4\pi^2}(1-\beta^2)^{\frac{3}{2}}\left(\beta \sin^{-1}\beta + \frac{\pi\beta}{2} + \sqrt{1-\beta^2}\right) \tag{4.5}$$

where

$$\beta = |\gamma| \cos\,(\Phi) \tag{4.6}$$

The corresponding variance has no closed form solution, but can be evaluated numerically:

$$\sigma_\Phi^2 = \int_{-\infty}^{\infty} \Phi^2 p(\Phi) d\Phi \tag{4.7}$$

This work formalizes the idea that differences in the transfer functions lead to differential phase biases or increased differential phase variances. For instance, if the motion compensation errors lead to differences in the PSF's between channels this will lead to a decrease in the inter-channel correlation and therefore an increased differential phase variance. It is shown in Appendix E that the inter-channel correlation coefficient factor due to inter-channel azimuth broadening of $\eta > 1$ is:

$$\gamma \propto \frac{1}{\sqrt{\eta}} \tag{4.8}$$

for sinc-like point spread functions. Therefore, inter-channel broadening of about 10 percent leads to a correlation factor of about 0.95.

But, this does not mean that defocussing common to both channels has no effect on the InSAR system. The amount of phase noise from certain sources, such as baseline decorrelation [10], depends upon the transfer function in each channel. In addition, a more local estimate of the terrain elevation is achieved with a narrower point spread function (PSF). Given that the height estimate is very sensitive to the differential phase, significant spatial averaging is required in InSAR to facilitate phase unwrapping and reduce the variance of the estimate. This relaxes the localization requirements because the averaging will typically take place over many resolution lengths. But, the narrower the PSF the more uncorrelated the samples are and thus better phase smoothing will be accomplished. The amount of spatial averaging may need to be reduced when the local elevation variation is large in order to avoid differential phase aliasing. This will increase the sensitivity to focussing problems.

Once the differential phase has been calculated it must be unwrapped into the absolute phase by adding some multiple of 2π. This is a two dimensional problem which requires continuity in the differential phase [19]. If the differential phase is discontinuous, for instance by reference track segmentation, then the unwrapping process becomes very complicated. Discontinuities will be inevitable in rugged terrain due to shadow and layover effects but should not be caused by motion compensation mechanisms.

In summary, identical, high resolution, geometrically correct, PSFs are desired for InSAR mapping. Phase errors in the compressed images that are common to both channels cancel out in the interferogram's differential phase. InSAR motion compensation has some of the conventional requirements, such as resolution and sidelobe level control, that exists in the single channel case. But, the primary concern is to maintain the similarity in the transfer functions between the two channels. Differential phase errors should be minimized at all costs. In addition, the differential phase should be continuous for phase unwrapping. The ability to meet these requirements of motion compensation for InSAR will now be examined for the

single and dual reference track approaches.

4.3 Ideal Motion Compensation

Ideal motion compensation for InSAR is very similar to the single channel scenario. Two parallel reference tracks can be defined, one for each channel. Given precise knowledge of the entire imaging geometry, including inertial data and terrain information, each target on the ground is processed independently as prescribed in the ideal single channel case. The compensated range compressed data then emulates transmission and reception from the two parallel tracks. The transmit/receive channel is processed as in the single channel case, but, the receive-only channel calculates corrections based on the transmission from the two-way antenna and reception at the one-way antenna.

As was the case in the single channel scenario there is a range varying phase correction that depends upon the displacement of each channel from its reference track. The possible side-effects from subsequent processing were outlined in the previous chapter, but, for InSAR the concern is what will lead to differential phase errors. If the displacements from the reference tracks are almost identical in each channel one would expect that the phase errors would essentially cancel out. This will be investigated further in Section 4.4.5.

Another approach could be to motion compensate both channels to the same reference track. If ideal compensation was carried out then the resulting differential phase would be zero everywhere because the phase would be the same in both channels (ignoring other effects such as noise). The usefulness of such an approach seems remote at present but it highlights the main differences between the two main approaches to motion compensation for InSAR, namely, using single and dual reference tracks. The single reference track approach attempts to undo the relative mapping between the two channels. The dual reference track, on the other hand,

attempts to make the parallax be with respect to the two reference tracks. The two approaches require different interpretations of the resulting differential phase.

4.3.1 Dual Reference Track Assuming Ideal Compensation

The approach taken by the Jet Propulsion Laboratory (JPL) [21, 22] is to assume that ideal motion compensation has been performed and they proceed to interpret the differential phase from the two reference tracks (Figure 12). The interpretation of the differential phase used is based purely on triangulation from the reference tracks (RT_a, RT_b):

$$\Phi = -\frac{2\pi}{\lambda}(R_{tah} - R_{tbh}) \tag{4.9}$$

The target coordinates are measured from the channel B reference track, requiring θ_b and R_{tbh}. Quoting their results [21, 22]:

$$\theta_b = \cos^{-1}\left(\cos\xi\sqrt{1-\sin(\theta_b-\xi)} - \sin\xi\sin(\theta_b-\xi)\right) \tag{4.10}$$

where

$$\sin(\theta_b-\xi) = \frac{\left(R_{tbh} - \frac{\lambda DP}{2\pi}\right)^2 - R_{tbh}^2 - b_{RT}^2}{2b_{RT}R_{tbh}} \tag{4.11}$$

and

$$\xi = \frac{\pi}{2} - \alpha_{ab} \tag{4.12}$$

This approach does not consider the possible biases that result when motion compensation is performed assuming flat terrain at some reference level. This assumption is required for InSAR because the terrain is not known apriori.

If there are large drifts from the reference tracks then segmentation of the reference tracks will be required due to the range varying phase correction (RVPC) problems. This will result in discontinuous differential phase because the interpretation of the differential phase is from the two reference track positions. This will complicate the phase unwrapping process.

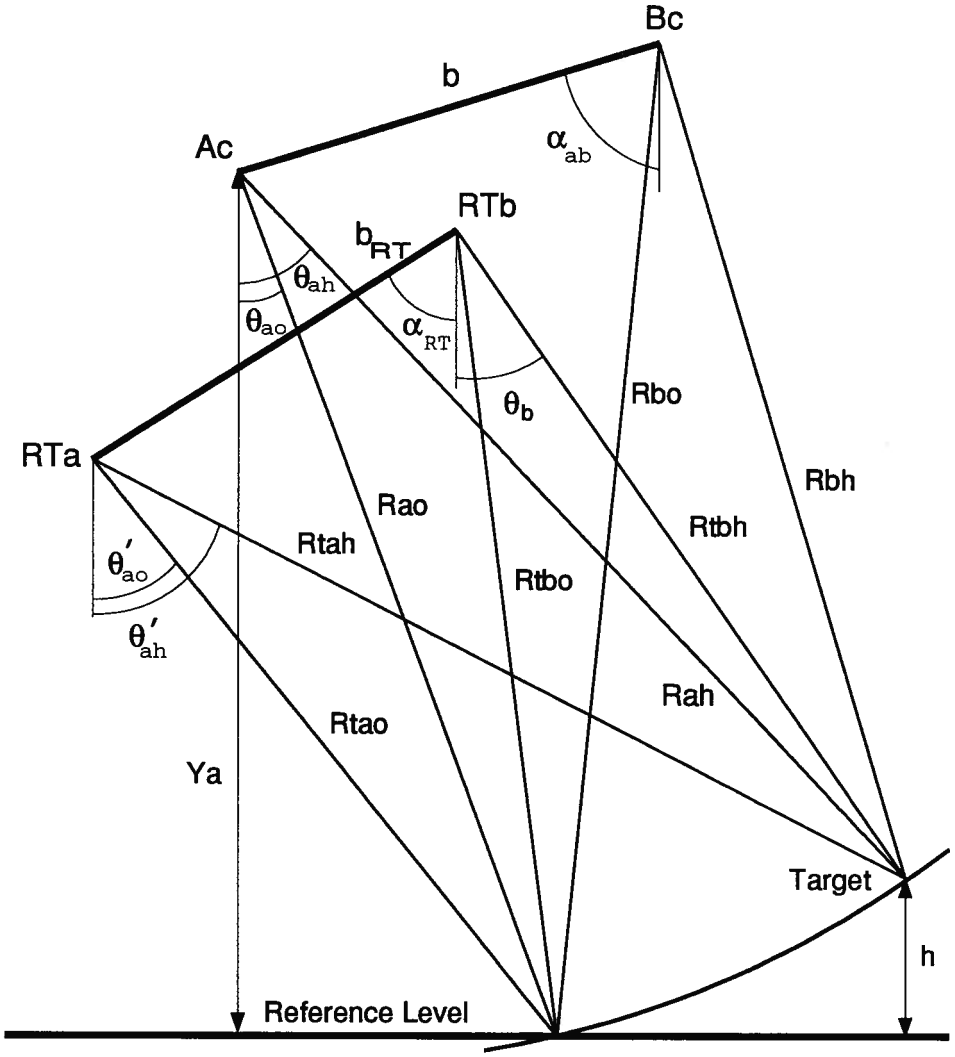

Figure 12 Double Reference Track Geometry

4.4 Non-Ideal Motion Compensation

Given that InSAR would be superfluous if the terrain elevation was initially known ideal motion compensation is not possible for InSAR. At best, each individual target could be processed as in the single channel ideal case but with flat terrain assumed. As in the single channel case, this is very computationally intensive and therefore zero Doppler pulse processing is most often used. In this section, two new approaches to interpreting the differential phase by considering the biases caused by unknown terrain will be presented. Following this, the

effects on the InSAR height estimate, due to the same sources of errors treated in the single channel case, will be investigated.

4.4.1 Single Reference Track with Unknown Terrain

The single reference track approach to motion compensation was first used for InSAR by the Canada Centre for Remote Sensing (CCRS) [25, 18]. Both channels are phase compensated to the same reference track using the geometry of Figure 13, assuming the terrain is flat at some reference level. For the following analysis the arc on which the target lies is assumed to be centered at the channel A antenna. An equally valid view centered on the channel B antenna could be used. The fact that there is a choice highlights the fact that the two channels are not perfectly registered due to the unknown terrain. When clutter data is processed the best 3D position estimate for the pixel is essentially midway between the two results.

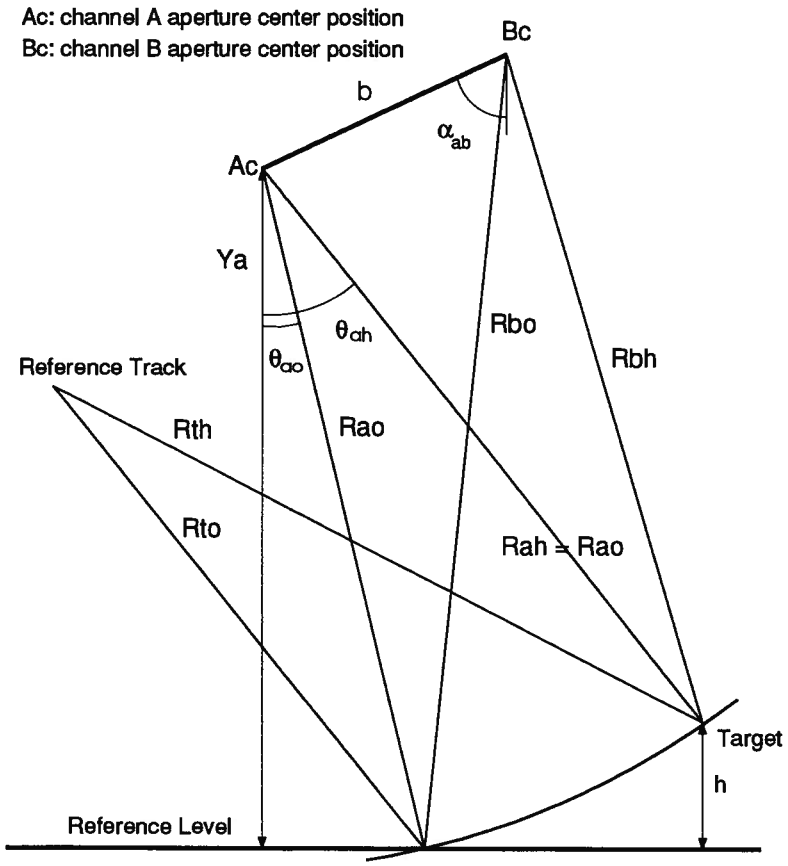

Figure 13 Single Reference Track Geometry

The applied phase correction for each channel assuming channel A is transmit/receive and channel B is receive-only is (Figure 13):

$$\begin{aligned}\phi_A(applied) &= -\frac{4\pi}{\lambda}(R_{to} - R_{ao}) \\ \phi_B(applied) &= -\frac{2\pi}{\lambda}((R_{to} - R_{ao}) + (R_{to} - R_{bo}))\end{aligned} \tag{4.13}$$

If ideal compensation had been applied (by virtue of θ being known):

$$\begin{aligned}\phi_A(ideal) &= -\frac{4\pi}{\lambda}(R_{th} - R_{ah}) \\ \phi_B(ideal) &= -\frac{2\pi}{\lambda}((R_{th} - R_{ah}) + (R_{th} - R_{bh}))\end{aligned} \tag{4.14}$$

the differential phase would be zero everywhere because the relative phase mapping due to the parallax would have been removed.

Due to the realities of non-ideal compensation it is necessary to make a "center of aperture assumption". The assumption is that motion compensation and the resulting differential phase of a compressed image sample of the interferogram is due only to the relative geometry of the InSAR system at the zero Doppler pulse. If the applied phase correction for a given pixel is "backed" out after compression, the resulting differential phase is due simply to the instantaneous relative geometry of the antennas and target for that pulse [18]. In addition, the inter-channel registration resampling that is performed on the range compressed data is assumed to carry over into the azimuth compressed data unchanged. The center of aperture assumption is in fact correct for trajectories which are parallel but offset from the reference track(s). This is the case because the applied phase correction is constant for a given slant range cell along the aperture and azimuth compression therefore does not alter the constant phase correction.

By invoking the center of aperture assumption the differential phase will be zero for scene patches that have the same elevation as the reference level because the motion compensation for these patches will have been done properly. The differential phase will be non-zero for any scene patch whose elevation differs from the reference level. The value of this phase is the difference in the errors in the phase correction applied between the two channels due to the

reference level assumption. These errors depend upon the imaging geometry and can be related explicitly to the elevation of the scene patch relative to the reference level. This interpretation applies for slowly varying drifts of the aircraft from the reference track. Higher frequency motions coupled with the unknown terrain will cause phase errors that deviate from the center of aperture assumption. These errors will be considered in Section 4.4.3.

The resulting single reference track differential phase Φ can easily be shown to be (Appendix F):

$$\begin{aligned} \Phi &= (\phi_A(applied) - \phi_A(ideal)) - (\phi_B(applied) - \phi_B(ideal)) \\ &= -\frac{2\pi}{\lambda}(R_{bo} - R_{bh}) \end{aligned} \tag{4.15}$$

The off-nadir angle θ_{ah}, measured from the instantaneous antenna position A_c, can be obtained in terms of known and measured parameters from simple trigonometry:

$$\begin{aligned} R_{bh}^2 &= b^2 + R_{ao}^2 + 2bR_{ao}\cos(\alpha_{ab} + \theta_{ah}) \\ R_{bo}^2 &= b^2 + R_{ao}^2 + 2bR_{ao}\cos(\alpha_{ab} + \theta_{ao}) \end{aligned} \tag{4.16}$$

yielding:

$$\Phi = \frac{2\pi}{\lambda}\left(\sqrt{b^2 + R_{ao}^2 + 2bR_{ao}\cos(\alpha_{ab} + \theta_{ah})} - R_{bo}\right) \tag{4.17}$$

and rearranging terms:

$$\theta_{ah} = \cos^{-1}\left(\frac{\left(\frac{\lambda}{2\pi}\Phi + R_{bo}\right)^2 - b^2 - R_{ao}^2}{2bR_{ao}}\right) - \alpha_{ab} \tag{4.18}$$

The scene patch elevation above the reference level is (Figure 13):

$$h = Y_a - R\cos\theta \tag{4.19}$$

By expanding the slant range values in a binomial series the following approximate solution results:

$$\theta_{ah} \approx \cos^{-1}\left(\frac{\lambda\Phi}{2\pi b} + \cos(\theta_{ao} + \alpha_{ab})\right) - \alpha_{ab} \tag{4.20}$$

Using the channel B antenna as the arc center, by symmetry the following results:

$$\theta_{bh} \approx \cos^{-1}\left(\frac{\lambda\Phi}{2\pi b} + \cos\left(\theta_{bo} + \alpha_{ab}\right)\right) - \alpha_{ab} \tag{4.21}$$

A more accurate position estimate can be obtained by using the slant range:

$$R = \frac{R_{ao} + R_{bo}}{2} \tag{4.22}$$

and the off-nadir angle:

$$\theta = \frac{\theta_{ah} + \theta_{bh}}{2} \tag{4.23}$$

measured from the center of the antenna baseline. The sensitivity of the height estimate to errors in the differential phase can be shown to be:

$$\frac{\partial h}{\partial \Phi} \approx -\frac{\lambda R \sin\theta}{2\pi b \sin\left(\theta + \alpha_{ab}\right)} \tag{4.24}$$

The single reference track differential phase (Equation 4.15) is independent of the reference track positions. Rather, it depends upon the actual slant range to the target from channel B (R_{bh}) relative to the slant range used for resampling channel B to register with channel A at the reference level (R_{bo}). If the reference track is segmented along azimuth to better follow the drifts of the aircraft, the differential phase will still be continuous provided the reference level is continuous across the segments. This is a very important feature of the single reference track approach.

Another benefit of the single reference track approach comes from the fact that the differential phase will vary depending upon the variation of the terrain about the assumed reference level. In other words, the flat earth fringes have been removed. This implies that the range spectrum of the interferogram is approximately at baseband. This simplifies the phase smoothing operation because the flat earth fringe rate, inherent in the dual reference track approach, does not need to be considered. Typically, the phase smoothing would have

to estimate the local fringe rate and smooth about this slope [19]. But, in either case range filtering of the interferogram must be considered carefully so as not to break the required symmetry of the spectrum [34].

4.4.2 Dual Reference Track with Unknown Terrain

One thing that is missing in the ideal motion compensation dual reference track interpretation of the differential phase is consideration of the phase errors in each channel that result from motion compensation assuming flat terrain. When these systematic terrain induced phase errors are included (or equivalently, motion compensation is backed out after compression) a new double reference track approach is obtained. The approach proceeds as in the single reference track case by considering the difference in the errors in the applied phase correction between channels. The center of aperture assumption is used here in the same was as in the single track case. Therefore, this approach attempts to handle errors due to unknown terrain coupled with slowly varying drifts from the reference tracks.

The applied and ideal phase correction in channel A is (Figure 12):

$$\begin{aligned} \phi_A(applied) &= -\frac{4\pi}{\lambda}(R_{tao} - R_{ao}) \\ \phi_A(ideal) &= -\frac{4\pi}{\lambda}(R_{tah} - R_{ah}) \end{aligned} \tag{4.25}$$

The channel B (receive-only) applied and ideal phase correction is:

$$\begin{aligned} \phi_B(applied) &= -\frac{2\pi}{\lambda}((R_{tao} - R_{ao}) + (R_{tbo} - R_{bo})) \\ \phi_B(ideal) &= -\frac{2\pi}{\lambda}((R_{tah} - R_{ah}) + (R_{tbh} - R_{bh})) \end{aligned} \tag{4.26}$$

The resulting differential phase will be the ideal component (Equation 4.9) plus the difference in the errors (Appendix G):

$$\begin{aligned} \Phi &= -\frac{2\pi}{\lambda}(R_{tah} - R_{tbh}) + \\ &(\phi_A(applied) - \phi_A(ideal)) - (\phi_B(applied) - \phi_B(ideal)) \\ &= -\frac{2\pi}{\lambda}(R_{tao} - R_{tbo} + R_{bo} - R_{bh}) \end{aligned} \tag{4.27}$$

The off-nadir angle θ_{ah} can be explicitly related to the measured differential phase and other known parameters using Equation 4.16:

$$\theta_{ah} + \alpha_{ab} = \cos^{-1}\left(\frac{\left(\frac{\lambda}{2\pi}\Phi + R_{tao} - R_{tbo} + R_{bo}\right)^2 - b^2 - R_{ao}^2}{2bR_{ao}}\right) \tag{4.28}$$

By expanding the slant range values in binomial series the following approximate solution results:

$$\theta_{ah} + \alpha_{ab} \approx \cos^{-1}\left(\left(\frac{1}{b}\right)\left(\frac{\lambda\Phi}{2\pi} + R_{tao} - R_{tbo}\right) + \cos\left(\theta_{ao} + \alpha_{ab}\right)\right) \tag{4.29}$$

Again, the symmetric formulation using the channel B antenna as the arc center leads to:

$$\theta_{bh} + \alpha_{ab} \approx \cos^{-1}\left(\left(\frac{1}{b}\right)\left(\frac{\lambda\Phi}{2\pi} + R_{tao} - R_{tbo}\right) + \cos\left(\theta_{ao} + \alpha_{ab}\right)\right) \tag{4.30}$$

The unbiased position estimates use the same Equations 4.22-4.23 as before. The conventional approach measures the off-nadir angle from the reference track but the single and new double track approaches measure from the instantaneous antenna positions. This is consistent with the backing out motion compensation viewpoint.

The differential phase bias error that the new dual reference track approach recovers, that is inherent to the conventional approach, is shown in Appendix G to be:

$$E(A) - E(B) \approx \left(\frac{2\pi h b_{los}}{\lambda R \sin\theta}\right)(\alpha_{RT} - \alpha_{ab}) \tag{4.31}$$

For unsegmented reference tracks, rugged terrain, and typical aircraft motion, this can correspond to height estimation biases of several meters. If the reference tracks are segmented to remain close to the antennas and the antenna and reference track baseline angles are similar, the errors become quite small.

The sensitivity of the height estimate to differential phase errors is identical to the single track case (Equation 4.24). But, the differential phase depends upon the reference track

position through R_{tao} and R_{tbo}. This means that reference track segmentation will result in discontinuous differential phase across the boundaries which will complicate the phase unwrapping process. One solution to this is to undo the originally applied phase correction to each channel after compression. The resulting differential phase is then interpreted with respect to the instantaneous antenna positions, removing the reference track dependence and making the differential phase continuous. Another more efficient approach that combines the single and dual track approaches to obtain the benefits of both will be described later in this chapter (Section 4.5.2).

4.4.3 Effects of Unknown Terrain

When the terrain is assumed to be flat at the reference level and there are higher frequency flight motions then there will be phase errors that vary along the aperture for each channel. This was analyzed already for the single channel case (Section 3.3.2). For InSAR, of concern is the difference in these phase errors. The error in each channel has the same form. Specifically, for channel A (from Appendix B):

$$\Delta\phi_a(t) \approx \frac{8\pi d_a(t)}{\lambda} \sin\left(\alpha_a(t) + \theta_{ao}(t) + \frac{\Delta\theta(t)}{2}\right) \sin\left(\frac{\Delta\theta(t)}{2}\right) \tag{4.32}$$

where $\theta_a(t)$ is the assumed angle to the target, and $\Delta\theta(t)$ is the error in that assumed angle. All of these parameters will change along the aperture for a given target due to the changing flight motion. It is shown in Appendix F that for the single reference track case the phase error for channel B is the same as channel A plus an additional term:

$$\begin{aligned}\Delta\phi_b(t) &\approx \Delta\phi_a(t) + \Delta\phi_{ab}(t) \\ &\approx \Delta\phi_a(t) + \frac{4\pi b}{\lambda} \sin\left(\alpha_{ab}(t) + \theta_{ao}(t) + \frac{\Delta\theta(t)}{2}\right) \sin\left(\frac{\Delta\theta(t)}{2}\right)\end{aligned} \tag{4.33}$$

where b is the baseline length between the two antennas (fixed) and $\alpha_{ab}(t)$ is the off-vertical angle of the baseline (aircraft roll angle). The portion of this relative term that is constant along the aperture will appear as a bias in the differential phase. This is precisely what is

considered in the preceding interpretations of the differential phase that includes the unknown terrain effects. Further approximations, following Appendix F, yields:

$$\Delta\phi_{ab}(t) \approx \frac{2\pi h b_{\perp los}(t)}{\lambda R \sin\theta} \tag{4.34}$$

where

$$b_{\perp los} = b \sin\left(\alpha_{ab} + \frac{\theta_{ao} + \theta_{ah}}{2}\right) \tag{4.35}$$

The same analysis can be done for the dual reference track case (Appendix G), yielding:

$$\begin{aligned}
\Delta\phi_a(t) &\approx \frac{8\pi d_a(t)}{\lambda} \sin\left(\alpha_a(t) + \theta_{ao}(t) + \frac{\Delta\theta_a(t)}{2}\right) \sin\left(\frac{\Delta\theta_a(t)}{2}\right) \\
\Delta\phi_b(t) &\approx \frac{8\pi d_b(t)}{\lambda} \sin\left(\alpha_b(t) + \theta_{bo}(t) + \frac{\Delta\theta_b(t)}{2}\right) \sin\left(\frac{\Delta\theta_b(t)}{2}\right) \\
&= \Delta\phi_a(t) + \Delta\phi_{ab}(t)
\end{aligned} \tag{4.36}$$

The difference in the errors is shown in Appendix G to be:

$$\Delta\phi_{ab}(t) = -\frac{2\pi}{\lambda}(R_{tao} - R_{tah} + R_{tbh} - R_{tbo} + R_{bo} - R_{bh}) \tag{4.37}$$

Expanding these slant ranges in binomial series yields (Appendix G):

$$\begin{aligned}
&\Delta\phi_{ab}(t) \approx \\
&-\left(\frac{2\pi b_{RT}}{\lambda}\right)\left(\cos\left(\alpha_{RT} + \theta'_{ao}\right) - \cos\left(\alpha_{RT} + \theta'_{ah}\right)\right) + \\
&\left(\frac{2\pi b}{\lambda}\right)\left(\cos\left(\alpha_{ab}(t) + \theta_{ao}(t)\right) - \cos\left(\alpha_{ab}(t) + \theta_{ah}(t)\right)\right) \\
&\approx \left(\frac{4\pi b_{RT}}{\lambda}\right) \sin\left(\alpha_{RT} + \theta'_{ao} + \frac{\Delta\theta'}{2}\right) \sin\left(\frac{\Delta\theta'}{2}\right) - \\
&\left(\frac{4\pi b}{\lambda}\right) \sin\left(\alpha_{ab}(t) + \theta_{ao}(t) + \frac{\Delta\theta(t)}{2}\right) \sin\left(\frac{\Delta\theta(t)}{2}\right)
\end{aligned} \tag{4.38}$$

The first sinusoidal term involving the reference track is constant for a given target because the reference track is fixed over the aperture. The second sinusoidal term is identical to the residual phase error in the single reference track case. This term varies along the aperture governed by aircraft roll and translation. Therefore, the interpretation of the differential phase is different between the two approaches but the phase errors due to unknown terrain coupled with higher frequency flight motion are the same (Equation 4.34).

Aircraft Roll

It is useful to evaluate how the difference term (Equation 4.34) varies along the aperture, as this will indicate the source of differential phase errors. The effect of a changing roll angle dominates over the effect of the changing angles to the target. Assuming the roll angle variation is very small and expanding in a Taylor's series:

$$\Delta\phi_{ab}(t) \approx \Delta\phi_{ab}(0) + \frac{\partial\Delta\phi_{ab}(0)}{\partial\alpha_{ab}}(\alpha_{ab}(t) - \alpha_{ab}(0)) \tag{4.39}$$

and

$$\frac{\partial\Delta\phi_{ab}}{\partial\alpha_{ab}} \approx \frac{4\pi b}{\lambda}\cos\left(\alpha_{ab}(t) + \theta_{ao} + \frac{\Delta\theta}{2}\right)\sin\left(\frac{\Delta\theta}{2}\right) \tag{4.40}$$

with

$$b_{los} = b\cos\left(\alpha_{ab} + \frac{\theta_{ao} + \theta_{ah}}{2}\right) \tag{4.41}$$

yields:

$$\begin{aligned}\Delta\phi_{ab}(t) &\approx \Delta\phi_{ab}(0) + \frac{2\pi h b_{los}}{\lambda R\sin\theta}(\alpha_{ab}(t) - \alpha_{ab}(0)) \\ &\approx \Delta\phi_{ab}(0) + \frac{2\pi h b_{los}\Delta\alpha_{ab}(t)}{\lambda R\sin\theta}\end{aligned} \tag{4.42}$$

where $\Delta\alpha_{ab}(t)$ is the variation in the roll angle about the center of aperture position. Of interested is the time varying term, as the bias will be removed in later processing and does not affect compression. This yields a varying differential phase error along the aperture of:

$$\Delta\Phi(t) \approx \frac{2\pi h b_{los}\Delta\alpha_{ab}(t)}{\lambda R\sin\theta} \tag{4.43}$$

Angular Velocity For linearly varying roll one might expect to observe a relative mis-positioning between the two channels due to the unknown terrain elevation. Using the results of linear phase errors on compression from Appendix C one can define:

$$\Delta\Phi(t) \approx \frac{2\pi h b_{los}\Delta\alpha_{ab}(t)}{\lambda R\sin\theta} = \pi L t \tag{4.44}$$

Differentiating yields:

$$\pi L \approx \frac{2\pi h b_{los}}{\lambda R \sin\theta} \frac{\partial \Delta\alpha_{ab}(t)}{\partial t} \tag{4.45}$$

The resulting differential phase at the peak is:

$$\Delta\Phi = \frac{\pi L^2}{4K} = \frac{\pi h^2 b_{los}^2}{2v^2 \lambda R \sin^2\theta} \left(\frac{\partial \Delta\alpha_{ab}}{\partial t} \right)^2 \tag{4.46}$$

For any reasonable roll this differential phase error is negligible.

The resulting differential shift in samples is:

$$\Delta P = -\frac{L\ PRF}{2K} \approx -\frac{b_{los} h\ PRF}{2v^2 \sin\theta} \frac{\partial \Delta\alpha_{ab}(t)}{\partial t} \quad (samples) \tag{4.47}$$

The effect of this differential shift on the variance of the differential phase can be evaluated by considering the inter-channel correlation coefficient [27]. When the differential shift is less than about 1/16 of a resolution width (or about one twelfth of a sample for the CCRS case) the correlation coefficient factor is greater than about 0.99. This will be used to limit the allowed differential shift. With 1/16 of a sample as a bound on the relative shift one obtains:

$$\frac{\partial \Delta\alpha_{ab}(t)}{\partial t} < \frac{v^2 \sin\theta}{8 b_{los} h PRF} \tag{4.48}$$

Note that the line-of-sight component of the baseline is usually a small fraction of the baseline length. For typical CCRS parameters (Table 1) and a worse case $b_{los} = 1\ m$, yields:

$$\frac{\partial \Delta\alpha_{ab}(t)}{\partial t} < \frac{290}{h} \left(\frac{deg.}{s} \right) \tag{4.49}$$

Angular Acceleration If consideration is made for quadratic roll motion (uniform angular acceleration) the phase error is quadratic. When Equation 4.4 is evaluated for a differential quadratic phase error one obtains the same result as linear FM compression with a quadratic phase error evaluated at the peak of the compressed result (Appendix A), except that it is normalized [27]. Therefore, the expected phase bias (which is the angle of the correlation

coefficient) is 1/3 of the value of the quadratic phase error at the band edge. Therefore, the peak error along the aperture must be less than 1/3 of the maximum allowed differential phase error (Appendix A):

$$\Delta\Phi_{peak\ max} > \frac{2\pi b_{los} h}{3\lambda R \sin\theta} \Delta\alpha_{ab_{quad.\ max}} \tag{4.50}$$

In terms of uniform angular acceleration:

$$\Delta\alpha_{ab}(t) = \frac{1}{2} a_{roll} t^2 \tag{4.51}$$

The resulting differential quadratic phase error, as before, can be transformed into a differential phase bias error in the compressed image:

$$\Delta\Phi_{bias} \approx \frac{a_{roll}\pi b_{los} h T^2}{12\lambda R \sin\theta} \tag{4.52}$$

When processing to the 3 dB width of the antenna beam pattern,

$$T = T_{3dB} = \frac{\lambda R}{Dv} \tag{4.53}$$

and conversion to a height estimate bias is made using Equation 4.24, one obtains:

$$\frac{\Delta h_{bias}}{h} \approx -\frac{\lambda^2 R^2 b_{los} a_{roll}}{24 b v^2 D^2 \sin(\theta + \alpha_{ab})} \tag{4.54}$$

For typical CCRS parameters (Table 1), a bias ratio of 1 m in 1000 m, and a worse case $b_{los} = 1\ m$, yields:

$$a_{roll} < 0.07\ \frac{deg.}{s^2} \tag{4.55}$$

In addition to the differential phase bias there is decorrelation given by the magnitude of the correlation coefficient. For quadratic differential phase errors along the aperture the magnitude of the inter-channel correlation coefficient can be shown to be [27]:

$$|\gamma| = \frac{\sqrt{S^2\left(\sqrt{\Psi}\right) + C^2\left(\sqrt{\Psi}\right)}}{\sqrt{\frac{2\Psi}{\pi}}} \tag{4.56}$$

where the Fresnel integrals are defined as:

$$S(x) = \sqrt{\frac{2}{\pi}} \int_0^x \sin u^2 du$$
$$C(x) = \sqrt{\frac{2}{\pi}} \int_0^x \cos u^2 du \tag{4.57}$$

and Ψ is the differential phase error at the band edge. For a typical allowed differential quadratic phase error of 75 mrad at the band edge for the bias result (yields about a 1 m elevation bias error), this leads to an insignificant decorrelation factor of about 0.995 by numerical integration. Therefore, future decorrelation due to differential quadratic phase errors will be ignored as the bias component is the dominant effect.

Sinusoidal Roll The dominant roll motion is often oscillatory. This leads to oscillatory differential phase errors along the aperture. It is not possible to analytically evaluate the effect on the differential phase of such motion, even if it is approximated by a sinusoid. An approximate solution can be obtained by considering the instantaneous angular acceleration of a sinusoid and extrapolating from the angular acceleration results.

Let the roll motion be described by:

$$\Delta\alpha_{ab}(t) = G \sin \frac{2\pi t}{T_{roll}} \tag{4.58}$$

where G and T_{roll} are the amplitude and period of the roll motion, respectively. The corresponding instantaneous acceleration by differentiating twice is:

$$a_{roll} = -G\left(\frac{2\pi}{T_{roll}}\right)^2 \sin \frac{2\pi t}{T_{roll}} \tag{4.59}$$

The effective angular acceleration will depend upon the length of the aperture compared to the period of the roll, but will always be less than 1. By using the previous results from Equation 4.52, and defining a constant $f <= 1$, which relates the instantaneous to effective angular

acceleration, the resulting differential bias error is:

$$\Delta\Phi_{bias} \approx -\frac{\pi b_{los} h T^2}{12\lambda R \sin\theta} f G \left(\frac{2\pi}{T_{roll}}\right)^2 \sin\frac{2\pi t}{T_{roll}} \tag{4.60}$$

Therefore, the bias error will follow the roll motion.

The roll motion will also change the expected differential phase. This change can be estimated from differentiating Equation 4.43, yielding:

$$\begin{aligned} \Delta\Phi_{exp} &\approx \frac{2\pi b_{los} h \Delta\alpha_{ab}(t)}{\lambda R \sin\theta} \\ &\approx \frac{2\pi b_{los} h}{\lambda R \sin\theta} G \sin\frac{2\pi t}{T_{roll}} \end{aligned} \tag{4.61}$$

When the difference between the change in the expected and error in the differential phase are compared, the following results:

$$\Delta\Phi_{bias} - \Delta\Phi_{exp} \approx \frac{2\pi b_{los} h}{\lambda R \sin\theta} G \sin\frac{2\pi t}{T_{roll}} \left(1 - \frac{f\pi^2 T^2}{6T_{roll}^2}\right) \tag{4.62}$$

Therefore, the effect of the sinusoidal roll is to smooth out the measured differential phase. When the last bracket in this expression is zero, the roll does not effect the measured differential phase. The resulting height estimate using the instantaneous antenna positions will therefore have an error term that follows the sinusoidal roll. When $\frac{T}{T_{roll}} \ll 1$ then $f \sim 1$, and when $\frac{T}{T_{roll}} \gg 1$ then $f \sim 0$. Thus, the amount of smoothing depends upon the specific parameters of a given situation. If the smoothing is significant then the conventional (ideal) dual reference track interpretation of the differential phase will be less sensitive to sinusoidal roll coupled with unknown terrain.

Translational Motion

It is now helpful to evaluate how translational motion of the aircraft contributes to the differential phase error. Beginning with the change in the error in the off-nadir angle to the target:

$$\Delta\phi_{ab}(t) \approx \frac{4\pi b}{\lambda} \sin\left(\alpha_{ab} + \theta_{ao} + \frac{\Delta\theta(t)}{2}\right) \sin\left(\frac{\Delta\theta(t)}{2}\right) \tag{4.63}$$

and differentiating, yields:

$$\frac{\partial \Delta\phi_{ab}(t)}{\partial \Delta\theta} \approx \frac{2\pi b_{\perp los}}{\lambda} \tag{4.64}$$

Expanding in an Taylor's series yields:

$$\Delta\phi_{ab}(t) \approx \Delta\phi_{ab}(0) + \frac{2\pi b_{\perp los}}{\lambda}(\Delta\theta(t) - \Delta\theta(0)) \tag{4.65}$$

By considering displacements M from the center of aperture position one obtains:

$$\Delta\theta(t) - \Delta\theta(0) \approx \frac{M_{los}(t)\Delta\theta(0)}{R} \tag{4.66}$$

This yields a differential phase error that varies along the aperture governed by the translational deviation of the antenna baseline:

$$\begin{aligned} \Delta\Phi_{\Delta\theta}(t) &\approx \frac{2\pi b_{\perp los} M_{los}(t)\Delta\theta(0)}{\lambda R} \\ &\approx \frac{2\pi b_{\perp los} M_{los}(t) h}{\lambda R^2 \sin\theta} \end{aligned} \tag{4.67}$$

If this analysis is repeated for changes in the assumed off-nadir angle to the target:

$$\Delta\phi_{ab}(t,1) \approx \frac{4\pi b}{\lambda} \sin\left(\alpha_{ab} + \theta_{ao}(t) + \frac{\Delta\theta}{2}\right) \sin\left(\frac{\Delta\theta}{2}\right) \tag{4.68}$$

, differentiating yields:

$$\frac{\partial \Delta\phi_{ab}(t,1)}{\partial \theta_a} \approx \frac{2\pi b_{los} h}{\lambda R \sin\theta} \tag{4.69}$$

Expanding in an Taylor's series yields:

$$\Delta\phi_{ab}(t) \approx \Delta\phi_{ab}(0) + \frac{2\pi b_{los} h}{\lambda R \sin\theta}(\theta_a(t) - \theta_a(0)) \tag{4.70}$$

By considering displacements M from the center of aperture position one obtains:

$$\theta_a(t) - \theta_a(0) \approx \frac{M_{\perp los}(t)}{R} \tag{4.71}$$

This yields a differential phase error that varies along the aperture governed by the translational deviation of the antenna baseline:

$$\Delta\Phi_{\theta_a}(t) \approx \frac{2\pi b_{los} M_{\perp los}(t) h}{\lambda R^2 \sin\theta} \tag{4.72}$$

Combining these two error sources gives:

$$\Delta\Phi(t) \approx \frac{2\pi h}{\lambda R^2 \sin\theta}(b_{los} M_{\perp los}(t) + b_{\perp los} M_{los}(t)) \tag{4.73}$$

It is easy to show that:

$$\begin{aligned} b_{los} M_{\perp los}(t) + b_{\perp los} M_{los}(t) &= bM(t)\sin(\theta_{blos} + \theta_{Mlos}) \\ &\leq bM(t) \end{aligned} \tag{4.74}$$

where the angles are measured from the line-of-sight direction. Therefore, the effective differential phase error along the aperture is:

$$\Delta\Phi(t) \approx \frac{2\pi h b M(t)}{\lambda R^2 \sin\theta} \tag{4.75}$$

When linear and quadratic motions are analyzed for differential shifts and phase errors, the results are negligible for realistic aircraft motions and rugged terrain. This is presented in Appendix H. Therefore, the differential phase errors along the aperture caused by the unknown terrain coupled with translational motion pose no problem. It should be noted that the effects, such as defocussing, observed for the single channel case will still apply to both channels in the InSAR case. Therefore, the predominant effect from translational motion is the azimuth shift and defocussing that occurs essentially identically in both channels.

4.4.4 FM Rate Induced Differential Phase Errors

An analysis of the effect of motion compensation induced FM rate errors for a single channel was made in the previous chapter. A quadratic phase error was observed along the aperture that was proportional to the constant offset displacement between the antenna position and the position used to generate the matched filter (Equation 3.28). In the interferometric case,

the displacement to the track used to generate the matched filters may be different between channels. This leads to a different quadratic phase error in each channel. This differential phase error along the aperture is:

$$\Delta\Phi(t) \approx \frac{2\pi v^2 t^2 \Delta R_{ab}}{\lambda R^2} \tag{4.76}$$

where ΔR_{ab} is the difference in the displacements to the track(s) used to generate the filters or equivalently the inter-channel difference in the slant range matched filter errors. Using the results from [27] it is known that the differential phase bias error is about 1/3 of the magnitude of the differential quadratic phase error at the edge of the processed aperture. Therefore, one can estimate the differential phase error at the peak:

$$\Delta\Phi_{bias} \approx \frac{1}{3}\frac{2\pi v^2 \left(\frac{T}{2}\right)^2 \Delta R_{ab}}{\lambda R^2} \tag{4.77}$$

If processing to the 3 dB azimuth beamwidth is performed,

$$T = T_{3dB} = \frac{\lambda R}{Dv} \tag{4.78}$$

and using the sensitivity in height estimate to differential phase errors result from Equation 4.24, one can obtain the bias in the height estimate:

$$\Delta h_{bias} \approx -\frac{\lambda^2 R \Delta R_{ab} \sin\theta}{12 b D^2 \sin\left(\theta + \alpha_{ab}\right)} \tag{4.79}$$

This expression can be used to limit the difference in the displacements for matched filter generation. If typical CCRS parameters are used (Table 1), and a 1 m height bias error is allowed, one finds that the difference in the displacements must be:

$$\Delta R_{ab} < 1.3 \ \ m \tag{4.80}$$

This gives a good indication of how often each matched filter must be updated in order to keep the difference in the quadratic phase errors between channels very small. Clearly, the matched filters must be updated for every azimuth line across the range swath.

In addition to this, the inter-channel resampling that is performed prior to motion compensation will result in data along azimuth that requires different matched filters. If block azimuth processing is performed then the length of the block is limited by the amount of flight motion along the block. Errors in the matched filter along azimuth that are different between channels will result in differential phase biases according to the above expressions.

4.4.5 RCMC Induced Differential Phase Errors

In the previous chapter the effect of motion compensation induced errors when RCMC was performed for a single channel was described. It was observed that a quadratic phase error along the aperture exists that is proportional to the constant offset displacement between the antenna position and the reference track (Equation 3.37). In the interferometric case, the displacement to the track used to apply the phase correction can be different between channels. This leads to a different quadratic phase error in each channel. The resulting differential phase error along the aperture is:

$$\Delta\Phi(t) \approx \frac{2\pi v^2 t^2}{\lambda R^2 \tan\theta} \frac{\Delta d_{\perp los}}{2} \tag{4.81}$$

where $\Delta d_{\perp los}$ is the difference in the displacements from the reference track(s). The relative displacement is divided by two because of the one-way path difference between the two channels (channel B is receive-only). Using the results from [27] it is known that the differential phase bias error is about 1/3 of the magnitude of the quadratic phase error at the edge of the processed aperture. Therefore, one can estimate the differential phase error resulting from the difference in the displacements to the track(s):

$$\Delta\Phi_{bias} \approx \frac{2\pi v^2 T^2}{12\lambda R^2 \tan\theta} \frac{\Delta d_{\perp los}}{2} \tag{4.82}$$

If processing is to the 3 dB azimuth beamwidth and using Equation 4.24 one can obtain the corresponding height estimate bias:

$$\Delta h_{bias} \approx -\frac{\lambda^2 R \cos\theta \, \Delta d_{\perp los}}{24 b D^2 \sin(\theta + \alpha_{ab})} \tag{4.83}$$

This expression can be used to limit the difference in the displacements from the reference track when RCMC is performed. If typical CCRS parameters are used (Table 1), and a 1 m height bias is allowed, one finds that the difference in the displacements must be less than:

$$\Delta d_{\perp los} < 3.5 \ m \tag{4.84}$$

For the single reference track case the difference in the displacements to the reference track are on the order of the baseline length. It would appear that this RCMC induced error may be significant for the single reference track case.

In the dual reference track approach the displacements from the reference tracks will be very similar in the two cases, greatly reducing the sensitivity to the RCMC errors. Referring to Figure 12 the effective difference in the displacements between the two channels can be estimated from the difference in the applied phase correction:

$$\phi_A - \phi_B = -\frac{2\pi}{\lambda}\frac{\Delta d}{2} = -\frac{2\pi}{\lambda}((R_{tao} - R_{tbo}) + (R_{bo} - R_{ao})) \tag{4.85}$$

Expanding the slant range values in binomial series yields:

$$\frac{\Delta d}{2} \approx b\cos\left(\theta_{ao}(t) + \alpha_{ab}(t)\right) - b_{RT}\cos\left(\theta'_{ao} + \alpha_{RT}\right) \tag{4.86}$$

The antenna baseline is naturally chosen to be the same as the reference track baseline, thus:

$$\begin{aligned}\frac{\Delta d}{2} \approx 2b\sin\frac{1}{2}\Big(&\alpha_{RT} + \alpha_{ab}(t) + \theta'_{ao} + \theta_{ao}(t)\Big) \\ &\sin\frac{1}{2}\Big(-\alpha_{RT} + \alpha_{ab}(t) - \theta'_{ao} + \theta_{ao}(t)\Big)\end{aligned} \tag{4.87}$$

Defining:

$$\Delta\alpha_{ab}(t) = \alpha_{ab}(t) - \alpha_{RT} \tag{4.88}$$

and approximating:

$$\theta_{ao}(t) - \theta'_{ao} \approx \frac{d_{\perp los}(t)}{R} \tag{4.89}$$

which gives:

$$\frac{\Delta d}{2} \approx b_{\perp los}\left(\Delta\alpha_{ab}(t) + \frac{d_{\perp los}}{R}\right) \tag{4.90}$$

For typical offsets from the reference track and roll of several degrees this effective difference in the displacement from the tracks is negligible. It is clear that if RCMC is to be performed, the dual reference track approach should be used.

4.4.6 Effects of No Motion Compensation Resampling

The idea of neglecting to resample during motion compensation for the single channel case was introduced in the previous chapter. It is now important to extend this to consider what differential phase errors might occur. More specifically, there may be a slight difference in the effect on the PSF for each channel that decreases the correlation. If this difference can be characterized as a differential residual range migration then one can use the results from [27] to evaluate the correlation coefficient. Appendix I considers the difference in the range migration errors between channels due to neglecting to resample the data during motion compensation. The resulting differential migration error along the aperture is:

$$\Delta R(t) \approx \frac{b_{\perp los} M_{\perp los}(t)}{R} \tag{4.91}$$

where $M_{\perp los}(t)$ is the linear deviation over the aperture from the center of aperture position.

For a linear flight variation leading to uncompensated differential linear range migration, the inter-channel correlation coefficient can be shown to be [27]:

$$|\gamma| = \frac{2}{\pi\beta}\int_0^{\frac{\pi\beta}{2}} \frac{\sin\alpha}{\alpha} d\alpha = \frac{Si\left(\frac{\pi\beta}{2}\right)}{\frac{\pi\beta}{2}} \tag{4.92}$$

where β is the range walk at the band edge in fractions of a range resolution cell. For typical CCRS parameters, the effect on the correlation resulting from numerical integration is negligible ($\gamma > 0.99$).

For quadratic flight motion leading to uncompensated differential quadratic range migration, the correlation coefficient can be shown to be [27]:

$$|\gamma| = \frac{1}{\sqrt{\epsilon}} \int_0^{\sqrt{\epsilon}} sinc(\alpha^2) d\alpha \tag{4.93}$$

where ϵ is the uncompensated quadratic migration at the band edge. Again, for typical CCRS parameters the effect on the correlation resulting from numerical integration is negligible ($\gamma > 0.99$).

4.4.7 Effects of Inertial Data Errors

Inertial data errors can have a significant impact on the accuracy of InSAR. Errors in the baseline length or angle translate directly to height estimation errors. In the single channel case it was shown that errors in the assumed position of the antenna led to phase correction errors during motion compensation. In the clutter data case the compression operation does not smooth the phase noise like it does in the point target case. The compressed impulse response will be broadened and have phase errors. In the InSAR case, the effect of INS errors on the height estimate can be calculated by differential analysis. The differential analysis for the general case of errors in baseline length and angle has been performed [10]. This work also applies for the conventional dual track approach with INS errors.

The single reference track approach and new dual track method result in the same sensitivities to baseline length and angle as previously reported [10]:

$$\frac{\partial h}{\partial b} \approx \frac{R \sin\theta}{b \tan(\theta + \alpha_{ab})} \tag{4.94}$$

and

$$\frac{\partial h}{\partial \alpha_{ab}} \approx R \sin\theta \tag{4.95}$$

It is therefore straightforward to calculate the effect of INS bias errors on the height estimates. The bias errors will have a small impact at the motion compensation stage, but, can cause significant errors in the estimated elevation through the above equations.

High frequency INS errors will translate into high frequency differential phase errors. The effect on the height estimate can be estimated from Equation 4.24. In addition, there will be defocussing that will increase smoothly with increased phase noise. Provided the statistics of the INS errors are about the same in both channels then the broadening will be about the same. Differential broadening will lead to an increased height estimate variance through Equation 4.8.

Given that all three methods, conventional double, new double, and single, all have the same sensitivity to INS errors there is no preferred approach to handle these errors. In all cases, differential phase smoothing will help reduce the effect of high frequency INS errors. Bias errors are much more difficult to deal with. In most cases control points will be necessary in order to obtain height estimates on the order of one meter accuracy.

4.4.8 Summary of Errors and Constraints for InSAR

In ideal motion compensation all the required geometric parameters are known and there is no restrictions placed on the processing. This leads to accurate compensation except that the range varying phase correction induces a range spectral shift. This can be minimized by keeping the reference track close to the antenna position by segmenting the track. Ideal compensation is not possible in the InSAR case because the terrain elevation is not known.

In realistic InSAR processing situations non-ideal motion compensation must be used. The following tables summarize the resulting errors and limitations given the assumptions made at the beginning of the chapter.

- The range varying phase correction causes a range spectral shift as in the single channel case. Subsequent processing, such as inter-channel registration, can lead to decorrelation if baseband data is assumed.
- The coupling between the RCMC and the range varying phase correction, which can be different between channels, can lead to differential phase biases.

- Differences in the errors in the FM rates between channels can lead to differential phase biases.
- The effect of unknown terrain that is common to both channels is the azimuth peak shift and azimuth defocussing seen in the single channel case.
- The differential effects of the unknown terrain can lead to differential phase biases when angular acceleration occurs.
- Most other effects will be almost identical in both channels and thus cancel out.
- Errors in the inertial data can lead to differential phase errors and biases in the height estimates. The high frequency INS data errors can be reduced by filtering the interferogram but INS bias errors will remain.

Table 6 outlines the main differences or similarities between the single and dual reference track approaches. It is clear that each approach has certain advantages and disadvantages.

The issues compared are:

- Whether the differential phase is continuous if the reference track(s) are segmented.
- Whether there are differential range spectral shifts caused by the range varying phase correction (RVPC). The effect of this will depend upon subsequent processing.
- Whether there are biases caused by the coupling effect of RCMC and the range varying phase correction (RVPC).
- Whether biases due to slowly varying aircraft drifts coupled with unknown terrain can be compensated for.
- Whether there is a range dependent fringe in the interferogram phase even for flat terrain at the reference level.

Table 4 InSAR Motion Compensation Errors and Limitations #1

Physical Effect	Error or Limitation
Displacement Offset (range varying phase correction)	Range Oversampling Factor O_r: $$1 + \frac{2c\lvert d_{\perp los}\rvert}{\lambda R \tan\theta B W_r} < O_r$$
RCMC Induced Bias Errors (range varying phase correction)	Differential Phase Error Along Aperture: $$\Delta\Phi(t) \approx \frac{2\pi v^2 t^2}{\lambda R^2 \tan\theta}\frac{\Delta d_{\perp los}}{2}$$ Differential Phase Bias Error: $$\Delta\Phi_{bias} \approx \frac{\pi v^2 T^2 \Delta d_{\perp los}}{12\lambda R^2 \tan\theta}$$ Height Estimate Bias (processing to 3 dB): $$\Delta h_{bias} \approx -\frac{\lambda^2 R\cos\theta \Delta d_{\perp los}}{24 b D^2 \sin(\theta + \alpha_{ab})}$$
FM Rate Induced Bias Errors	Differential Phase Error Along Aperture: $$\Delta\Phi(t) \approx \frac{2\pi v^2 t^2 \Delta R_{ab}}{\lambda R^2}$$ Differential Phase Bias Error: $$\Delta\Phi_{bias} \approx \frac{\pi v^2 T^2 \Delta R_{ab}}{6\lambda R^2}$$ Height Estimate Bias (processing to 3 dB): $$\Delta h_{bias} \approx -\frac{\lambda^2 R \Delta R_{ab}\sin\theta}{12 b D^2 \sin(\theta + \alpha_{ab})}$$

Table 5 InSAR Motion Compensation Errors and Limitations #2

Effect of Unknown Terrain	Error or Limitation
Effects Common to Both Channels	Phase Error Along Aperture: $$\Delta\phi_{err}(t) \approx \frac{4\pi h d_{\perp los}(t)}{\lambda R \sin\theta}$$ Azimuth Peak Shift: $$\Delta P \approx -\frac{h}{v^2 \sin\theta}\frac{\partial d_{\perp los}}{\partial t} \ (sec)$$ 5% Defocussing: $$a_{\perp los} < \frac{\lambda R \sin\theta}{hT^2}$$ Processing to 3 dB: $$a_{\perp los} < \frac{\lambda \sin\theta D^2 v^2}{h\lambda^2 R}$$
Differential Effects	Differential Phase Error Along Aperture: $$\Delta\Phi(t) \approx \frac{2\pi h b_{\perp los}(t)}{\lambda R \sin\theta}$$ Differential Phase Bias due to Angular Acceleration: $$\Delta\Phi_{bias} \approx \frac{a_{roll}\pi b_{los} T^2}{12\lambda R \sin\theta}$$ Height Estimate Bias due to Angular Acceleration (processing to 3 dB): $$\frac{\Delta h_{bias}}{h} \approx -\frac{\lambda^2 R^2 b_{los} a_{roll}}{24 b v^2 D^2 \sin(\theta + \alpha_{ab})}$$

Table 6 Comparison of Single and Dual Reference Track Motion Compensation

Properties		Single	Dual
1	Continuity of Differential Phase with Segmented Reference Track(s)	Yes	No
2	Equal Range Spectral Shifts between channels due to RVPC	No	Yes
3	Insensitive to Bias Errors caused by RCMC and RVPC	No	Yes
4	Compensation for Unknown Terrain coupled with low freq. motion	Yes	Yes
5	Removal of flat earth fringes	Yes	No

4.5 Proposed Motion Compensation Approaches

Given the analysis of the interferometric motion compensation problem presented above, it is now possible to define recommended approaches. This section will begin with a review of the system requirements followed by a discussion of the possible processing approaches. A new approach will be proposed which combines the benefits of the dual and single reference track methods.

4.5.1 Realization of Requirements

A general purpose InSAR system will require the following in order to generate topographic maps accurately and efficiently:

1. Differential phase fidelity. This means that all bias errors are minimized and random errors are reduced by spatial filtering. Optimum smoothing is obtained when the samples are uncorrelated. This may require full resolution azimuth processing making RCMC necessary.
2. Capable of mapping rugged terrain (+/- 1 *km*) under typical flight conditions. This will likely require segmentation of the reference tracks to follow the flight motion.
3. Continuous differential phase over the entire image scene is desirable. This means that only one tie point is required to unwrap the phase of the entire image.

The ability to meet the above requirements can be evaluated by considering the summary of errors and limitations of motion compensation in the previous section. A quantitative analysis can be carried out for a specific InSAR system. But, a qualitative approach can be formulated for the general case.

Typical CCRS System Approach

For the typical InSAR scenario for the CCRS system a fairly simple approach to motion compensation is adequate. This would include:

1. No motion compensation resampling.
2. Phase correction to a single reference track that may be segmented, if necessary.
3. No RCMC.
4. Azimuth matched filters determined separately for each channel based on the reference level positions.
5. Phase unwrapping that assumes continuous differential phase (as far a motion compensation is concerned)
6. Differential phase to elevation conversion based on the new formulation (Section 4.4.1).

Apart from the possible defocussing problems for severe terrain and translational acceleration this approach should yield a motion compensation approach which contributes on the order of a meter to the height estimate error budget.

Most Accurate Approach

The most accurate approach would be to implement the following:

1. Perform motion compensation resampling.
2. Phase correction to dual reference track that may be segmented if necessary.
3. Perform RCMC.

4. Azimuth matched filters determined separately for each channel based on the reference level positions.
5. Phase unwrapping that assumes discontinuous differential phase (as far as motion compensation is concerned).
6. Differential phase to elevation conversion based on the new dual track formulation (Section 4.4.2).

The main problem with this approach is the discontinuous differential phase as a result of segmentation of the reference tracks. A modification to this approach will now be presented that combines the benefits of the single and dual reference track approaches.

4.5.2 Combination of Single and Dual Reference Tracks

A new approach to InSAR motion compensation will now be proposed which is a simple, yet effective, extension to the dual reference track approach. It is clear that performing dual reference track motion compensation is preferred for the compression operation, but, it is desirable to have the single reference track differential phase for phase smoothing and phase unwrapping. The proposal is to convert back to the single reference track form after dual track motion compensation, optional RCMC, and azimuth compression have been performed.

This conversion can be accomplished by a post-compression phase correction that converts the channel B reference track to the channel A reference track. Given that the reference track positions are parallel over the segment, and the position of each range cell on the ground is fixed if motion compensation resampling is performed, this means simply adding a range depending phase constant to each azimuth matched filter. The resulting differential phase of this two step approach is equivalent to performing motion compensation in one step to a single track. In other words, the differential phase will be zero if each step is performed properly. Again, because of the unknown terrain, errors will arise and the differential phase will be

given by these errors. The combined errors from each step are in fact the same as if one step of single track compensation were performed, except that the RCMC induced phase bias (characteristic of single track motion compensation) will not be present (Equation 4.83). This will now be described in detail.

From Equation G.9 of Appendix G and Figure 12, the differential phase error resulting from the unknown terrain after dual track motion compensation, optional RCMC, and azimuth compression is:

$$E_d(A) - E_d(B) = -\frac{2\pi}{\lambda}(R_{tao} - R_{tah} - R_{tbo} + R_{bo} + R_{tbh} - R_{bh}) \tag{4.109}$$

The next step is to apply a phase correction which makes the channel B reference track data appear as though it were at the channel A reference track. The applied phase correction to channel B is:

$$\phi_B(applied) = -\frac{2\pi}{\lambda}(R_{tao} - R_{tbo}) \tag{4.110}$$

Notice that this is constant along the aperture if motion compensation resampling is performed and can therefore be applied as a range varying constant phase term for each azimuth matched filter. Otherwise, it must be applied pixel by pixel on the compressed image or to the interferogram. Due to the unknown terrain the ideal correction should have been:

$$\phi_B(ideal) = -\frac{2\pi}{\lambda}(R_{tah} - R_{tbh}) \tag{4.111}$$

Therefore, there is a differential phase error from this operation which is:

$$E_s(B) = -\frac{2\pi}{\lambda}(R_{tao} - R_{tbo} + R_{tbh} - R_{tah}) \tag{4.112}$$

The resulting differential phase after the two operations will be zero if all corrections were ideal. Therefore, the differential phase is equal to the residual errors:

$$\Phi = E_d(A) - E_d(B) - E_s(B) \tag{4.113}$$

which results in:

$$\Phi = -\frac{2\pi}{\lambda}(R_{bo} - R_{bh}) \tag{4.114}$$

which is precisely the same result as if one step single track compensation had been applied (Equation 4.15), except without the RCMC induced errors.

Most Accurate and Most Convenient Approach

The resulting most accurate and convenient approach would therefore be to implement the following:

1. Perform motion compensation resampling.
2. Phase correction to dual reference tracks that may be segmented if necessary.
3. Perform RCMC.
4. Azimuth matched filters determined separately for each channel based on the reference level positions. Apply the extra phase constant term to each matched filter for Channel B (Equation 4.110).
5. Phase unwrapping that assumes continuous differential phase.
6. Differential phase to elevation conversion based on the new dual/single track formulation (Equation 4.114).

If motion compensation resampling is not performed the extra phase correction must be applied after azimuth compression on the entire image. The benefits versus the extra computation would have to be weighed. The validity of such approaches to motion compensation will be verified by simulation and processing of real InSAR data in the next chapter.

Chapter 5 Evaluation of Non-Ideal InSAR Motion Compensation

In order to ensure that the modelling and analysis of the previous chapters is correct experiments were performed using a point target simulator as well as processing real InSAR data from the CCRS Convair 580 system [25]. The simulation and real data processing used the zero-Doppler pulse processing and flat earth assumptions of non-ideal InSAR motion compensation. This chapter will begin with a description of the point target simulator and the corresponding results and conclude with results from real InSAR data processing.

5.1 Point Target Simulation

A comprehensive simulation of the InSAR data acquisition and processing mechanism was performed. Dual channel range compressed raw SAR point target data was generated for any desired flight motion and target location. An InSAR processor was then used to process the data into an interferogram and finally into a height estimate for the target. In this section, the simulator will first be described followed by the modelling of typical flight motion. The results obtained using the modelled motions will be described as well as the results from using real motion data from the CCRS Convair 580 aircraft. When the predicted results are compared to the simulation results good agreement is found.

5.1.1 The Point Target Simulator

The point target simulator consists of three parts. First, range compressed point target echo data is generated for any aircraft trajectory, including roll effects, and for any target elevation. Next, both channels of the raw data are processed by the InSAR processor. This consists of motion compensation phase correction, azimuth compression and two-fold oversampling, interferogram creation, phase unwrapping, and differential phase to elevation conversion. The

third component of the simulator is the evaluation routines that monitor the results along the way. This consists of performing point target analysis on the two compressed channels and on the interferogram, as well as analyzing the final height estimate. The simulator was implemented in the MATLAB simulation language. The simulator is based on typical C-band airborne systems, but the specific parameters were taken from the CCRS InSAR system for the Convair 580 aircraft. The simulation algorithm will now be described in more detail.

Simulation Algorithm

The simulation algorithm consists of the following processing steps:

1. Generate range compressed point target data for a particular flight and target position for two channels (one transmit receive, one receive-only) assuming receive-only channel is registered with main channel assuming flat terrain. The registration is implicit in the sampling of the raw data. The data is 2048 samples in azimuth and 21 samples in range (variable).
2. Apply phase correction to each channel assuming flat terrain and using either one or two reference tracks. No motion compensation resampling is performed.
3. Perform azimuth Fourier Transform.
4. Optionally, perform RCMC in the frequency domain by baseband interpolation for each channel. An 8 point FIR kernel is used and interpolation is made to 1/16 of a sample.
5. Performed azimuth compression using a matched filter for each channel. The slant range used to generate the matched filter is correct at the zero Doppler pulse. Terms up to fourth order in time are used.
6. Perform azimuth Inverse Fourier Transform including two-fold zero padding to prepare for interferogram creation. This is required as interferogram generation doubles the bandwidth.

7. Interpolate by a factor of 16 and analyze the compressed peak characteristics in each channel.
8. Generate the interferogram using the original (not interpolated) compressed data from each channel.
9. Interpolate by a factor of 16 and analyze the compressed peak characteristics in the interferogram.
10. Unwrap the differential phase using the terrain elevation knowledge.
11. Convert the differential phase into a height estimate.

5.1.2 Modelling of Typical Aircraft Motions

In order to use the simulator, aircraft flight motions are required. Antenna displacement data obtained from CCRS for the Convair 580 was used to come up with classes of motions that could be compared with the predicted results (Figures 14 and 15). Data from a number of flights was analyzed. From this data the following motions were selected for use in the simulator:

Table 7 Typical Flight Motion for CCRS Convair 580

Motion Type	Peak Flight Motion
Translational Velocity	$0.5\ \frac{m}{s}$
Translational Acceleration	$0.01\ g\ \frac{m}{s^2}$
Baseline Angular Velocity (roll)	$0.2\ \frac{deg}{s}$
Baseline Angular Acceleration (roll)	$0.3\ \frac{deg}{s^2}$
Sinusoidal Baseline Variation (roll)	$0.15\ deg\ peak$
Displacement Offset	$10\ m$

5.1.3 Simulation Results of Modelled Motions

The typical peak flight motion shown in Table 7 were used, one at a time, in the simulator using the parameters of Table 1 (unless otherwise specified). The motions were divided into separate components in the line-of-sight direction and perpendicular to this to allow the theoretical error analysis to be evaluated. Both single and dual reference track

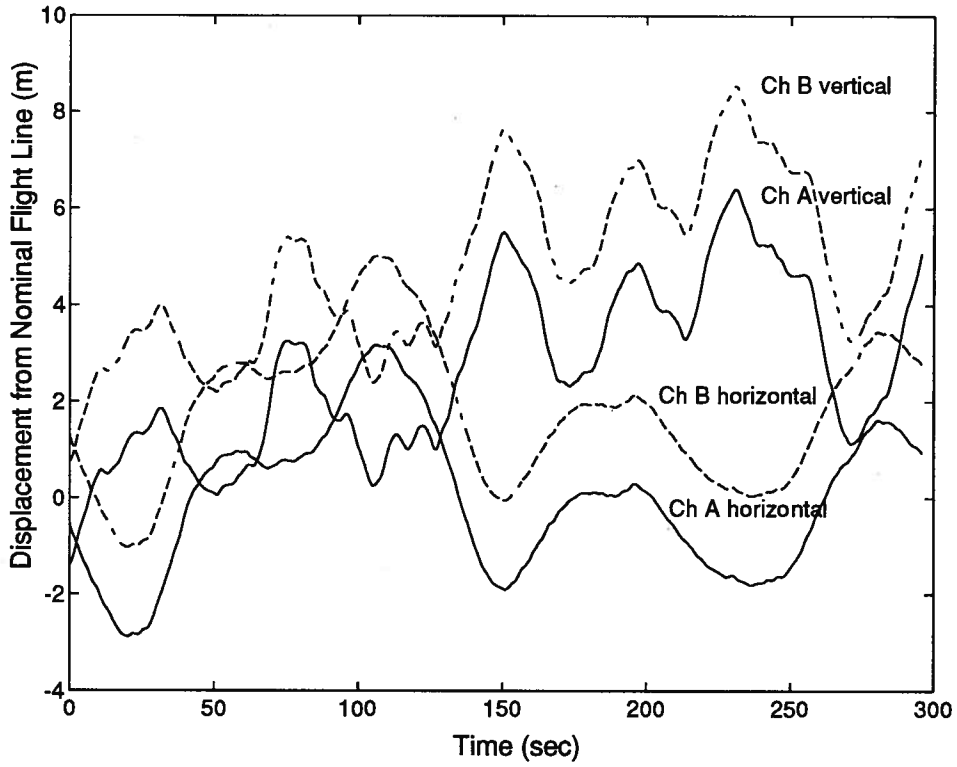

Figure 14 Convair 580 Flight Displacement Data

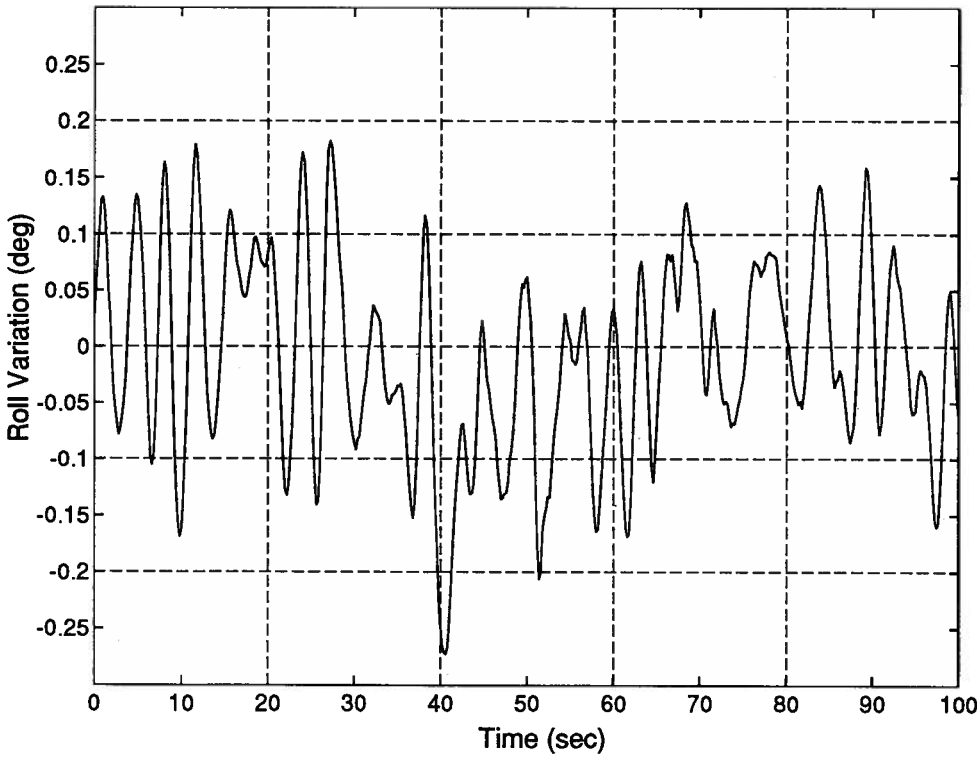

Figure 15 Convair 580 Roll Variation

motion compensation was performed. Apart from the differential phase errors the results were essentially identical between the single and dual track approaches. The dual track results will be presented first, followed by the single track results.

Dual Reference Tracks with RCMC

Table 8 shows the results for the dual reference track approach for target elevations less than or equal to 1000 m from the reference track and for motions that yielded insignificant errors. In addition, there was no measurable inter-channel shifts. This indicates that these flight motions are acceptable for the simulator algorithm (including the assumptions contained there such as the center of aperture assumption, neglecting to resample, and non-ideal motion compensation). The results for targets below the reference track are similar except for the change in the angle to the target which makes the above/below results slightly asymmetric.

Table 8 Dual Reference Track Motion Compensation with RCMC

Flight Motion	h <= 1000 m				
	Δh (m)	Azimuth Broadening (%)	Azimuth Shift (m)	Range Broadening (%)	Inter-channel Broadening (%)
ll with $d <= 10\,m$	< 0.05	< 1	0	< 1	< 1
$\frac{\partial d_{los}}{\partial t} = 0.5\ \frac{m}{s}$	< 0.05	< 1	0	< 1	< 1
$a_{los} = 0.01g$	< 0.05	< 1	0	< 1	< 1
$\frac{\partial \alpha_{ab}}{\partial t} = 0.2\ \frac{deg}{s}$	< 0.05	< 1	0	< 1	< 1

The most significant results are shown in the following figures. Figure 16 shows the resulting azimuth shift from translational velocity perpendicular to the line-of-sight direction. The predicted shift of Equation 3.48 agrees well with the simulation result.

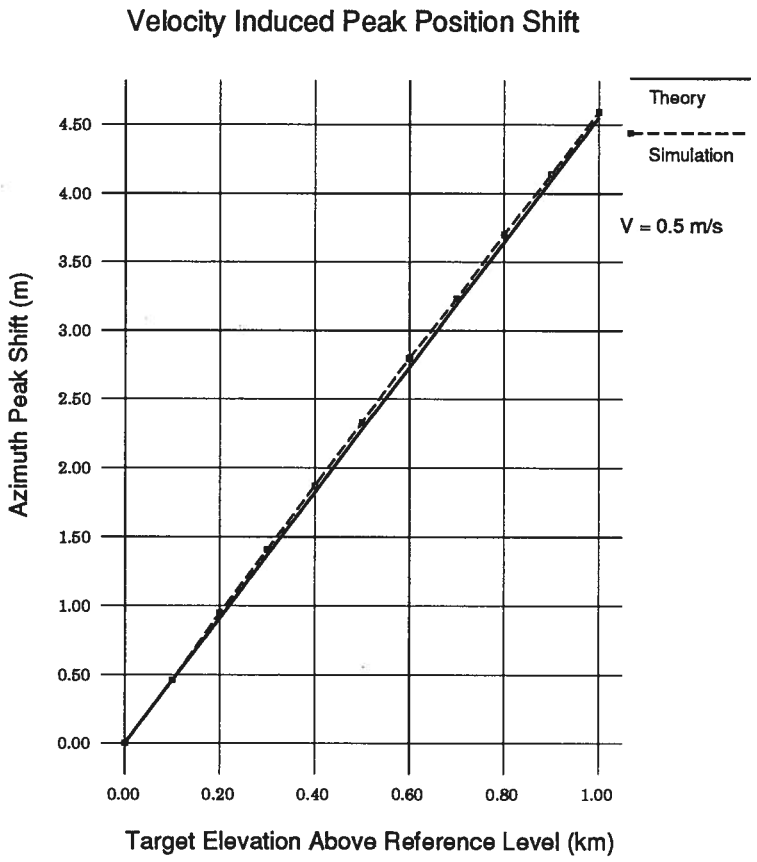

Figure 16 Unknown Terrain with $v_{\perp los} = 0.5\ \frac{m}{s}$, and $R = 10\ km$

Figure 17 shows the resulting azimuth defocussing occurring in both channels for a uniform translation acceleration perpendicular to the line-of-sight of 0.01 g. By using Equation 3.55 there should be about 5 % defocussing for a terrain elevation of 500 m. This agrees quite well with the simulation results.

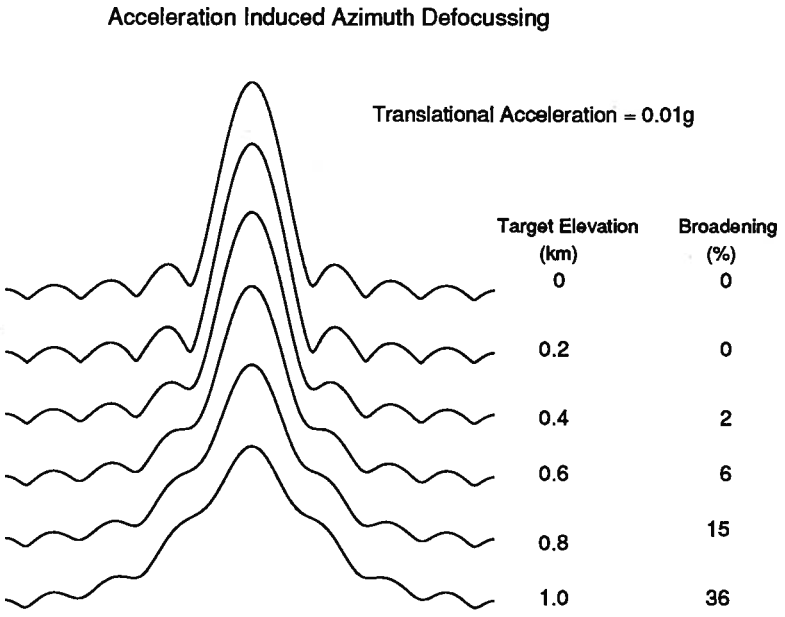

Figure 17 Unknown Terrain with $a_{\perp los} = 0.01g$, and $R = 10\ km$

Table 9 shows the results from an angular acceleration of 0.3 $\frac{deg}{s^2}$ for a range of slant range values. Predicted differential phase errors using Equation 4.52 and height estimate biases using Equation 4.54 were compared with the simulation results (using no antenna beam pattern) yielding good agreement. The larger discrepancy at near range is due to the errors in estimating the effective baseline perpendicular to the line-of-sight as it gets smaller.

Table 9 Effects of Angular Acceleration, $a_{roll} = 0.3\ \frac{deg}{s^2}$, $h = 1\ km$, and no antenna pattern

Slant Range (km)	Processed Aperture (sec)	$\Delta\Phi_{theory}$ (mrad)	$\Delta\Phi_{sim}$ (mrad)	Δh_{theory} (m)	Δh_{sim} (m)
10	3	19	26	-0.5	-0.7
15	3	14	15	-0.7	-0.7
15	4.6	32	34	-1.6	-1.6
20	4.6	30	31	-2.1	-2.1
20	6	53	55	-3.8	-3.7

Figures 18 and 19 show the results from sinusoidal roll of 0.15 *deg peak* and with *period* = 3 *sec*. As was suggested by Equation 4.62, the effect of the phase bias error being about equal and opposite to the change in the expected phase, and the smoothing performed by the compression operation, combined to result in a very smooth measured differential phase. The expected phase followed the roll motion thus leading to a sinusoidally varying height estimation error. This smoothing effect was even more pronounced at far range due to the longer aperture processed. It should be noted that using a smoothed version of the inertial data to convert the differential phase to elevation will not solve this problem. What will happen is that new height errors will occur even for targets at the reference level. At least under the current approach it is only targets that deviate appreciably from the reference level which are affected.

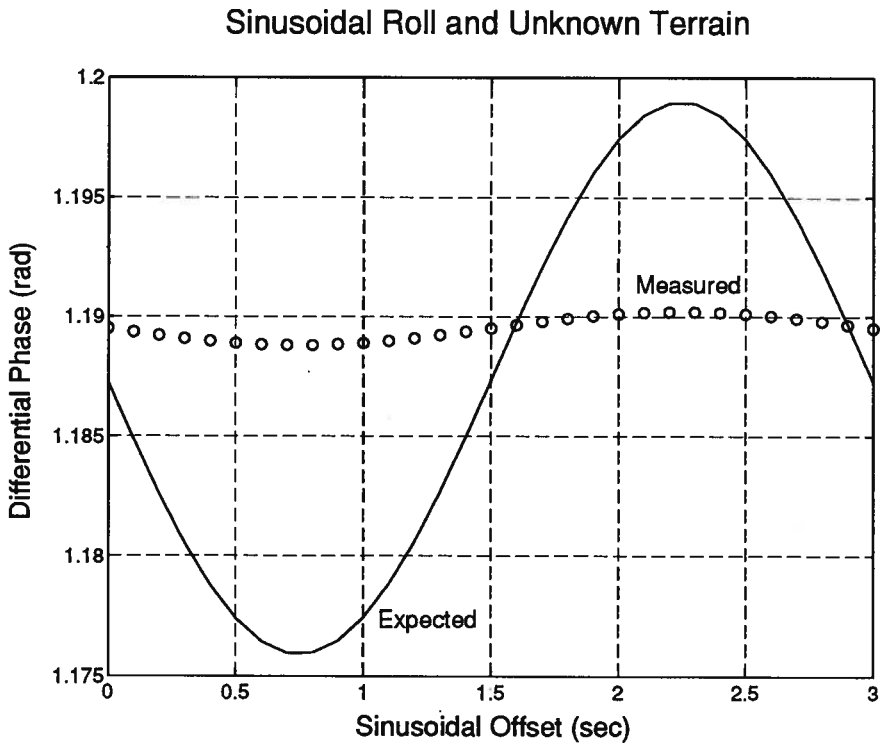

Figure 18 Effect of Sinusoidal Roll on Differential Phase

(0.15 *deg peak*, *period* = 3 *sec*, $h = 1\ km$, $R = 10\ km$)

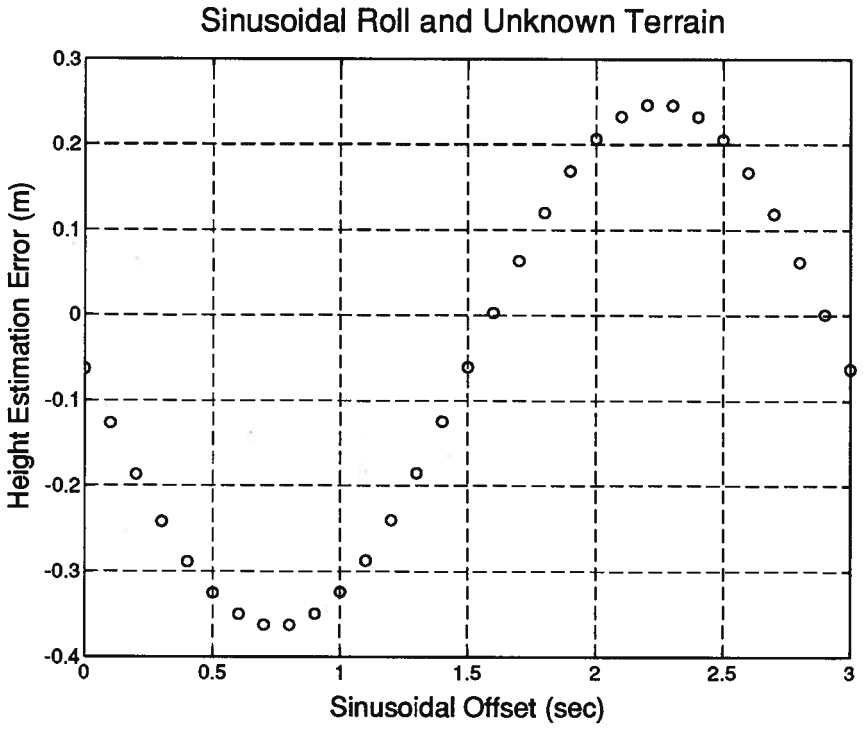

Figure 19 Effect of Sinusoidal Roll on Height Estimate

($0.15\ deg\ peak,\ period = 3\ sec,\ h = 1\ km,\ R = 10\ km$)

Single Reference Track with RCMC

The only difference between the results from the single and dual reference track approaches was that involving an extra differential phase bias in the single reference track case. This was predicted by Equation 4.82 to occur when RCMC was performed. Figure 20 shows how the theory and simulation results agreed very well.

5.1.4 Simulation Results of Actual Motion Data

Actual motion data from Figures 14 and 15 were also used in the simulator. This data corresponds to pass 6 of the Kananaskis flights in February 1992 of the Convair 580. Point target simulation results were obtained along the flight line every 0.2 seconds and dual reference track motion compensation with RCMC and single track without RCMC were performed. This is equivalent to simulating a strip of point targets along azimuth separated by about 25 m. The

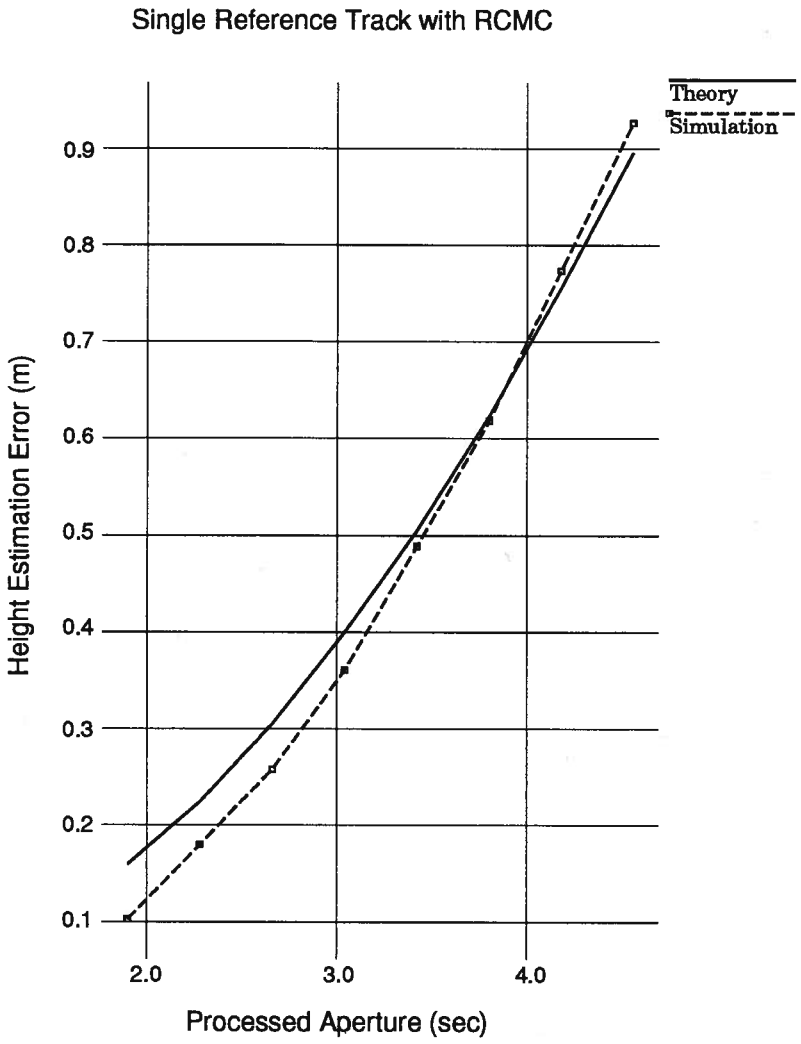

Figure 20 Single Track Bias Errors, $R = 10\ km$, and no antenna pattern

following results indicate the errors that would results from typical Convair 580 flight motion coupled with unknown terrain and precise inertial data measurements.

Dual Reference Tracks with RCMC

The results from dual reference track motion compensation with RCMC and real motion data were similar to those using the modelled motion data. Most effects were almost identical in both channels. The significant results of differential phase errors, height estimation errors, azimuth defocussing, and azimuth shifts will now be described.

Differential Phase Errors The dominant differential phase error was due to the smoothing effect of unknown terrain coupled with aircraft roll (Figure 21). The expected differential phase itself followed the large scale motion of R_{tbo} and R_{tao} with a small scale ripple due to the aircraft roll. The measured differential phase followed the large scale motion but smoothed out some of the ripple. This leads to a ripple in the height estimate.

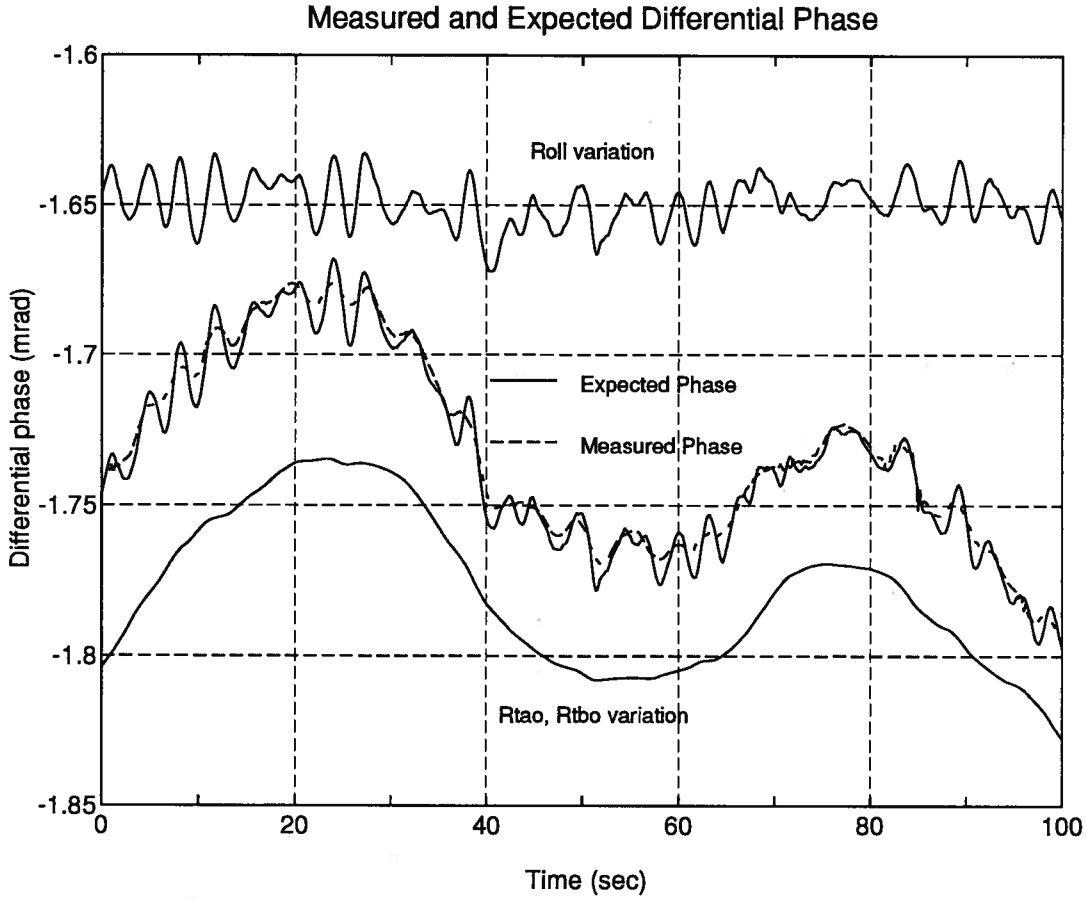

Figure 21 Measured Versus Expected Differential Phase Dual Track ($R = 10\ km$, $h = 1\ km$)

Height Estimation Errors Given that the differential phase errors follow the roll motion, then the resulting height estimation errors will also follow the roll motion. Figure 22 shows the resulting height estimation errors using the new double reference track interpretation of the differential phase.

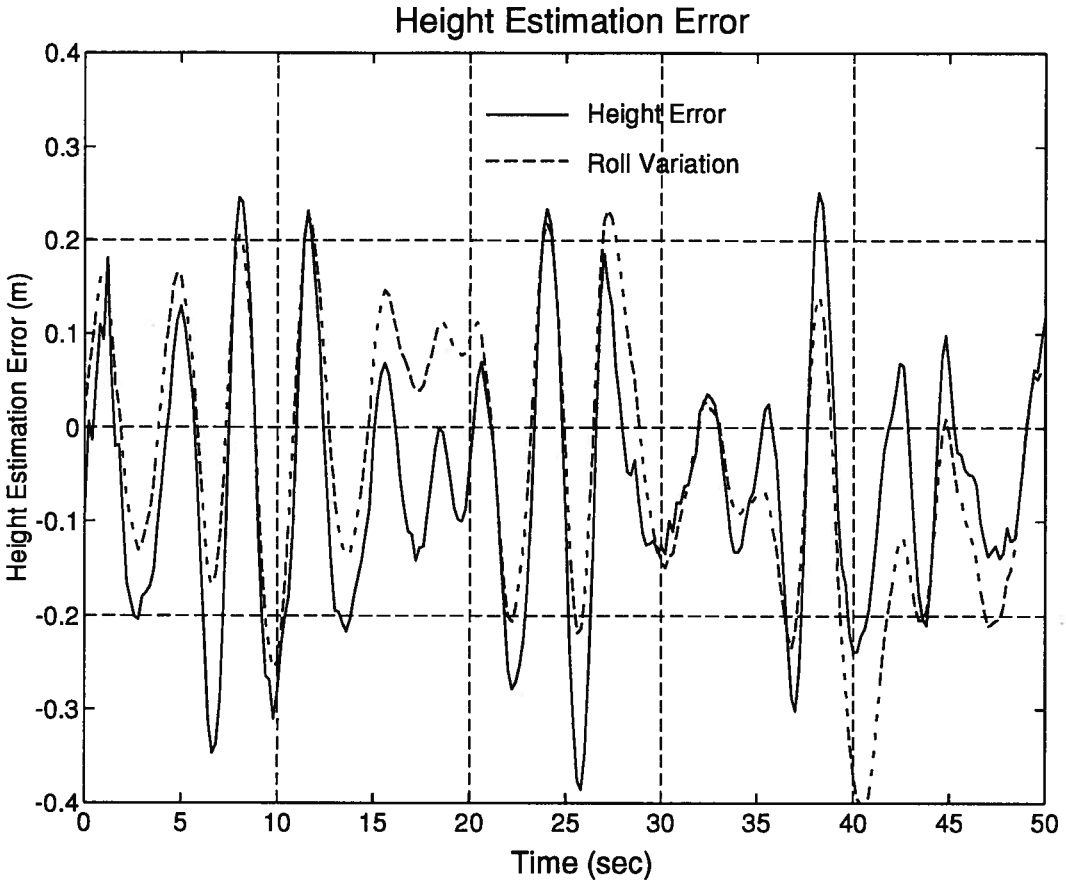

Figure 22 Height Estimation Errors and Roll ($R = 10\ km,\ h = 1\ km$)

Figures 23, 24, and 25 compare the height estimation errors for the conventional (ideal assumed) and new dual reference track approaches for different slant range values. The reference tracks were chosen to minimize the possible biases that can occur in the conventional approach. At near range the errors resulting from the aircraft roll are small in the new approach compared to the residual biases of the conventional approach. At mid and far range the errors are about the same size but the new approach has higher frequency errors due to the roll. An explanation for this was given above for the case of point targets and sinusoidal roll. The impulsive height errors come from regions where extreme defocussing occurred.

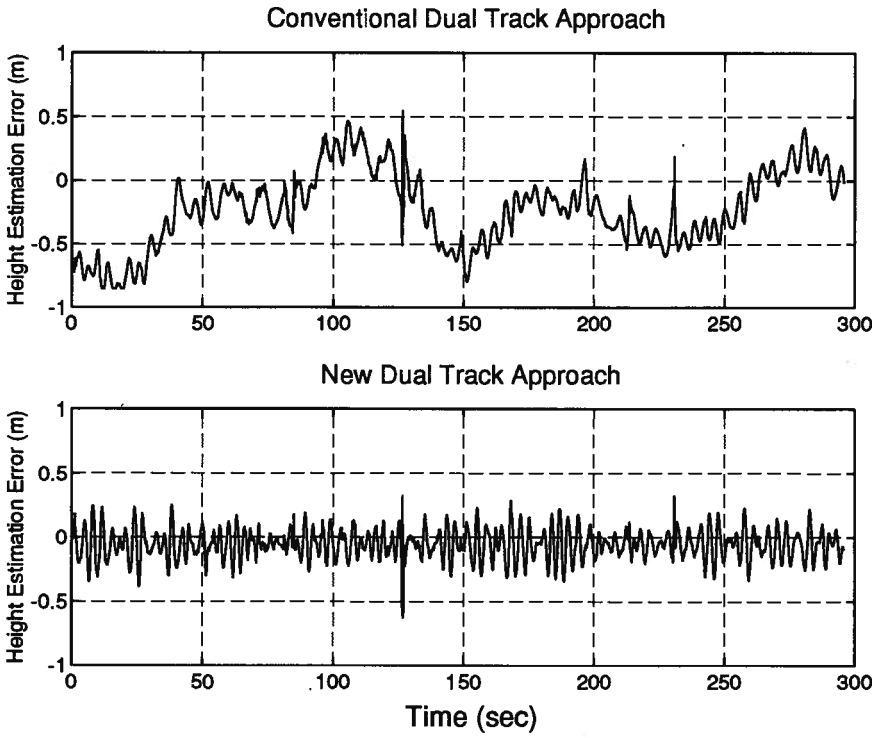

Figure 23 Height Estimation Errors ($R = 10\ km,\ h = 1\ km$)

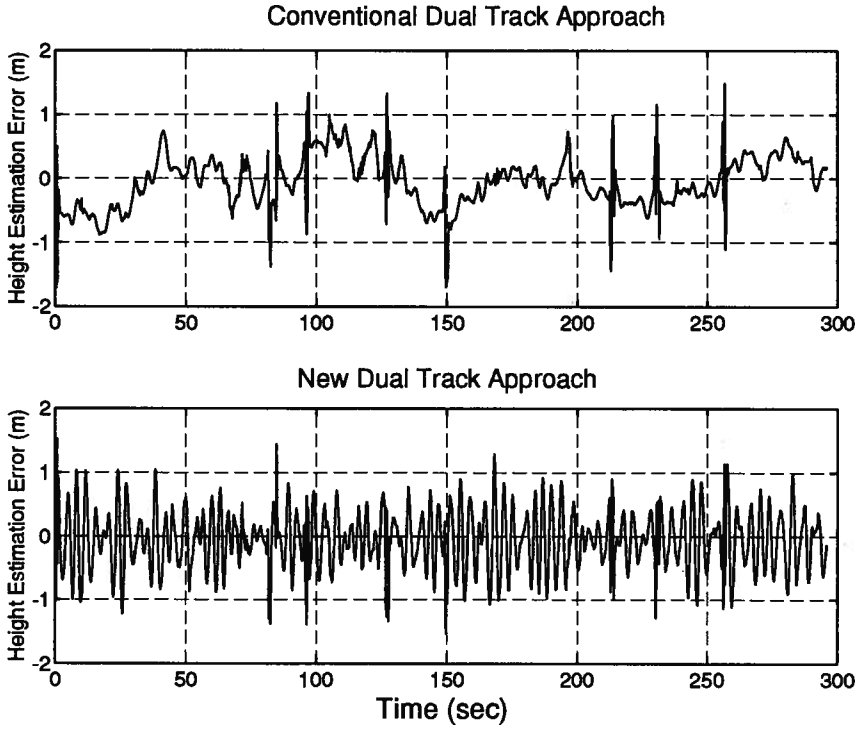

Figure 24 Height Estimation Errors ($R = 15\ km,\ h = 1\ km$)

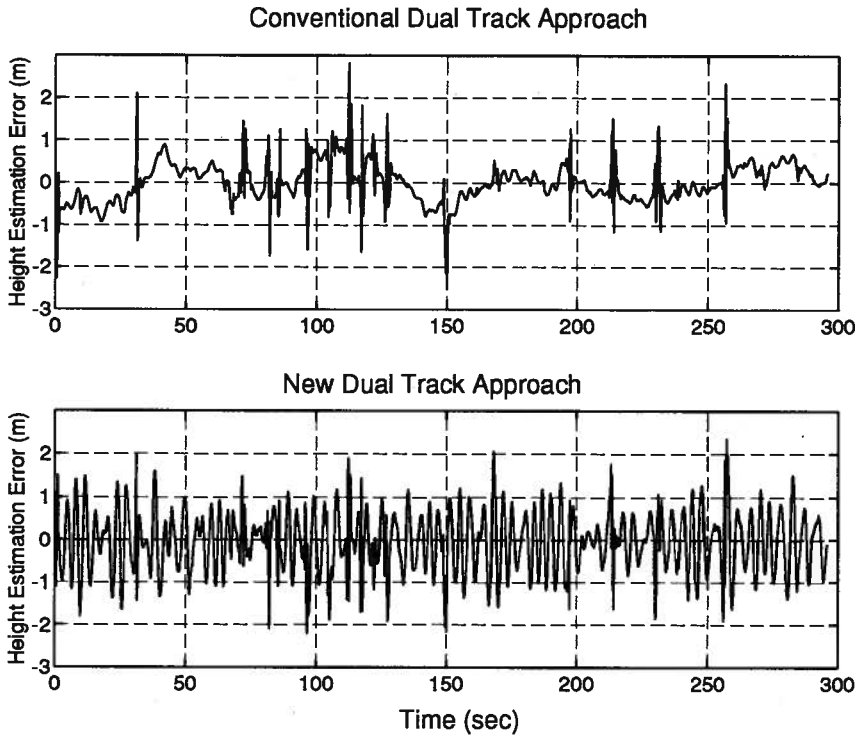

Figure 25 Height Estimation Errors ($R = 20\ km$, $h = 1\ km$)

Azimuth Defocussing The theory predicted that acceleration perpendicular to the line-of-sight would lead to defocussing in both channels. Figure 26 shows the resulting 3 dB width azimuth broadening for a target elevation of $h = 1\ km$ above the reference track. Also plotted is the general variation of the displacement from the reference tracks perpendicular to the line-of-sight direction. The total variation over the processed extent was about 6 m. At a few positions along the flight line significant defocussing occurs. Figure 27 shows the same experiment but with $h = 500\ m$. By halving the target elevation the defocussing is reduced to reasonable levels. In either case, the inter-channel differential defocussing is less than a few percent provided significant defocussing does not occur. When significant defocussing occurs the interpretation of a 3 dB width loses its meaning as the sidelobes have joined the main lobe.

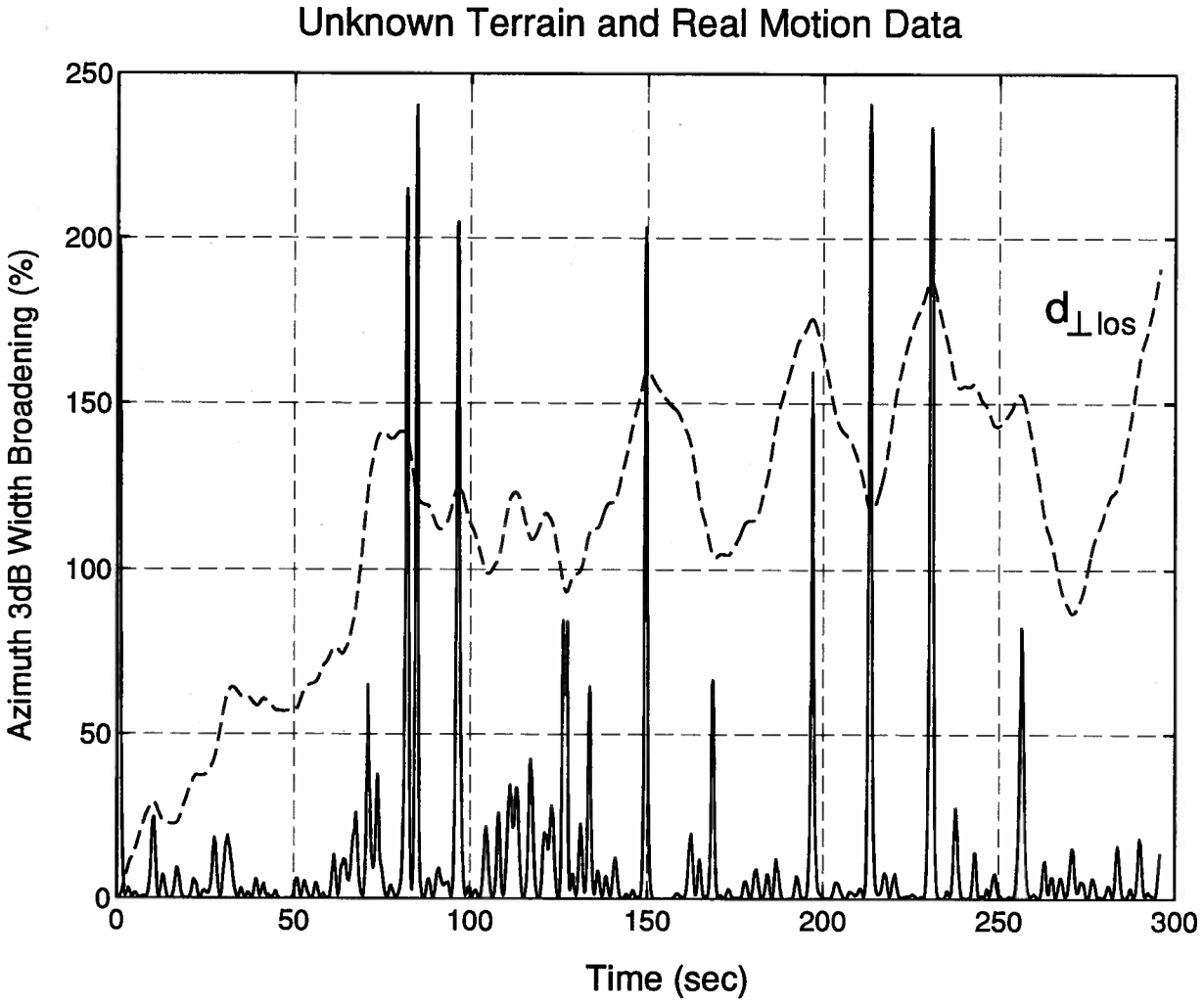

Figure 26 Azimuth Broadening with Unknown Terrain ($R = 10\ km$, $h = 1\ km$)

Azimuth Shift Figure 28 shows the resulting mis-positioning of the peak in azimuth for a target with $h = 1\ km$. The results were the same across the range swath. Using Equation 3.48, and by low pass filtering the motion data with a 1 second long box-car filter to estimate the velocity, the predicted shift was calculated. It is clear that the prediction and measured results agree.

Single Reference Track without RCMC

The above simulations were repeated but with single reference track motion compensation and no RCMC was performed. Most of the results were essentially the same as the dual

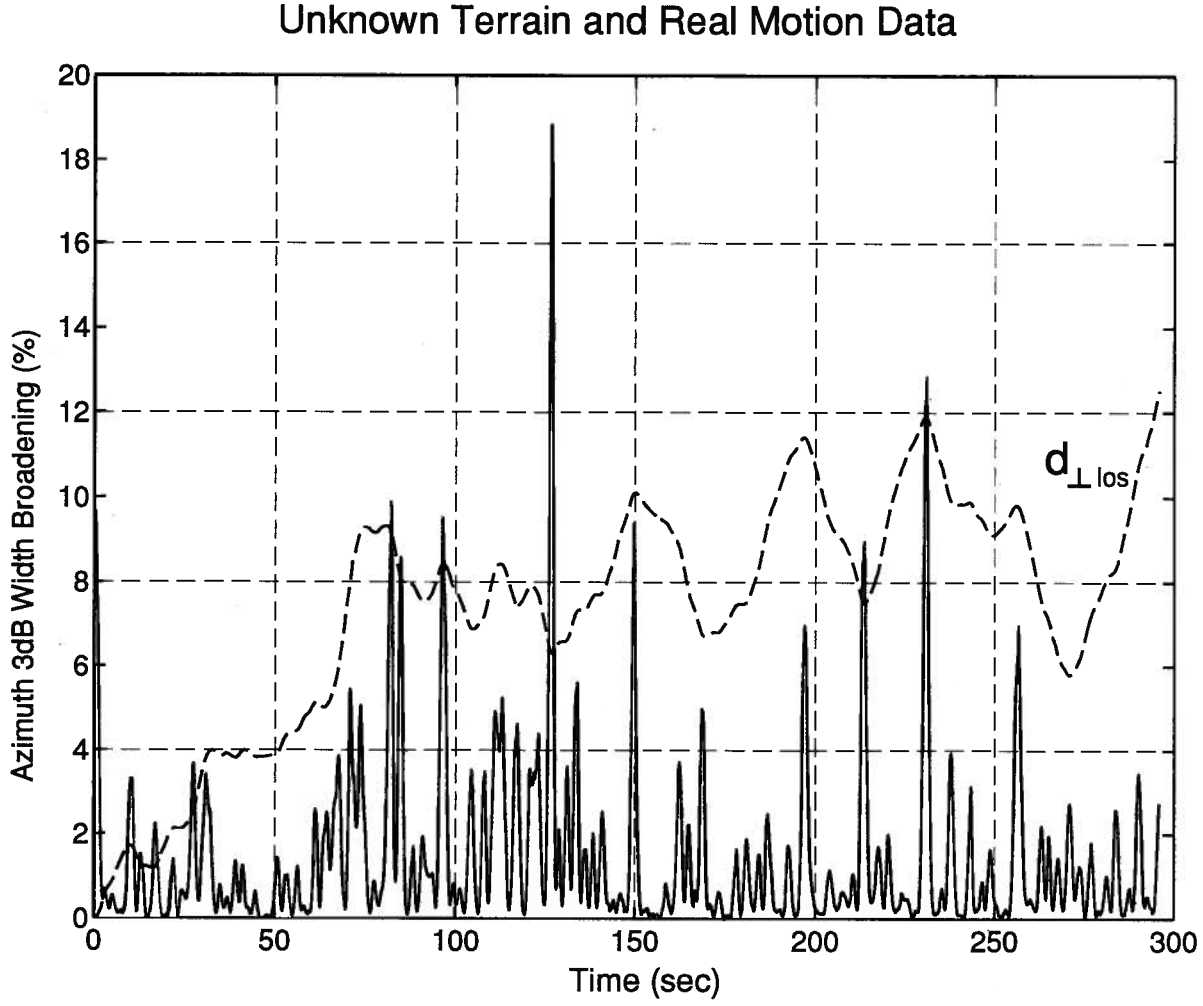

Figure 27 Azimuth Broadening with Unknown Terrain ($R = 10\ km$, $h = 500\ m$)

reference track with RCMC results. The exceptions to this were the resulting differential phase and a small bias error. Figure 29 shows how the expected differential phase follows the roll motion but is otherwise unaffected by the larger drifts. The corresponding height estimation errors are shown in Figure 30. The small bias at the peak is due to a coupling between the range phase ramp in the interferogram PSF, caused by the difference in the range varying phase corrections between channels, and a small migration of the compressed peak across range due to the uncompensated range migration. If the phase at the correct slant range (slant range of peak if RCMC had been performed) is evaluated, no bias is found. This bias does not occur for dual reference track motion compensation without RCMC because there is no range phase

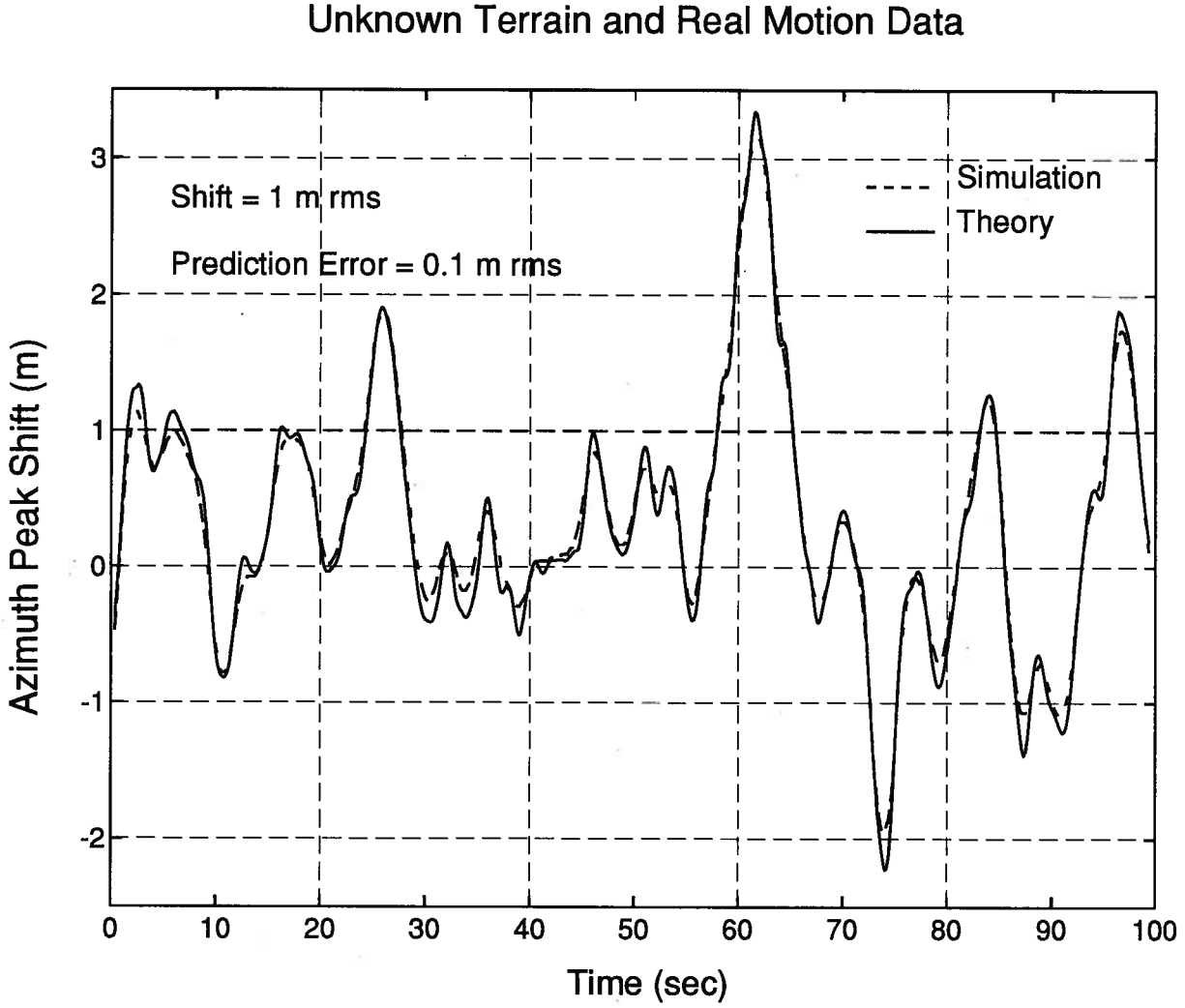

Figure 28 Azimuth Shift with Unknown Terrain ($h = 1\ km$)

ramp in the interferogram. This error can be minimized for the single reference track case by keeping the processed bandwidth small.

The azimuth broadening and azimuth shift are slightly smaller than the dual track with RCMC case due to the shorter effective aperture processed.

Processing with Segmented Tracks

In order to investigate the continuity in the differential phase of the new dual/single track approach the point target simulator was used. The segmented tracks are handled by overlapping the azimuth data sufficiently to ensure a constant reference track for a given compression operation. The point target simulator was run using the real motion data for two cases of

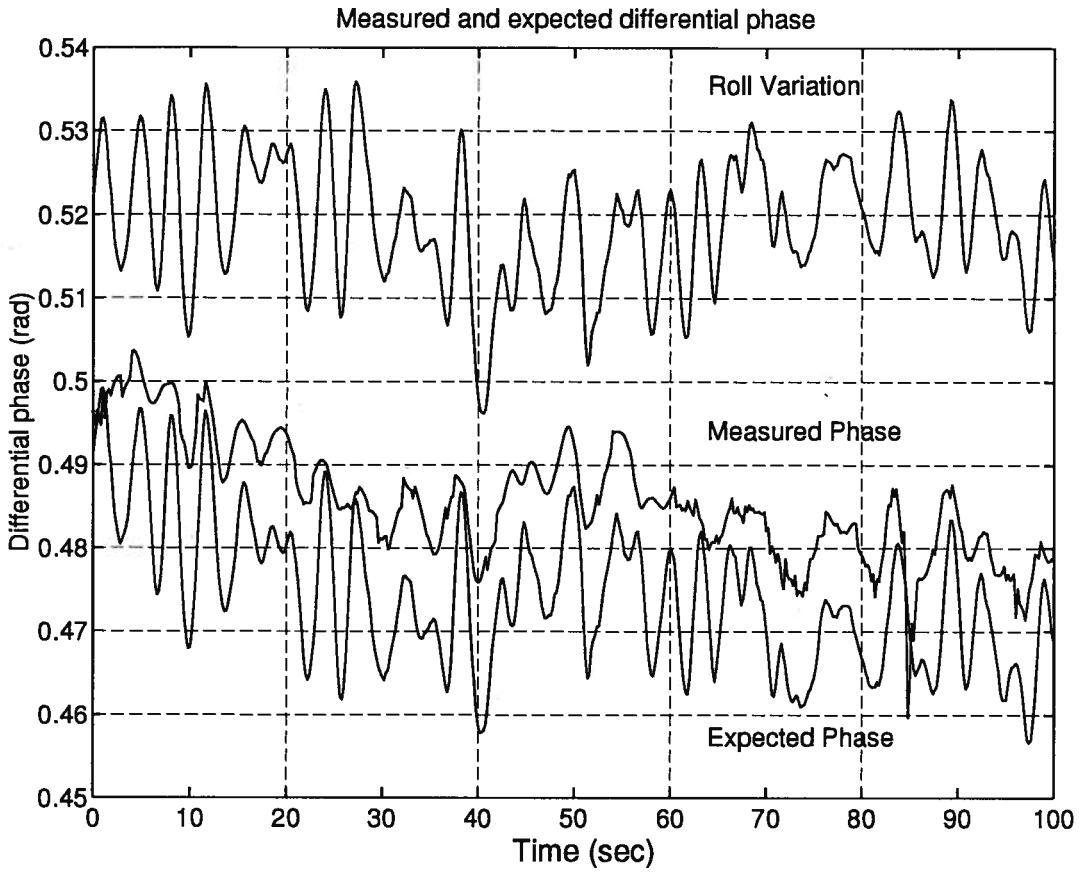

Figure 29 Measured Versus Expected Differential Phase Single Track ($R = 10\ km$, $h = 1\ km$)

reference tracks. The resulting two strips of data were then cut and pasted together at the midway point. This was performed for the dual reference track approach and for the new dual/single track approach where a phase correction is applied after compression to convert from the dual track to the single track formulation. Figure 31 shows the resulting differential phase of the interferogram. It is clear that the dual track approach results in discontinuous differential phase. The new dual/single track approach has continuous differential phase across the boundary. When the height estimates were compared between the two approaches the results were identical, as expected (Figure 32).

5.1.5 Discussion of Point Target Results

There is a convincing correlation between the theoretical error modelling presented in this

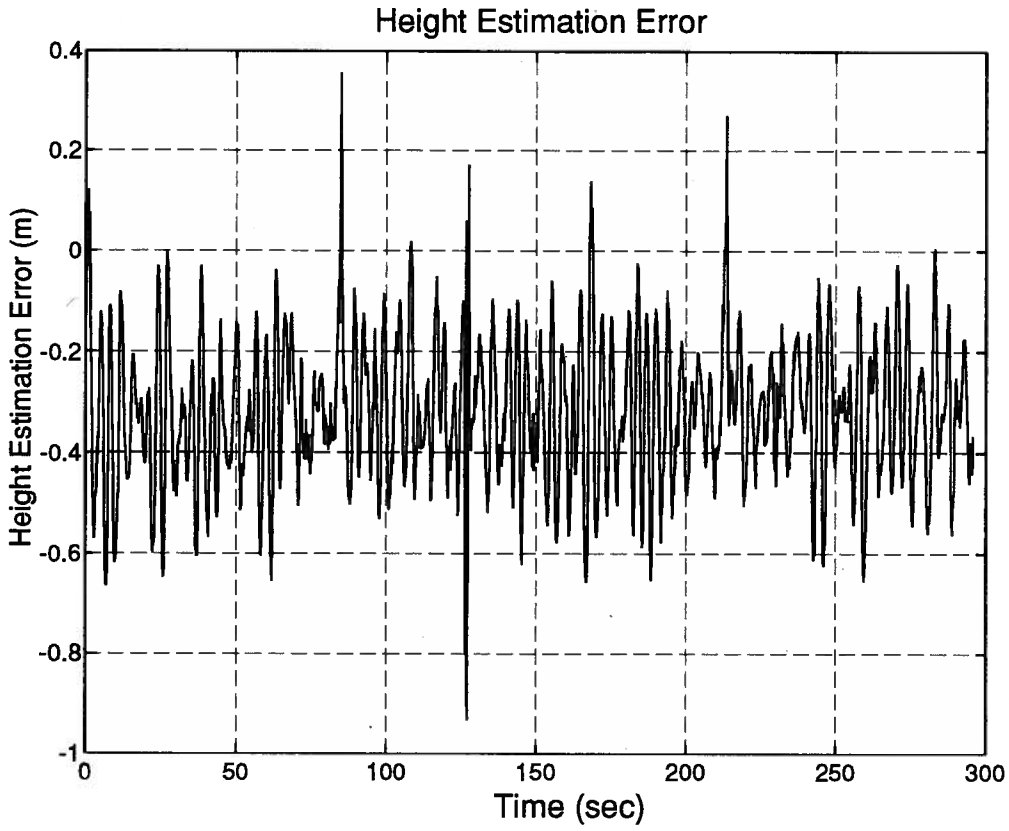

Figure 30 Height Estimation Errors Single Track no RCMC ($R = 10\ km$, $h = 1\ km$)

work and the simulated results using the point target simulator. As predicted, the following main results were observed:

1. The majority of errors resulting from non-ideal motion compensation cancel out between the two channels leading to accurate height estimation.
2. Unknown terrain coupled with velocity perpendicular to the line-of-sight direction leads to an azimuth shift of the compressed peak in both channels identically. Provided this is only a few meters the subsequent differential phase smoothing by spatial filtering will reduce the impact of this error. Alternately, if the error is large the shift can be predicted once a height estimate is available and corrected by a resampling operation. The predictive ability of the theory is very good. But, this correction should not be necessary for the CCRS InSAR system.

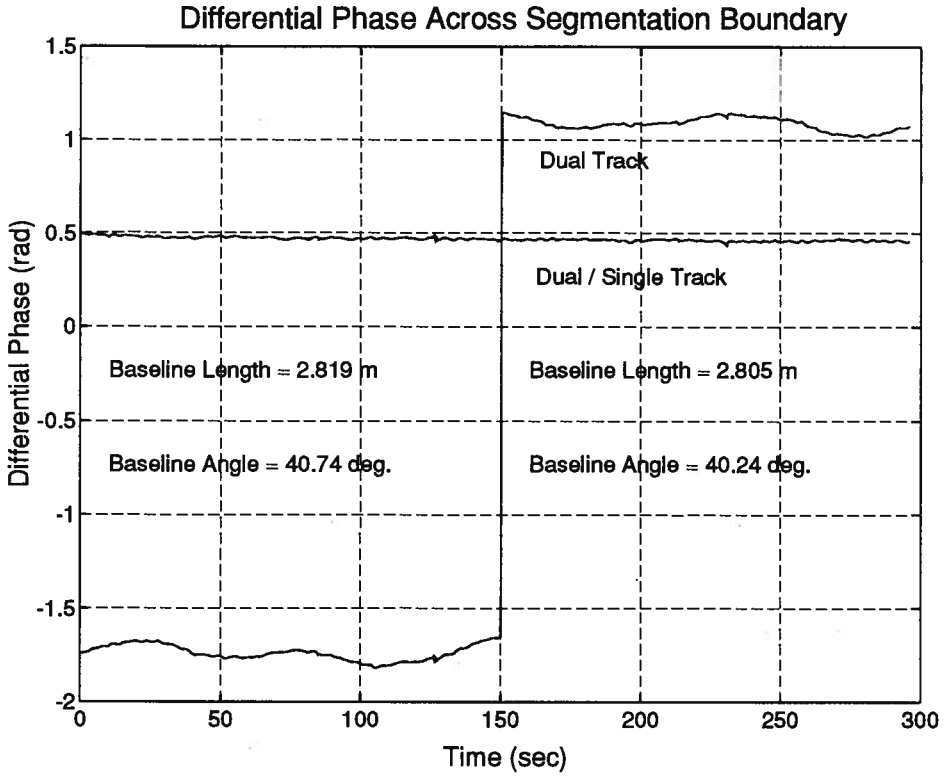

Figure 31 Differential Phase with Segmented Reference Tracks ($R = 10\ km$, $h = 1\ km$)

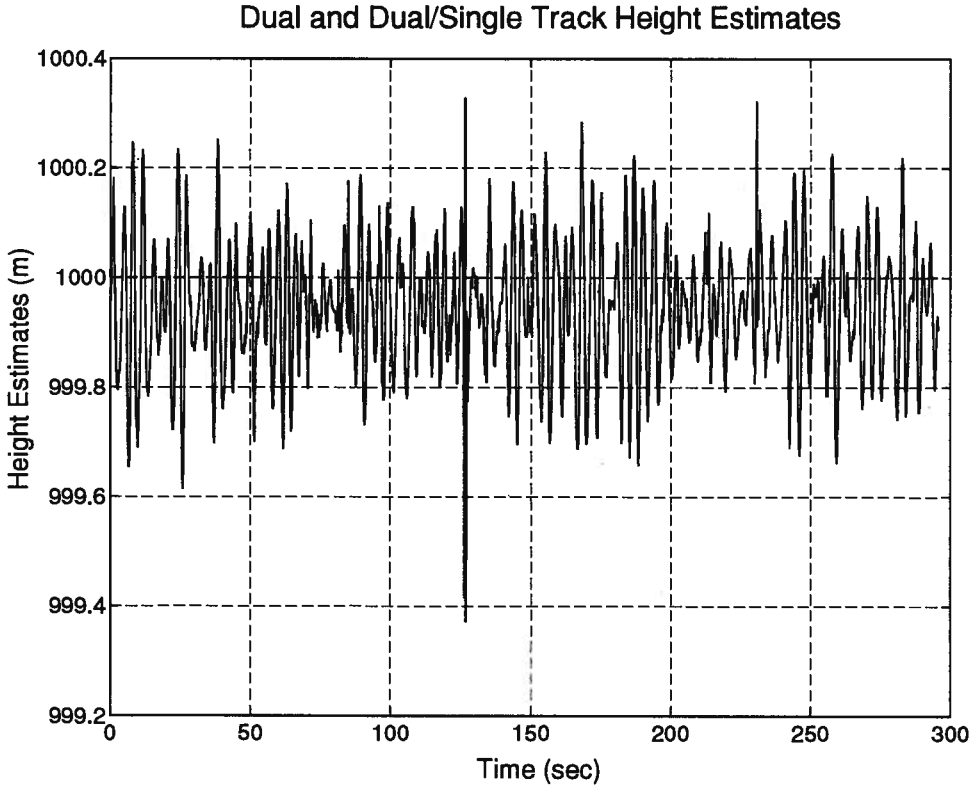

Figure 32 Height Estimates with Segmented Reference Tracks ($R = 10\ km$, $h = 1\ km$)

3. Unknown terrain coupled with acceleration perpendicular to the line-of-sight direction leads to similar defocussing in both channels. For rugged terrain significant defocussing can occur at a few positions along the flight line for the CCRS InSAR system. Only knowledge of the terrain elevation and complete time domain motion compensation and processing can reduce this effect.
4. The single reference track approach with RCMC has an inherent differential phase bias due to the difference in the displacements from the reference track coupled with RCMC. This bias did not occur in the double reference track approach, as expected.
5. The single reference track approach without RCMC also has a small bias error in the height estimate at the peak due to the difference in the displacements from the reference track coupled with the migration of the compressed peak due to uncompensated RCM. This bias did not occur in the double reference track approach.
6. The dominant source of differential phase errors, and thus height estimation errors, is due to aircraft roll coupled with unknown terrain. The roll motion produces angular accelerations which cause bias errors. In addition, the motions are often oscillatory allowing for smoothing to occur due to the compression operation. This resulted in smoothed measured differential phase which did not follow the higher frequency expected differential phase. The conventional approach to interpreting the differential phase is not as sensitive to this effect as the new single and new dual track approaches. But, the conventional approach is sensitive to the choice of reference tracks for a given segment.

5.2 Processing CCRS InSAR Data

In addition to the successful results from the point target simulations, processing with real CCRS InSAR data was carried out to demonstrate the ability to obtain quality interferograms for the various proposed approaches. In this section, the InSAR processor will be described

followed by a description and display of the resulting interferograms and a slant range topographic map. Some additional experiments with inertial data errors will also be described.

A basic InSAR processor was implemented in the MATLAB simulation language following the process flow of Figure 2. The main processing steps included:

1. Resample channel B to register with channel A at the reference level.
2. Perform motion compensation phase correction to each channel using single or dual reference tracks.
3. Perform azimuth compression using fast convolution without RCMC.
4. Form interferogram.
5. Perform phase smoothing and phase unwrapping.
6. Convert differential phase to elevation.

The processor was designed to operate on one block of range data at a time. The blocks could then be pieced together to form a complete image. The processing parameters were those of Table 1.

5.2.1 Three Hills Data Results

The data set processed was of the Three Hills area in Alberta. The data was acquired by the CCRS InSAR system in February 1992, pass 10. The scene is of farm land with rolling hills. The raw data was 12000 range lines with a swath width of 2048 samples. The interferograms were phase smoothed by sample averaging of 10 samples in azimuth and down sampled by 10 producing a final image 2048 samples in range by 1024 in azimuth. This yielded about equal sampling intervals of 4 m in each direction.

Figure 33 shows the interferogram square root of the magnitude image which is essentially equivalent to a single channel SAR image. The image looks distorted because of the slant range perspective.

Figure 34 shows the resulting interferogram differential phase for the dual reference track case. One cycle of the color wheel corresponds to a change of 2π radians. The dominant variation is due to the flat earth fringes which depend upon the position of the reference tracks. The discontinuity in the reference tracks at range line 512 will clearly cause phase unwrapping problems. The flat earth fringes have to be removed before the variation due to topography will be visible in the interferogram.

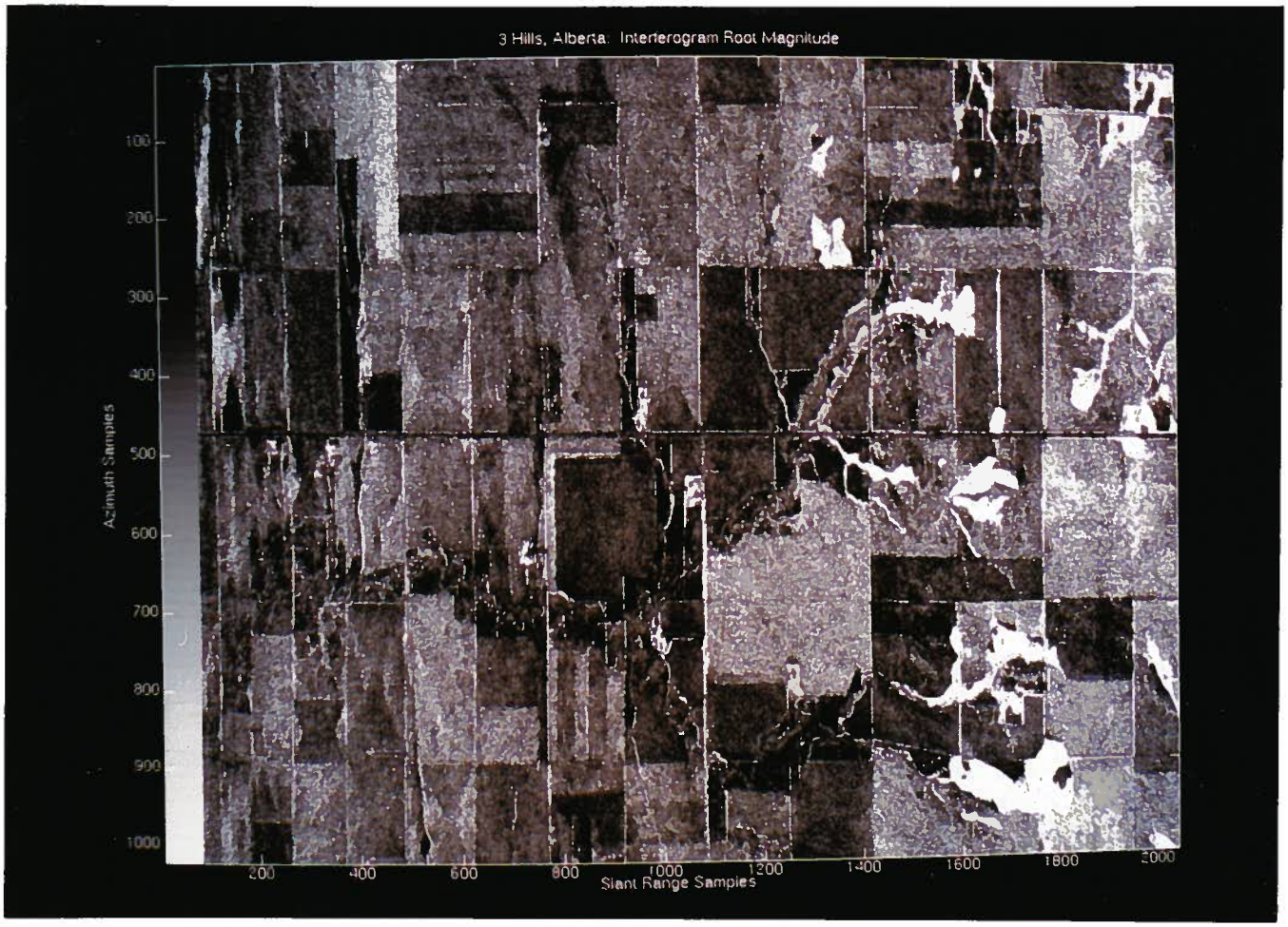

Figure 33 Square Root of Interferogram Magnitude Image

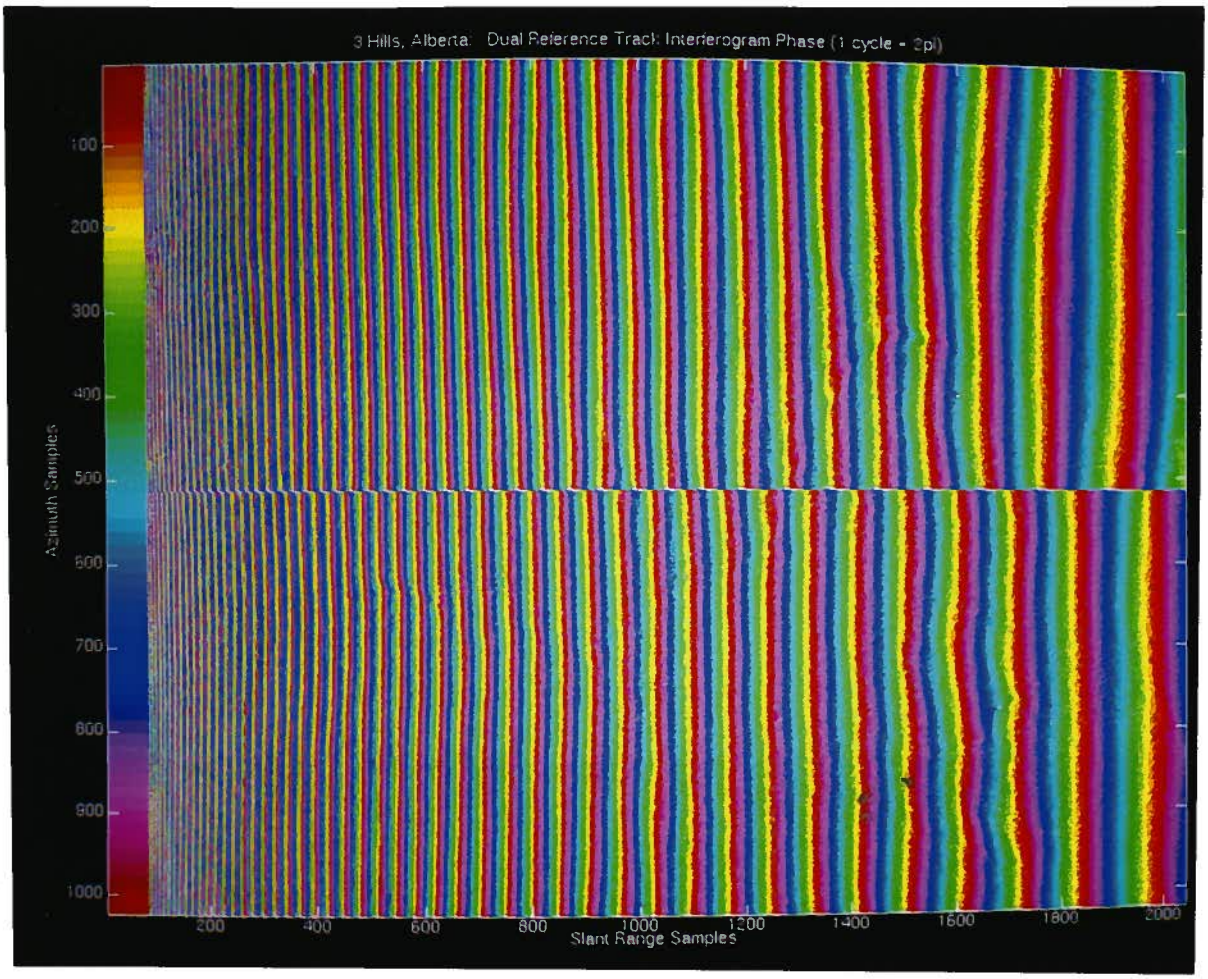

Figure 34 Dual Reference Track Interferogram Phase

Figure 35 shows the resulting interferogram differential phase for the new dual/single track case. One cycle of the color wheel corresponds to a change of π radians. The extra phase correction was applied to the phase smoothed and down sampled interferogram to reduce computation. The new dual/single approach has the expected continuous differential phase across the segmentation boundary.

Figure 36 shows the interferogram differential phase for the single reference track case. One cycle of the color wheel corresponds to a change in differential phase of π radians. It

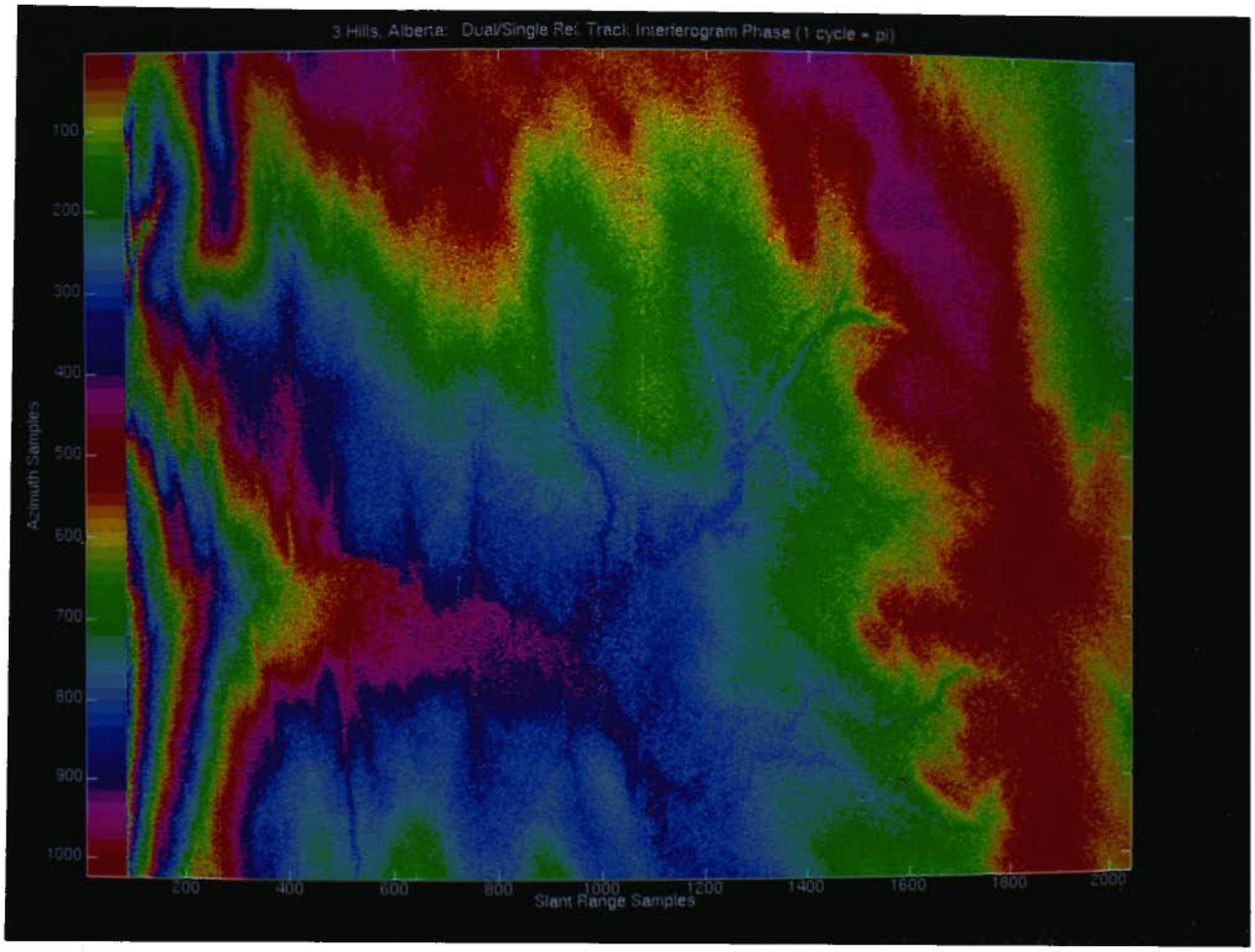

Figure 35 Dual/Single Reference Track Interferogram Phase

is clear that the differential phase is continuous across the discontinuity at range line number 512. This result was compared to the interferogram using the new dual/single reference track approach yielding a negligible mean difference of 2 *mrad* or 6 *cm* in elevation and 6 *mrad rms* or 3 *cm rms* in elevation across the image. This result shows that the bias errors that occur solely for the single reference track case without RCMC are small when the processed bandwidth is small.

Further interferometric processing of the single reference track interferogram was per-

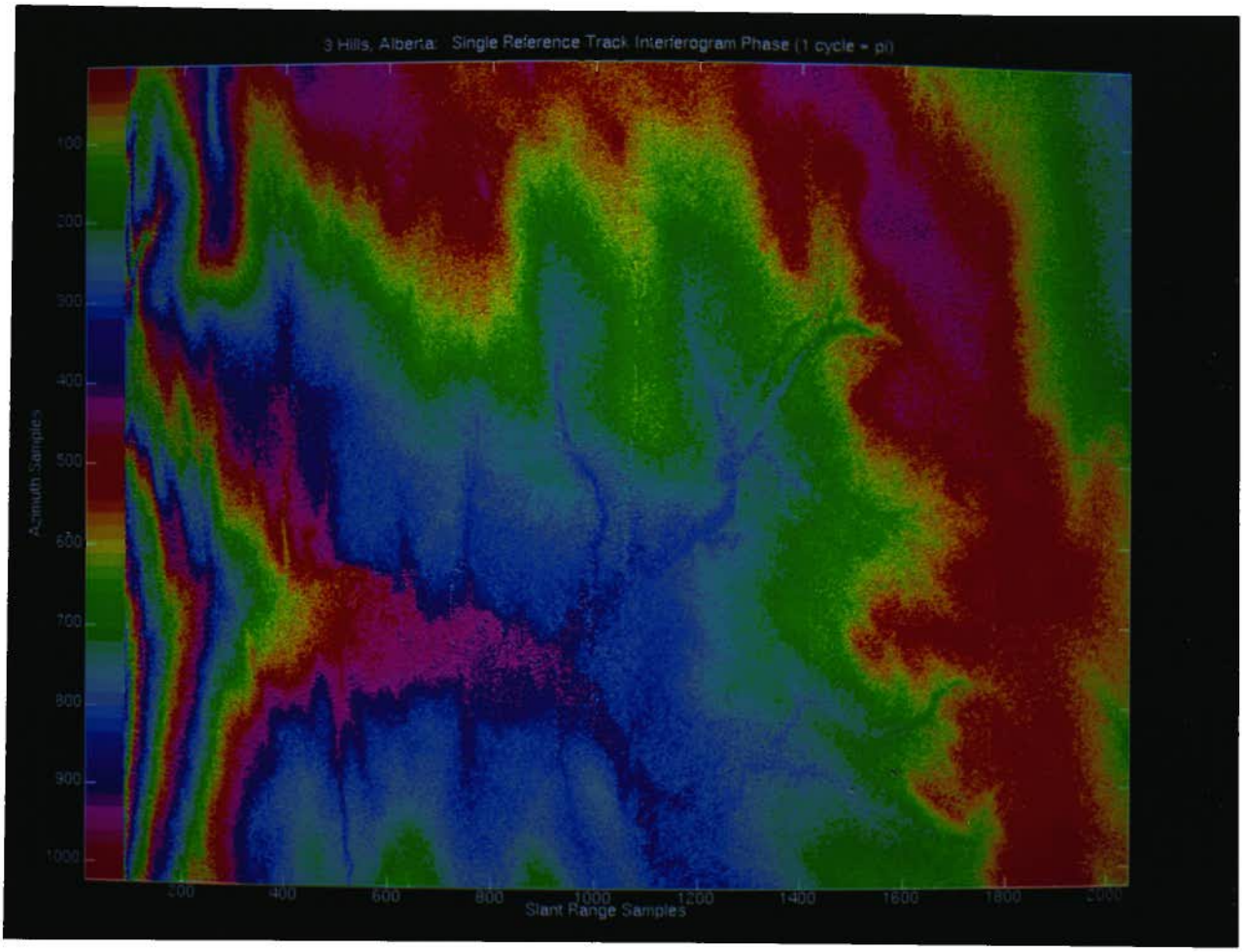

Figure 36 Single Reference Track Interferogram Phase

formed. The differential phase was phase unwrapped and converted into elevation estimates without any control points or phase calibration. Figure 37 shows the resulting slant range topography with one cycle of the color wheel corresponding to 50 feet. Figure 38 shows the 1:50 000 contour map for the region with contour intervals of 25 feet. A visual comparison of the two demonstrates the effectiveness of SAR interferometry. The spatial distortion would be removed if a projection to ground range were made.

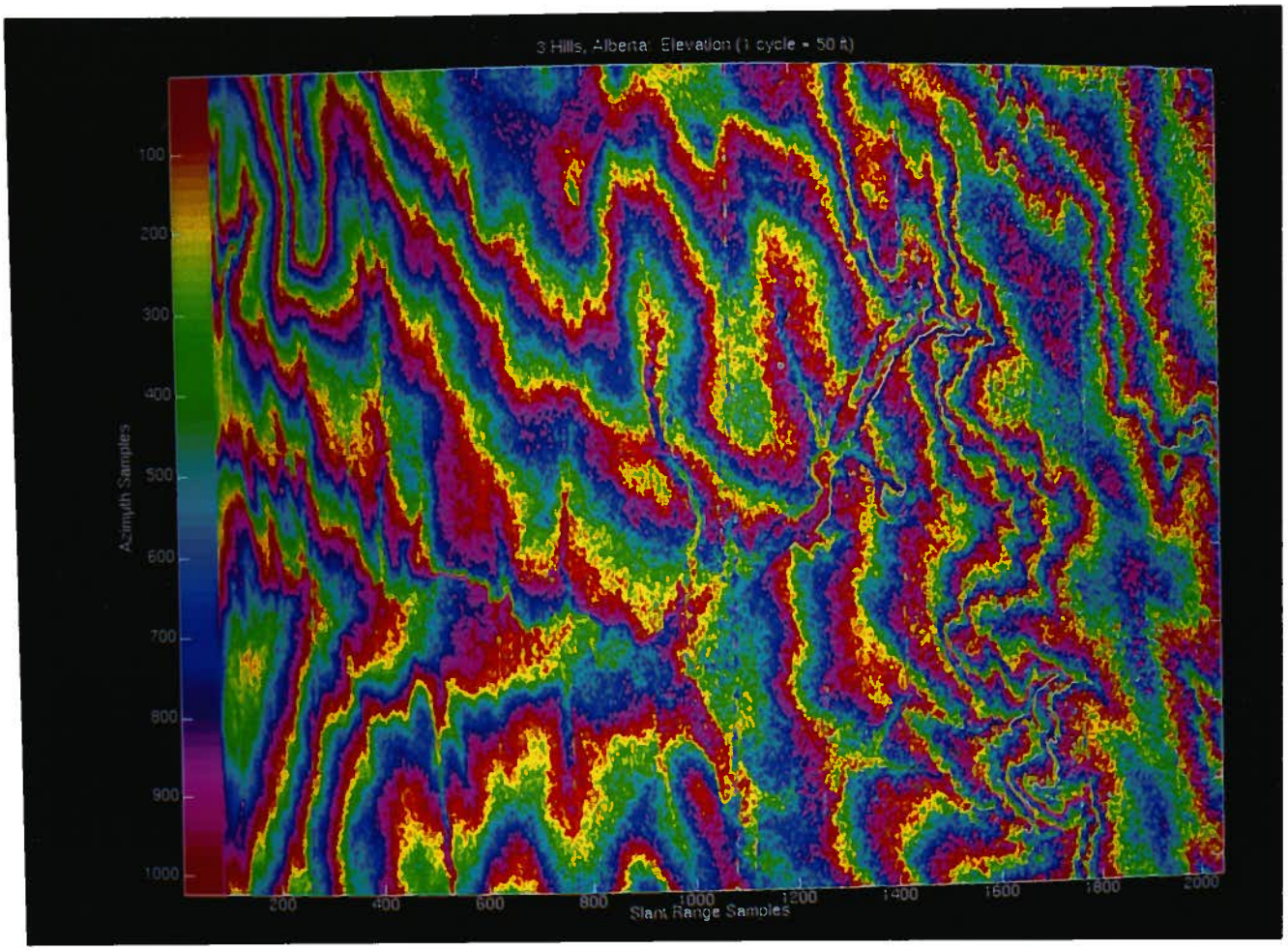

Figure 37 Elevation Estimates

5.2.2 Inertial Data Errors

In order to ensure the equality of all approaches with regard to inertial data errors real data experiments were carried out. A baseline clutter data set was constructed from the Three Hills data which used the INS data supplied by CCRS for motion compensation and elevation estimation. In the test data set the same raw data was processed but with zero mean, independent, Gaussian errors in the INS data. The single and dual track motion compensation approaches were used as well as the conventional dual track interpretation of the resulting

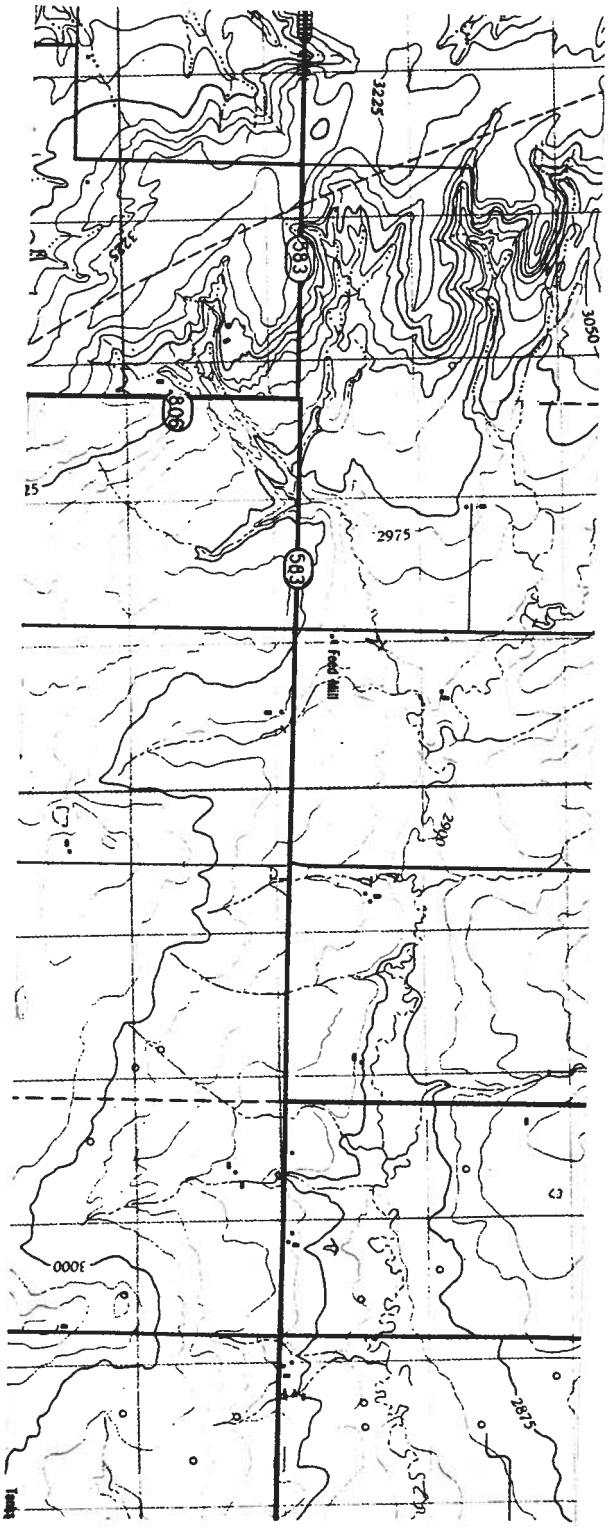

Figure 38 1:50 000 Contour Map of 3 Hills Area (51°45′ lat. 113°30′ long.),

25 ft contours (82 P/11/12 Energy, Mines, and Resources Canada, 1990)

differential phase. The height estimates were compared to the height estimates from the baseline data set and the errors computed. As expected, all methods produced the same variance of height errors. As an example of the results for the CCRS processing parameters, a 1 *mm rms* error in the position of the receive-only antenna produced about a 0.4 *m rms* height estimation error at near range.

Another similar experiment was conducted, except that the INS errors were constant over the aperture. As expected, all methods produced the same bias in the height estimates. For example, with a 1 *mm* bias error in the horizontal and vertical position of the receive-only antenna position lead to a height estimation bias of about 0.5 *m* at near range.

It would appear that an important limiting factor for airborne InSAR motion compensation is in the ability to estimate the baseline length and angle. For the single and new dual track formulations the errors arise in the differential phase to elevation equations. In the conventional dual track approach the instantaneous baseline must be known in order to motion compensate accurately to the two reference tracks. The resulting baseline induced errors appear as differential phase biases. In either case, the effect on the height estimates are the same.

Chapter 6 Conclusions

In this chapter the main conclusions drawn from this work will be listed and briefly described. Following this, the ensuing recommended motion compensation approaches for InSAR will be summarized. The following specific conclusions were made from this work:

1. The effect of motion compensation with unknown terrain on focussing can be severe for turbulent flights and moderate terrain or typical flights and rugged terrain. The translational velocity causes the compressed peak positions to be shifted (Equation 3.48) and translational acceleration leads to peak broadening (Equation 3.54).
2. Due to the range varying phase correction (RVPC) and the ensuing range spectral shift induced, the allowed displacement offset between the reference track and the antenna track is limited by the range oversampling factor if subsequent baseband processing is used (Equation 3.21). This spectral shift may cause problems for interpolation in RCMC or subsequent range filtering.
3. Differential phase bias, and thus a height estimation bias, can occur that dependent upon the difference in the displacements between each channel and the reference track due to the range varying phase correction (RVPC). This difference is much larger in the single reference track case and can lead to significant differential phase biases. This difference is typically very small in the double reference track case. When RCMC is performed the bias is due to differences in quadratic phase errors (Equations 4.82 and 4.83). When RCMC is not performed, the bias is due to the peak shift caused by uncompensated RCM coupled with the range phase ramp of the differential RVPC.
4. The effect of motion compensation with unknown terrain on the differential phase is small in most cases due to the phase errors cancelling out between channels. Differential phase biases can occur if the offset between the antennas and the reference tracks become large,

combined with rugged terrain (Equation 4.31). These effects can be compensated for in the differential phase to elevation equations. The single reference track approach handles this automatically (Equation 4.15) but the double reference track case must include an extra term in the equation (Equation 4.27). Severe angular (roll) acceleration coupled with rugged terrain can lead to differential phase biases (Equations 4.52, 4.54, and 4.60).

5. If block azimuth processing is used then the length of the block is limited by the amount of range resampling performed over that block as this determines the slant range required for the matched filter. The important parameter is the difference in the errors in the matched filters between the two channels as this leads to differential phase biases (Equations 4.77 and 4.79).
6. Neglecting to resample for motion compensation does not have much effect for typical flights but will cause broadening and a reduction of the useful part of the aperture for very turbulent flights.
7. Errors in the inertial data can lead to differential phase errors and biases in the height estimates. The high frequency errors can be reduced by filtering the interferogram but bias errors will remain. An important factor for airborne InSAR motion compensation is in the ability to estimate the baseline length and angle. For the single and new dual track formulations the errors arise in the differential phase to elevation equations. In the conventional dual track approach the instantaneous baseline must be known in order to motion compensate accurately to the two reference tracks. The resulting baseline induced errors appear as differential phase biases. In either case, the effect on the height estimates are the same, requiring extremely accurate inertial data. In the absence of this correction, control points will be required.
8. The single reference track approach yields continuous differential phase even when the reference track is segmented (Equation 4.15). In addition, the flat earth fringes have been

removed.

9. The dual reference track approach yields discontinuous differential phase when the reference tracks are segmented (Equation 4.27).
10. The benefits of both the single and dual reference track approaches can be realized by using the dual track for motion compensation followed by a conversion to a single track by a subsequent phase correction. If motion compensation resampling is performed then this extra correction can be very efficiently applied as a constant to the receive-only channel azimuth matched filter for each azimuth line in the segment (Equation 4.110). If motion compensation resampling is not performed the correction must be applied pixel by pixel to the entire receive-only image or to the phase smoothed and down sampled interferogram.

6.1 Recommended Approach for CCRS System

For the typical C-band InSAR scenario for the CCRS system a fairly simple approach to motion compensation is adequate. This would include:

1. No motion compensation resampling.
2. Phase correction to a single reference track that may be segmented, if necessary.
3. No RCMC.
4. Azimuth matched filters determined separately for each channel based on the reference level positions.
5. Phase unwrapping that assumes continuous differential phase (as far as motion compensation is concerned).
6. Differential phase to elevation conversion based on the new single track formulation.

Apart from the possible defocussing problems for severe terrain coupled with translational acceleration, this approach should yield a motion compensation approach which contributes on the order of a meter to the height estimate error budget.

6.2 Recommended General Approach

A very accurate approach, which might be required for system parameters other than that of the CCRS case, would be to implement the following:

1. Perform motion compensation resampling.
2. Phase correction to dual reference track that may be segmented if necessary.
3. Perform RCMC.
4. Azimuth matched filters determined separately for each channel based on the reference level positions. Apply the extra phase constant term to each matched filter for channel B to convert the channel B reference track to the channel A reference track.
5. Phase unwrapping that assumes continuous differential phase (as far as motion compensation is concerned).
6. Differential phase to elevation conversion based on the new dual/single track formulation.

Chapter 7 Suggestions for Future Work

The following is a list of possible extensions to the current work or new ideas that have come up:

1. Remove the restriction in the current work of a yaw steered antenna and zero Doppler processing. Investigate how this changes the sensitivities and recommended processing for motion compensation for InSAR.
2. Investigate the role of Autofocus for InSAR motion compensation. For instance,
   a. Investigate the potential of absolute phase ambiguity determination by manipulating the defocussing sensitivity to unknown terrain.
   b. Use Autofocus to handle defocussing caused by unknown terrain.
3. Investigate the modifications to motion compensation for InSAR that might be required if the Split-frequency approach [21] is needed.

Bibliography

[1] R. O. Harger. *Synthetic Aperture Radar Systems Theory and Design.* Academic Press, New York, 1970.

[2] C. J. Oliver. Synthetic-aperture radar imaging. *Journal of Physics D [Applied Physics]*, 22(7), July 1989.

[3] John C. Curlander and Robert N. McDonough. *Synthetic Aperture Radar Systems and Signal Processing*. John Wiley and Sons, Inc., 1991.

[4] I. Cumming, D. Hawkins, and A. L. Gray. All-weather Mapping with Interferometric Radar. In *23rd International Symposium on Remote Sensing of the Environment, Bangkok*, April 1990.

[5] F. W. Leberl, J. Raggam, and M. Kobrick. On Stereo Viewing of SAR Images. *IEEE Transactions on Geoscience and Remote Sensing*, 23(2), March 1985.

[6] L. C. Graham. Synthetic Interferometer Radar for Topographic Mapping. *Proceeding of IEEE*, 62(6), June 1974.

[7] H. Zebker and R. Goldstein. Topographic Mapping From Interferometric SAR Observations. *Journal of Geophysical Research*, 91(B5):4993–4999, 1986.

[8] A. K. Gabriel and R. M. Goldstein. Crossed Orbit Interferometry: Theory and Experimental Results from SIR-B. *International Journal of Remote Sensing*, 9(5):857–872, 1988.

[9] M. Seymour. Height Estimation by SAR Interferometry Theory and Error Analysis. Technical report, RX-TN-50–3688 MacDonald Dettwiler and Associates, 1992.

[10] E. Rodriguez and J. M. Martin. Theory and Design of Interferometric Synthetic Aperture Radars. *IEE Proceedings-F*, 139(2), April 1992.

[11] A. Moccia and S. Vetrella. A Tethered Interferometric Synthetic Aperture Radar (SAR) for a Topographic Mission. *IEEE Transactions on Geoscience and Remote Sensing*, 30(1), January 1992.

[12] H. A. Zebker, M. J. Sander, T. Farr, and R. P. Salazar. Global Topographic Satellite (TOPSAT) Mission. Jet Propulsion Laboratory, April 1993.

[13] C. Elachi. *Spaceborne Radar Remote Sensing: Applications and Techniques*. IEEE Press, New York, 1988.

[14] J. C. Kirk. Motion Compensation for Synthetic Aperture Radar. *IEEE Transactions on Aerospace and Electronic Systems*, 11(3), May 1975.

[15] D. Blacknell, A. Freeman, S. Quegan, I. A. Ward, I. P. Finley, C. J. Oliver, R. G. White, and J. W. Wood. Geometric Accuracy in Airborne SAR Images. *IEEE Transactions on Aerospace and Electronic Systems*, 25(2), March 1989.

[16] J. R. Moreira. A New Method of Aircraft Motion Error Extraction From Radar Raw Data For Real Time Motion Compensation. *IEEE Transactions on Geoscience and Remote Sensing*, 28(4), July 1990.

[17] P. Hoogeboom, P. Snoeij, P. J. Koomen, and H. Pouwels. The PHARUS Project, Results of the Definition Study Including the SAR Testbed PHARS. *IEEE Transactions on Geoscience and Remote Sensing*, 30(4), July 1992.

[18] A. L. Gray, P. Vachon, K. Mattar, and P. Farris-Manning. Airborne SAR Interferometry at CCRS: Project Status and Height Bias Error Minimization. In *CEOS CAL/VAL Workshop, September 1992, Ottawa, Canada*, 1992.

[19] R. M. Goldstein, H. A. Zebker, and C. L. Werner. Satellite Radar Interferometry: Two-dimensional Phase Unwrapping. *Radio Science*, 23(4):713–720, 1988.

[20] C. Prati, M. Giani, and N. Leuratti. SAR Interferometry: a 2–D Phase Unwrapping Technique Based on Phase and Absolute Value Information. In *Proceedings of the International Geoscience and Remote Sensing Society*, 1990.

[21] S. Madsen, H. Zebker, and J. Martin. Topographic Mapping Using Radar Interferometry: Processing Techniques. *IEEE Transactions on Geoscience and Remote Sensing*, 31(1), January 1993.

[22] H. Zebker, S. Madsen, and J. Martin. The TOPSAR Interferometric Radar Mapping Instrument. *IEEE Transactions on Geoscience and Remote Sensing*, 30(5), September 1992.

[23] A. L. Gray and P. J. Farris-Manning. Repeat-Pass Interferometry with Airborne Synthetic Aperture Radar. *IEEE Transactions on Geoscience and Remote Sensing*, 31(1), January 1993.

[24] S. A. Hovanessian. Introduction to Synthetic Array and Imaging Radars. Technical report, Hughes Aircraft Company, Radar Systems Group, March 1979.

[25] A. L. Gray, K. Mattar, and P. Farris-Manning. Airborne SAR Interferometry for Terrain Elevation. In *Proceedings of the International Geoscience and Remote Sensing Society, Houston, Texas*, 1992.

[26] Leland B. Jackson. *Digital Filters and Signal Processing*. Kluwer Academic Publishers, 1989.

[27] R. Bamler and D. Just. Phase Statistics and Decorrelation in SAR Interferograms. In *Proceedings of the International Geoscience and Remote Sensing Society, Tokyo, Japan*, 17-21 August 1993.

[28] P. L. Bogler. Motion-Compensated SAR Image ISLR. *IEEE Transactions on Geoscience and Remote Sensing*, 25(6), November 1987.

[29] I. Cumming. The Effect of Matched Filters on Phase Errors. Technical report, AB-RP-50–2412 MacDonald Dettwiler and Associates, 1990.

[30] P. Beckmann. *Probability in Communication Engineering*. Harcourt, Brace & World, Inc., 1967.

[31] I. S. Gradshteyn and I. M. Ryzhik. *Table of Integrals, Series, and Products (Corrected and Enlarged)*. Academic Press Inc., 1980.

[32] T. Sos. ERIM/ARPA/ARMY TEC IFSARE Program. In *Proceedings of the DARPA Interferometric SAR Technology and Applications Symposium*, 13-14 April 1993.

[33] J. C. Dainty. *Topics in Applied Physics: Laser Speckle and Related Phenomena*. Springer-Verlag, Berlin, 1984.

[34] F. Gatelli, A. Monti Guarnieri, F. Parizzi, P. Pasquali, C. Prati, and F. Rocca. Developments in ERS-1 SAR Interferometry: Use of the Spectral Shift. In *International Workshop on SAR Interferometry, Naples, Italy*, 18-20 May 1993.

Appendix A Effect of Quadratic Phase Errors on Compression

It is useful to evaluate the effect of quadratic phase errors on the compression of a linear FM pulse. The ideal signal is:

$$s(t) = e^{-j\pi Kt^2} \tag{A.1}$$

The signal to be considered is:

$$s(t) = e^{-j\pi(K+\Delta K)t^2} \tag{A.2}$$

By requiring a large time-bandwidth product ($KT^2 > 50$, from Oliver, 1989) one can obtain an accurate approximation to the true compression by correlating with the following matched filter:

$$s(t) = rect\left(\frac{t}{T}\right)e^{j\pi Kt^2} \tag{A.3}$$

where T is the processed aperture time. The compressed peak is therefore:

$$\begin{aligned} p(t) &= \int_{-\infty}^{\infty} rect\left(\frac{\tau}{T}\right)e^{-j\pi\left((K+\Delta K)(t+\tau)^2\right)}e^{j\pi K\tau^2}d\tau \\ &= \int_{-\frac{T}{2}}^{\frac{T}{2}} e^{-j\pi\left((K+\Delta K)(t^2+2t\tau)\right)}e^{-j\pi\Delta K\tau^2}d\tau \\ &= e^{-j\pi(K+\Delta K)t^2}\int_{-\frac{T}{2}}^{\frac{T}{2}} e^{-j2\pi(K+\Delta K)t\tau}e^{-j\pi\Delta K\tau^2}d\tau \end{aligned} \tag{A.4}$$

The remaining integral can be evaluated resulting in Fresnel integrals. As the phase at the peak is of most importance, one can simplify:

$$p(0) = \int_{-\frac{T}{2}}^{\frac{T}{2}} e^{-j\pi\Delta K\tau^2}d\tau \tag{A.5}$$

This expression is a complex Fresnel Integral or Cornu Spiral. Of interest is the angle of the Cornu Spiral. The following substitution can be used to put this into a more recognizable form:

$$\pi\Delta K\tau^2 = u^2 \tag{A.6}$$

yielding,

$$p(0) = \frac{1}{\sqrt{\pi\Delta K}} \int_{-\frac{T}{2}\sqrt{\pi\Delta K}}^{\frac{T}{2}\sqrt{\pi\Delta K}} e^{-ju^2} du = \frac{2}{\sqrt{\pi\Delta K}} \int_{0}^{\frac{T}{2}\sqrt{\pi\Delta K}} e^{-ju^2} du \tag{A.7}$$

Now the Cornu Spiral can be evaluated using an asymptotic expansion for small values of x:

$$S(x) = \sqrt{\frac{2}{\pi}} \int_0^x \sin u^2 du \approx \sqrt{\frac{2}{\pi}} \left(\frac{x^3}{3} - \frac{x^7}{7 \cdot 3!} \cdots \right)$$
$$C(x) = \sqrt{\frac{2}{\pi}} \int_0^x \cos u^2 du \approx \sqrt{\frac{2}{\pi}} \left(x - \frac{x^5}{5 \cdot 2!} \cdots \right) \tag{A.8}$$

The phase error at the peak is:

$$\Delta\Phi(x) = \tan^{-1}\left(-\frac{S(x)}{C(x)}\right) \approx -\frac{S(x)}{C(x)} \approx -\frac{x^2}{3} \tag{A.9}$$

Back substituting values gives:

$$\Delta\Phi \approx -\frac{\pi\Delta K T^2}{12} \tag{A.10}$$

In terms of the applied quadratic phase error at the edge of the processed band:

$$\Delta\phi = \frac{\pi\Delta K T^2}{4} \tag{A.11}$$

one obtains:

$$\Delta\Phi \approx -\frac{\Delta\phi}{3} \tag{A.12}$$

The exact solution was obtained using numerical integration and compared to this approximation. The approximate relation is an upper bound and is very accurate up to an applied error of about π at the band edge. In addition, the phase error across the compressed peak was observed from the numerical solutions. It was found that the phase was parabolic about the peak with the error initially decreasing toward the first null, passes through zero, then increases toward π at the first null. In other words, the expected zero phase response has zero phase over the main lobe and a change of π radians across each null. When a quadratic phase error is present along the aperture the edges of this step-like phase response are smoothed out. About 90 percent of the main lobe has a phase error less than that at the peak and the remaining 10 percent is around the null.

The effect of quadratic phase errors on the compressed peak 3dB width is very non-linear. For applied phase errors at the edge of the band of less than about $\pi/2$ the broadening is less than about 5%. For applied errors of about 2.5 radians the broadening is about 20%. Above this value the peak deformation becomes extreme and the broadening increases very rapidly.

The effect of quadratic phase errors on the compressed peak sidelobe levels is fairly linear. Above 2.5 radians the sidelobe level has dropped from –13 dB to –5 dB. It would appear that to maintain a reasonable peak shape the phase errors should be kept below about $\pi/2$ at the edges of the processed band.

For sinusoidal type motions with periods less than the processed aperture, the phase error must be less than $\pi/2$ for a maximum allowable broadening of 10% according to Hovanessian, 1979.

Appendix B Single Channel Phase Errors due to Unknown Terrain

Given that the off-nadir angle to the imaged patch is initially unknown, this leads to phase errors in the applied motion compensation phase correction. Referring to Figure 7 one applies a correction of:

$$\phi_{mc}(applied) = -\frac{4\pi}{\lambda}(R_{to} - R_{ao}) \tag{B.1}$$

for the zero Doppler pulse of a particular target. The proper correction is:

$$\phi_{mc}(ideal) = -\frac{4\pi}{\lambda}(R_{th} - R_{ao}) \tag{B.2}$$

Therefore, the phase mismatch between the data and the assumed data for matched filtering is:

$$\Delta\phi_{err} = -\frac{4\pi}{\lambda}(R_{to} - R_{th}) \tag{B.3}$$

One can expand this expression for the phase errors to first order to better understand what parameters are important by using the cosine law and a truncated binomial expansion:

$$\begin{aligned} R_{th} &= R_{ao}\sqrt{1 + \frac{d^2}{R_{ao}^2} - 2\frac{d}{R_{ao}}\cos(\alpha + \theta_{ah})} \\ &\approx R_{ao}\left(1 - \frac{d}{R_{ao}}\cos(\alpha + \theta_{ah})\right) \end{aligned} \tag{B.4}$$

$$\begin{aligned} R_{to} &= R_{ao}\sqrt{1 + \frac{d^2}{R_{ao}^2} - 2\frac{d}{R_{ao}}\cos(\alpha + \theta_{ao})} \\ &\approx R_{ao}\left(1 - \frac{d}{R_{ao}}\cos(\alpha + \theta_{ao})\right) \end{aligned} \tag{B.5}$$

Therefore, the phase error is

$$\Delta\phi_{err} \approx -\frac{4\pi d}{\lambda}(\cos(\alpha + \theta_{ah}) - \cos(\alpha + \theta_{ao})) \tag{B.6}$$

defining

$$\begin{aligned} \theta &= \theta_{ao} \\ \Delta\theta &= \theta_{ah} - \theta_{ao} \end{aligned} \tag{B.7}$$

and using

$$\cos a - \cos b = -2\sin\frac{1}{2}(a + b)\sin\frac{1}{2}(a - b) \tag{B.8}$$

yields:

$$\Delta\phi_{err}(t) \approx \frac{8\pi d(t)}{\lambda}\sin\left(\alpha(t) + \theta(t) + \frac{\Delta\theta(t)}{2}\right)\sin\frac{\Delta\theta(t)}{2} \tag{B.9}$$

The time dependence has been shown to indicate that the phase error for a particular target will vary across the aperture depending upon the flight motion, the applied motion compensation, and the error in the assumed off-nadir angle to the target. It is clear from this expression that the phase error is sensitive to flight motion perpendicular to the line-of-sight of the beam. The phase error variation over the aperture is therefore,

$$\Delta\phi_{err}(t) \approx \frac{8\pi d_{\perp los}(t)}{\lambda} \sin\frac{\Delta\theta(t)}{2} \tag{B.10}$$

where $d_{\perp los}(t)$ is the flight motion displacement variation perpendicular to the line-of-sight. One can approximate the error in the off-nadir angle with the upper bound:

$$\Delta\theta \approx \frac{h}{R_{ao}\sin\theta} \tag{B.11}$$

and another upper bound approximation:

$$\sin\frac{\Delta\theta}{2} \approx \frac{\Delta\theta}{2} \tag{B.12}$$

Therefore,

$$\Delta\phi_{err}(t) \approx \frac{4\pi\ h\ d_{\perp los}(t)}{\lambda R_{ao}\sin\theta} \tag{B.13}$$

Appendix C Effect of Linear Phase Errors on Compression

It is useful to evaluate the effect of linear phase errors on the compression of a linear FM pulse. The ideal signal is:

$$s(t) = e^{-j\pi Kt^2} \tag{C.1}$$

The signal to be considered is:

$$s(t) = e^{-j\pi(Kt^2+Lt)} \tag{C.2}$$

By requiring a large time-bandwidth product ($KT^2 > 50$, from Oliver, 1989) one can obtain an accurate approximation to the true compression by correlating with the following matched filter:

$$s(t) = rect\left(\frac{t}{T}\right)e^{j\pi Kt^2} \tag{C.3}$$

where T is the processed aperture time. The compressed peak is therefore:

$$\begin{aligned} p(t) &= \int_{-\infty}^{\infty} rect\left(\frac{\tau}{T}\right)e^{-j\pi\left(K(t+\tau)^2+L(t+\tau)\right)}e^{j\pi K\tau^2}d\tau \\ &= \int_{-\frac{T}{2}}^{\frac{T}{2}} e^{-j\pi\left(Kt^2+2Kt\tau+L(t+\tau)\right)}d\tau \\ &= e^{-j\pi(Kt^2+Lt)}\int_{-\frac{T}{2}}^{\frac{T}{2}} e^{-j2\pi Kt\tau}e^{-j\pi L\tau}d\tau \end{aligned} \tag{C.4}$$

$$\int_{-\frac{T}{2}}^{\frac{T}{2}} e^{-j2\pi Kt\tau}e^{-j\pi L\tau}d\tau = -\frac{T\sin\pi(2tK+L)\frac{T}{2}}{\pi(2tK+L)\frac{T}{2}} \tag{C.5}$$

Therefore, the final solution is:

$$p(t) = -\frac{T\sin\pi(2tK+L)\frac{T}{2}}{\pi(2tK+L)\frac{T}{2}}e^{-j\pi(Kt^2+Lt)} \tag{C.6}$$

The position of the peak is no longer at time zero but has been shifted to:

$$t_{peak} = -\frac{L}{2K} \quad (sec) \tag{C.7}$$

In addition, there is a phase error at the peak:

$$\theta_{err} = \frac{\pi L^2}{4K} \quad (rad) \tag{C.8}$$

Appendix D Directional Random Walk Model

The complex pixel result from azimuth compression with random phase noise can be described by a directional random walk model. The statistics of the complex summation result for the case of communication theory problems has been studied by Beckmann, 1967. The summation can be characterized by:

$$Re^{j\theta} = X + jY = \sum_{i=1}^{N} A_i e^{j\phi_i} \tag{D.1}$$

where each contribution is independent and the expectation of Y is zero (expect zero phase). The A_i's can be regarded as the modulated scattering strength along azimuth including any compression windowing. According to Beckmann, the probability density function (PDF) for the resultant phase is:

$$p(\theta) = \frac{Ke^{\left[-0.5B^2(1+K^2)\right]}}{2\pi\left(K^2\cos^2\theta + \sin^2\theta\right)}\left[1 + G\sqrt{\pi}e^{G^2}(1 + erf(G))\right] \tag{D.2}$$

where

$$G = BK\cos\theta\sqrt{\frac{1+K^2}{2\left(K^2\cos^2\theta + \sin^2\theta\right)}} \tag{D.3}$$

$$B = \frac{\bar{X}}{\sqrt{< \left(X - \bar{X}\right)^2 > + < Y^2 >}} \tag{D.4}$$

$$K = \sqrt{\frac{< Y^2 >}{< \left(X - \bar{X}\right)^2 >}} \tag{D.5}$$

$$\bar{X} = < X >$$

$$erf(G) = \frac{2}{\sqrt{\pi}}\int_0^G e^{-z^2}dz \tag{D.6}$$

Of interest is the variance of the resultant phase:

$$\sigma_\theta^2 = \int_{-\infty}^{\infty} \theta^2 p(\theta)d\theta \tag{D.7}$$

A closed form solution to this integral does not exist. But, in most cases of interest an approximate result is sufficient.

When the variance of X and Y are the same (K = 1) one obtains:

$$p(\theta) = \frac{e^{-B^2}}{2\pi}\left[1 + B\sqrt{\pi}\cos\theta(1 + erf(B\cos\theta))e^{B^2\cos^2\theta}\right] \tag{D.8}$$

Furthermore, when the mean of the real part of the resultant is much larger than its variance (B >> 1):

$$erf(B\cos\theta) = \frac{2}{\sqrt{\pi}} \int_0^{B\cos\theta} e^{-z^2} dz \approx 1 \tag{D.9}$$

and

$$\cos^2\theta \approx 1 - \theta^2 \tag{D.10}$$

yielding:

$$p(\theta) \approx \frac{B\cos\theta}{\sqrt{\pi}} e^{-B^2\theta^2} \tag{D.11}$$

Due to the very narrow peak of this function one can ignore the $\cos\theta$ term. Therefore, the PDF of the resultant phase is approximately Gaussian:

$$p(\theta) \approx \frac{B}{\sqrt{\pi}} e^{-B^2\theta^2} \tag{D.12}$$

The variance of the resultant phase is clearly:

$$\sigma_\theta^2 = \frac{1}{2B^2} = \frac{< (X - \bar{X})^2 >}{\bar{X}^2} \tag{D.13}$$

Of interest is to evaluate the phase variance for the case of Gaussian phase noise applied to the signal prior to compression as a result of high frequency inertial data errors. It is assumed that the phase noise is zero mean and independent from element to element. The result of compression including compression weighting is:

$$Re^{j\theta} = X + jY = \sum_{i=1}^{N} A_i e^{j\phi_i} = \sum_{i=1}^{N} A_i \cos\phi_i + j\sum_{i=1}^{N} A_i \sin\phi_i \tag{D.14}$$

The variance to be solved is:

$$\sigma_\theta^2 = \frac{< (X - \bar{X})^2 >}{\bar{X}^2} = \frac{< X^2 >}{\bar{X}^2} = \frac{< Y^2 >}{\bar{X}^2} \tag{D.15}$$

Furthermore,

$$< Y^2 > = \left(\int_{-\infty}^{\infty} \frac{\sin^2\phi}{\sqrt{2\pi}\sigma_\phi} e^{-\frac{\phi^2}{2\sigma_\phi^2}} d\phi \right) \sum_{i=1}^{N} A_i^2 = \frac{\left(1 - e^{-2\sigma_\phi^2}\right)}{2} \sum_{i=1}^{N} A_i^2 \tag{D.16}$$

$$\bar{X} = \left(\int_{-\infty}^{\infty} \frac{\cos\phi}{\sqrt{2\pi}\sigma_\phi} e^{-\frac{\phi^2}{2\sigma_\phi^2}} d\phi \right) \sum_{i=1}^{N} A_i = e^{-\frac{\sigma_\phi^2}{2}} \sum_{i=1}^{N} A_i \tag{D.17}$$

The exponential integrals are evaluated using Gradshteyn, 1980, p480. The resulting phase variance is:

$$\sigma_\theta^2 = \frac{\left(1 - e^{-2\sigma_\phi^2}\right)}{2\, e^{-\sigma_\phi^2}} \frac{\sum_{i=1}^{N} A_i^2}{\left\{\sum_{i=1}^{N} A_i\right\}^2} \tag{D.18}$$

where σ_ϕ^2 is the variance of the Gaussian phase noise. When there is uniform weighting this reduces to:

$$\sigma_\theta^2 = \frac{\left(1 - e^{-2\sigma_\phi^2}\right)}{2N\, e^{-\sigma_\phi^2}} \tag{D.19}$$

Appendix E Inter-channel Azimuth Broadening

It is possible to calculate the inter-channel correlation coefficient for distributed homogenous targets given the point spread function of each channel. The point spread functions will be assumed to be weighted sinc functions that are scaled relative to each other. To evaluate the effect of inter-channel azimuth broadening one needs to evaluate the following expression:

$$\gamma = \frac{\int_{-\infty}^{\infty} P_{a1}(x)P_{a2}(x)dx}{\sqrt{\left(\int_{-\infty}^{\infty} P_{a1}(x)P_{a1}(x)dx\right)\left(\int_{-\infty}^{\infty} P_{a2}(x)P_{a2}(x)dx\right)}} \tag{E.1}$$

where

$$P_{a1}(x) = \frac{\sin 2\pi Wx}{2\pi Wx} \otimes \widetilde{w}(x) \tag{E.2}$$

and

$$P_{a2}(x) = \frac{\sin \frac{2\pi Wx}{\eta}}{\frac{2\pi Wx}{\eta}} \otimes \widetilde{w}(x) \tag{E.3}$$

are the azimuth point spread functions for channel 1 and 2, respectively, and where $\eta > 1$, ($\otimes$ means convolution) and $\widetilde{w}(x)$ is the inverse Fourier Transform of the frequency domain applied window. These integrals are evaluated by invoking the following property of Fourier Transforms:

$$\begin{aligned} \mathcal{F}\{g(t)\} &= \widetilde{g}(f) \\ \int_{-\infty}^{\infty} g(t)dt &= \widetilde{g}(0) \end{aligned} \tag{E.4}$$

Therefore,

$$\int_{-\infty}^{\infty} P_{a1}(x)P_{a2}(x)dx = \int_{-\infty}^{\infty} \left\{ \left(\frac{\sin 2\pi Wx}{2\pi Wx} \otimes \widetilde{w}(x)\right)\left(\frac{\sin \frac{2\pi Wx}{\eta}}{\frac{2\pi Wx}{\eta}} \otimes \widetilde{w}(x)\right) \right\} dx \tag{E.5}$$

$$\begin{aligned} \mathcal{F}\left\{\frac{\sin 2\pi Wx}{2\pi Wx} \otimes \widetilde{w}(x)\right\} &= \frac{1}{2W} rect\left(\frac{f}{2W}\right) \times w(f) \\ \mathcal{F}\left\{\frac{\sin \frac{2\pi Wx}{\eta}}{\frac{2\pi Wx}{\eta}} \otimes \widetilde{w}(x)\right\} &= \frac{\eta}{2W} rect\left(\frac{\eta f}{2W}\right) \times w(f) \end{aligned} \tag{E.6}$$

$$\int_{-\infty}^{\infty} P_{a1}(x)P_{a2}(x)dx = \left[\left(\frac{1}{2W} rect\left(\frac{f}{2W}\right)w(f)\right) \otimes \left(\frac{\eta}{2W} rect\left(\frac{\eta f}{2W}\right)w(f)\right)\right]_{f=0} \tag{E.7}$$

then,

$$\int_{-\infty}^{\infty} P_{a1}(x)P_{a2}(x)dx = \frac{\eta}{4W^2}\int_{-\frac{W}{\eta}}^{\frac{W}{\eta}} w^2(f)df$$

$$\int_{-\infty}^{\infty} P_{a1}(x)P_{a1}(x)dx = \frac{1}{4W^2}\int_{-W}^{W} w^2(f)df \tag{E.8}$$

$$\int_{-\infty}^{\infty} P_{a2}(x)P_{a2}(x)dx = \frac{\eta^2}{4W^2}\int_{-\frac{W}{\eta}}^{\frac{W}{\eta}} w^2(f)df$$

Resulting in:

$$\gamma = \frac{\frac{\eta}{4W^2}\int_{-\frac{W}{\eta}}^{\frac{W}{\eta}} w^2(f)df}{\sqrt{\left\{\frac{1}{4W^2}\int_{-W}^{W} w^2(f)df\right\}\left\{\frac{\eta^2}{4W^2}\int_{-\frac{W}{\eta}}^{\frac{W}{\eta}} w^2(f)df\right\}}} = \sqrt{\frac{\int_{-\frac{W}{b}}^{\frac{W}{b}} w^2(f)df}{\int_{-W}^{W} w^2(f)df}} \tag{E.9}$$

If $w(f) = 1$ on [-W,W], then

$$\gamma = \frac{1}{\sqrt{\eta}} \tag{E.10}$$

For example, if there was 10 % inter-channel azimuth broadening this would reduce the inter-channel correlation coefficient by a factor of 0.95.

Appendix F Single Reference Track Phase Errors

In the single reference track case both channels are motion compensated to the same reference track (Figure 13). The channel A (transmit/receive) applied phase correction is:

$$\phi_A(applied) = -\frac{4\pi}{\lambda}(R_{to} - R_{ao}) \tag{F.1}$$

What should have been applied if the target elevation had been known is:

$$\phi_A(ideal) = -\frac{4\pi}{\lambda}(R_{th} - R_{ao}) \tag{F.2}$$

Therefore, the channel A phase correction error, due to the target height being above the reference level, for this particular range cell and this particular azimuth pulse is:

$$\begin{aligned} E(A) &= \phi_A(applied) - \phi_A(ideal) \\ &= -\frac{4\pi}{\lambda}(R_{to} - R_{ao} - (R_{th} - R_{ao})) \\ &= -\frac{4\pi}{\lambda}(R_{to} - R_{th}) \end{aligned} \tag{F.3}$$

The channel B (receive-only) applied phase correction is:

$$\phi_B(applied) = -\frac{2\pi}{\lambda}((R_{to} - R_{ao}) + (R_{to} - R_{bo})) \tag{F.4}$$

What should have been applied if the target elevation had been known is:

$$\phi_B(ideal) = -\frac{2\pi}{\lambda}((R_{th} - R_{ao}) + (R_{th} - R_{bh})) \tag{F.5}$$

Therefore, the channel B phase correction error for this range cell and this azimuth pulse is:

$$\begin{aligned} E(B) &= \phi_B(applied) - \phi_B(ideal) \\ &= -\frac{2\pi}{\lambda}(2R_{to} - R_{ao} - R_{bo} + R_{ao} + R_{bh} - 2R_{th}) \end{aligned} \tag{F.6}$$

The difference in the two errors, which is the differential phase, is:

$$\Phi = E(A) - E(B) = -\frac{2\pi}{\lambda}(R_{bo} - R_{bh}) \tag{F.7}$$

By expanding the slant range values into binomial series one obtains:

$$\Phi = \frac{2\pi b}{\lambda}(\cos(\alpha_{ab} + \theta_{ah}) - \cos(\alpha_{ab} + \theta_{ao})) \tag{F.8}$$

defining

$$\Delta\theta = \theta_{ah} - \theta_{ao} \tag{F.9}$$

and using

$$\cos a - \cos b = -2 \sin \frac{1}{2}(a+b) \sin \frac{1}{2}(a-b) \tag{F.10}$$

yields

$$\begin{aligned} \Phi &\approx -\frac{4\pi b}{\lambda} \sin\left(\alpha_{ab} + \theta_{ao} + \frac{\Delta\theta}{2}\right) \sin\frac{\Delta\theta}{2} \\ &\approx -\frac{4\pi b_{\perp los}}{\lambda} \sin\frac{\Delta\theta}{2} \end{aligned} \tag{F.11}$$

But,

$$\frac{\Delta\theta}{2} \approx \frac{h}{2R_{ao}\sin\theta} \tag{F.12}$$

therefore,

$$\Phi \approx -\frac{2\pi b_{\perp los} h}{\lambda R_{ao} \sin\theta} \tag{F.13}$$

Appendix G Dual Reference Track Phase Errors

In the dual reference track approach each channel is motion compensated to its own track (Figure 12). The applied phase correction in channel A is:

$$\phi_A(applied) = -\frac{4\pi}{\lambda}(R_{tao} - R_{ao}) \tag{G.1}$$

What should have been applied if the target elevation had been known is:

$$\phi_A(ideal) = -\frac{4\pi}{\lambda}(R_{tah} - R_{ao}) \tag{G.2}$$

Therefore, the channel A phase correction error for this range cell and this azimuth pulse is:

$$\begin{aligned} E(A) &= \phi_A(applied) - \phi_A(ideal) \\ &= -\frac{4\pi}{\lambda}(R_{tao} - R_{tah}) \end{aligned} \tag{G.3}$$

The channel B (receive-only) applied phase correction is:

$$\phi_B(applied) = -\frac{2\pi}{\lambda}((R_{tao} - R_{ao}) + (R_{tbo} - R_{bo})) \tag{G.4}$$

What should have been applied if the target elevation had been known is:

$$\phi_B(ideal) = -\frac{2\pi}{\lambda}((R_{tah} - R_{ao}) + (R_{tbh} - R_{bh})) \tag{G.5}$$

Therefore, the channel B phase correction error for this range cell and this azimuth pulse is:

$$\begin{aligned} &E(B) = \phi_B(applied) - \phi_B(ideal) = \\ &-\frac{2\pi}{\lambda}((R_{tao} - R_{ao}) + (R_{tbo} - R_{bo}) - (R_{tah} - R_{ao}) - (R_{tbh} - R_{bh})) \end{aligned} \tag{G.6}$$

In the dual reference track case, one would expect that the differential phase will be the path length difference phase, using the reference track positions, plus a component due to the errors in the applied phase correction because of the unknown target height.
The component of differential phase due to pure triangulation is:

$$\Phi_t = -\frac{2\pi}{\lambda}(R_{tah} - R_{tbh}) \tag{G.7}$$

Combining the conventional term with the new term results in:

$$\Phi = -\frac{2\pi}{\lambda}(R_{tah} - R_{tbh}) + E(A) - E(B) \tag{G.8}$$

where

$$E(A) - E(B) = -\frac{2\pi}{\lambda}(R_{tao} - R_{ao} - R_{tah} + R_{ao} - R_{tbo} + R_{bo} + R_{tbh} - R_{bh}) \tag{G.9}$$

which results in:

$$DP = -\frac{2\pi}{\lambda}(R_{tao} - R_{tbo} + R_{bo} - R_{bh}) \tag{G.10}$$

It is helpful to express the difference in the errors between the channels in a more understandable form. By pairing together terms that can be converted into known parameters and invoking the parallel ray approximation this yields:

$$\begin{aligned} R_{tao} - R_{tbo} &\approx -b_{RT}\cos\left(\theta'_{ao} + \alpha_{RT}\right) \\ R_{tbh} - R_{tah} &\approx b_{RT}\cos\left(\theta'_{ah} + \alpha_{RT}\right) \\ R_{bo} - R_{bh} &\approx b(\cos\left(\theta_{ao} + \alpha_{ab}\right) - \cos\left(\theta_{ah} + \alpha_{ab}\right)) \end{aligned} \tag{G.11}$$

Therefore,

$$\begin{aligned} E(A) - E(B) \approx \left(\frac{2\pi b_{RT}}{\lambda}\right)\left(\cos\left(\theta'_{ao} + \alpha_{RT}\right) - \cos\left(\theta'_{ah} + \alpha_{RT}\right)\right) + \\ \left(\frac{2\pi b}{\lambda}\right)(\cos\left(\theta_{ah} + \alpha_{ab}\right) - \cos\left(\theta_{ao} + \alpha_{ab}\right)) \end{aligned} \tag{G.12}$$

Extending this by defining:

$$\begin{aligned} \Delta\theta &= \theta_{ah} - \theta_{ao} \\ \Delta\theta' &= \theta'_{ah} - \theta'_{ao} \end{aligned} \tag{G.13}$$

and using

$$\cos a - \cos b = -2\sin\frac{1}{2}(a+b)\sin\frac{1}{2}(a-b) \tag{G.14}$$

yields:

$$\begin{aligned} E(A) - E(B) \approx \\ \left(\frac{4\pi b_{RT}}{\lambda}\right)\sin\left(\alpha_{RT} + \theta'_{ao} + \frac{\Delta\theta'}{2}\right)\sin\left(\frac{\Delta\theta'}{2}\right) - \\ \left(\frac{4\pi b}{\lambda}\right)\sin\left(\alpha_{ab}(t) + \theta_{ao}(t) + \frac{\Delta\theta(t)}{2}\right)\sin\left(\frac{\Delta\theta(t)}{2}\right) \end{aligned} \tag{G.15}$$

When the displacement from the reference track is small and the antenna baseline is the same as the reference track baseline (which it is):

$$\begin{aligned} E(A) - E(B) \approx \\ \left(\frac{4\pi b}{\lambda}\right)\sin\left(\frac{\Delta\theta}{2}\right)\left(\sin\left(\alpha_{RT} + \theta_{ao} + \frac{\Delta\theta}{2}\right) - \sin\left(\alpha_{ab}(t) + \theta_{ao} + \frac{\Delta\theta}{2}\right)\right) \end{aligned} \tag{G.16}$$

using

$$\Delta\theta \approx \frac{h}{R_o \sin\theta} \tag{G.17}$$

one obtains:

$$E(A) - E(B) \approx \left(\frac{4\pi bh}{\lambda R \sin\theta}\right)\left(\cos\left(\frac{\alpha_{RT} + \alpha_{ab}}{2} + \theta_{ao} + \frac{\Delta\theta}{2}\right)\sin\left(\frac{\alpha_{RT} - \alpha_{ab}}{2}\right)\right) \tag{G.18}$$

which gives:

$$E(A) - E(B) \approx \left(\frac{2\pi hb_{los}}{\lambda R \sin\theta}\right)(\alpha_{RT} - \alpha_{ab}) \tag{G.19}$$

This represents the error recovered by this new approach that is not considered in the conventional dual reference track approach.

Appendix H Unknown Terrain and Translational Motion

It is helpful to evaluate how translational motion of the aircraft contributes to the differential phase error. Using the result of Equation 4.75 for the differential phase error along the aperture the possible effects on the interferogram can be analyzed:

$$\Delta\Phi(t) \approx \frac{2\pi hbM(t)}{\lambda R^2 \sin\theta} \tag{H.1}$$

For linearly varying deviations one would expect to observe a relative mis-positioning between the two channels (Appendix C):

$$\pi Lt \approx \frac{2\pi hbM(t)}{\lambda R^2 \sin\theta} \tag{H.2}$$

Differentiating:

$$\pi L \approx \frac{2\pi hb}{\lambda R^2 \sin\theta}\frac{\partial M(t)}{\partial t} \tag{H.3}$$

The resulting differential phase at the peak is:

$$\Delta\Phi = \frac{\pi L^2}{4K} = \frac{\pi h^2 b^2}{2v^2 \lambda R^3 \sin^2\theta}\left(\frac{\partial M}{\partial t}\right)^2 \tag{H.4}$$

For any reasonable parameters this differential phase error is negligible.

The resulting differential shift in samples is:

$$\Delta P = -\frac{L\ PRF}{2K} \approx -\frac{hb\ PRF}{2v^2 R\sin\theta}\frac{\partial M(t)}{\partial t}\ (samples) \tag{H.5}$$

Using 1/16 of a sample as an upper bound we obtain:

$$\frac{\partial M(t)}{\partial t} < \frac{v^2 R\sin\theta}{8hb\ PRF} \tag{H.6}$$

For typical CCRS parameters (Table 1) this yields:

$$\frac{\partial M(t)}{\partial t} < \frac{18100}{h}\ \frac{m}{s} \tag{H.7}$$

Clearly, this is not a very limiting factor.

If one consider quadratic roll motion (uniform angular acceleration) the peak error along the aperture must be less than 1/3 of our maximum allowed differential phase error (Appendix A):

$$\Delta\Phi_{max} \approx \frac{2\pi hbM_{max}}{\lambda R^2 \sin\theta} \tag{H.8}$$

In terms of uniform acceleration:

$$a < \frac{12\lambda R^2 \sin\theta \Delta\Phi_{bias}}{\pi hbT^2} \tag{H.9}$$

For typical CCRS parameters (Table 1) this gives:

$$a < \frac{1742g}{h} \tag{H.10}$$

were g is the acceleration due to gravity. Again, it is clear that the differential phase errors due to translational motion coupled with unknown terrain elevation is negligible.

Appendix I Motion Compensation Resampling

When resampling for motion compensation is neglected there is a residual range migration error in each channel that varies along the aperture depending upon the geometry and flight motion. It is important to explore the nature of the difference in the errors between the two channels (Figure 39).

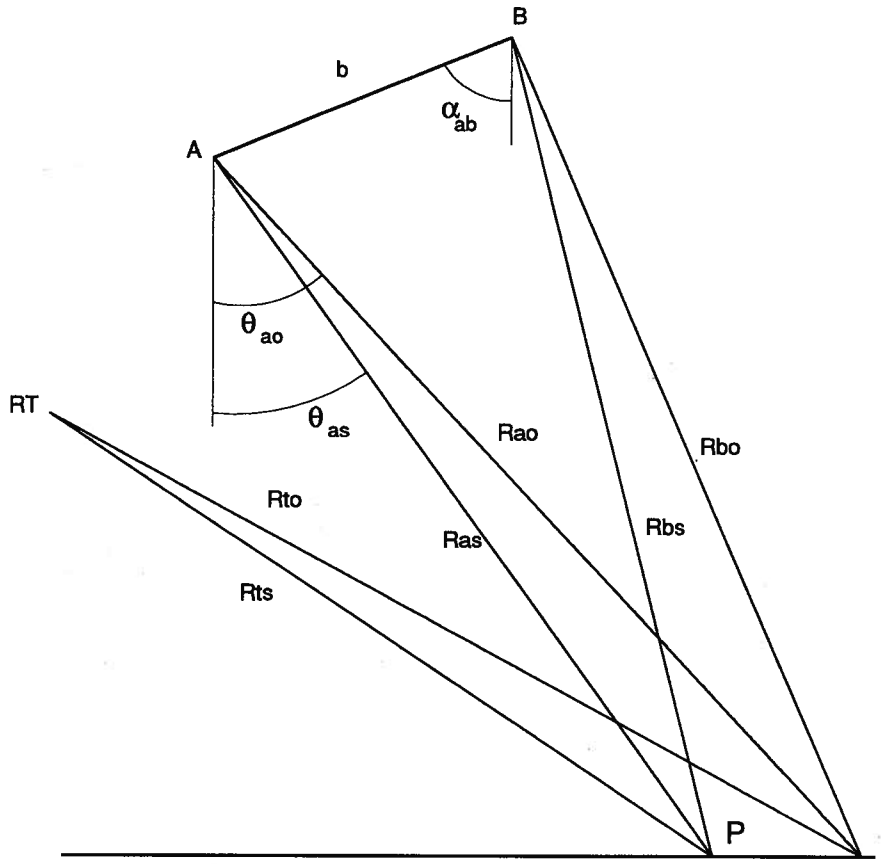

Figure 39 Differential Resampling Geometry

Assuming that the point P is the correct sample to follow (flat terrain) the energy of a target for flight motion parallel to the reference tracks, the residual migration in channel A is:

$$\Delta R(A) = R_{ao} - R_{as} \tag{I.1}$$

The residual migration error in channel B is:

$$\Delta R(A) = R_{bo} - R_{bs} \tag{I.2}$$

The difference between them is:

$$\Delta R(A) - \Delta R(B) = R_{ao} - R_{bo} + R_{bs} - R_{as} \tag{I.3}$$

This can be approximated from:

$$\begin{aligned} R_{bo} &= R_{ao}\sqrt{1+\frac{b^2}{R_{ao}^2}+2\frac{b}{R_{ao}}\cos\left(\alpha_{ab}+\theta_{ao}\right)} \\ &\approx R_{ao}\left(1+\frac{b}{R_{ao}}\cos\left(\alpha_{ab}+\theta_{ao}\right)\right) \end{aligned} \tag{I.4}$$

and

$$\begin{aligned} R_{bs} &= R_{as}\sqrt{1+\frac{b^2}{R_{as}^2}+2\frac{b}{R_{as}}\cos\left(\alpha_{ab}+\theta_{as}\right)} \\ &\approx R_{as}\left(1+\frac{b}{R_{as}}\cos\left(\alpha_{ab}+\theta_{as}\right)\right) \end{aligned} \tag{I.5}$$

Yielding:

$$\Delta R(A)-\Delta R(B)\approx -(\cos\left(\alpha_{ab}+\theta_{ao}\right)-\cos\left(\alpha_{ab}+\theta_{as}\right)) \tag{I.6}$$

defining

$$\begin{aligned} \theta &= \theta_{as} \\ \Delta\theta &= \theta_{ao}-\theta_{as} \end{aligned} \tag{I.7}$$

and using

$$\cos a-\cos b=-2\sin\frac{1}{2}(a+b)\sin\frac{1}{2}(a-b) \tag{I.8}$$

yields:

$$\Delta R(A)-\Delta R(B)\approx 2b\sin\left(\alpha_{ab}+\theta+\frac{\Delta\theta}{2}\right)\sin\frac{\Delta\theta}{2} \tag{I.9}$$

With further approximations from Figure 11:

$$\Delta\theta\approx\frac{x(t)\cos\xi(t)}{R_{ao}} \tag{I.10}$$

$$\Delta R(A)-\Delta R(B)\approx\frac{b\sin\left(\alpha_{ab}+\theta\right)x(t)\cos\xi(t)}{R} \tag{I.11}$$

Provided the roll angle $\alpha_{ab}(t)$ does not vary significantly over the aperture the resulting error is proportional to the product of the flight deviation and antenna separation perpendicular to the line-of-sight direction:

$$\Delta R(t)\approx\frac{b_{\perp los}M_{\perp los}(t)}{R} \tag{I.12}$$

Appendix J MATLAB Program Listings

The following is a sample of the macros used for the MATLAB simulator and InSAR processor. They are written in the MATLAB simulation language.

```
%%%%%%%%%%%%%%%%%%%%%%%%%%%%%%%%%%%%%%%%%%%%%%%%%%%%%%%%%%%%%%%%%%%%%%%%%%%%
% simulator1.m
%
%    Dual channel point target simulation with aircraft motion, motion
%    compensation to one or two reference tracks, RCMC, azimuth compression,
%    interferogram generation, and point target analysis
%
%
% Change control
%  June 8/93  Initial release, modified from rcmc1.m to add RCMC
%  June 10/93 added interpolation by 2 of ch A and B before i'gram generation
%  June 17/93 shifted azimuth profile by one sample
%  Dec  16/93 added sinusoidal roll
%
%%%%%%%%%%%%%%%%%%%%%%%%%%%%%%%%%%%%%%%%%%%%%%%%%%%%%%%%%%%%%%%%%%%%%%%%%%%%
% Initialize Parameters
%%%%%%%%%%%%%%%%%%%%%%%%%%%%%%%%%%%%%%%%%%%%%%%%%%%%%%%%%%%%%%%%%%%%%%%%%%%%
%
V = 131.0;              % A/C velocity m/s
PRF = 337;              % Hz
wave = 0.0565646;       % wavelength (m)
D = 1.0;                % antenna azimuth length (m)
Fr = 37.5E6;            % Range sampling rate Hz
c = 2.9979E8;           % speed of light (m/s)
slpix = c/(2*Fr);       % slant range pixel spacing (m)
slres = 5.6;            % slant range resolution (m)
H = 6000;               % reference altitude (m)
Rao = 10000;            % slant range at nearest approach (m)
                % from "nominal" antenna position (delh1c,delv1c)
Ka = 2*V^2/(wave*Rao);% Azimuth FM rate Hz/s
etac = 0;               % azimuth time of nearest approach (sec)
Na = 2048;              % number of azimuth samples generated
BWproc = 3;             % processed beamwidth (deg.)
%Nmf = BWproc*(pi/180)*Rao*PRF/V; % length of azimuth matched filter (sampl.)
Nmf = 1024;             % number of azimuth samples processed
K = 50;                 % azimuth beamwidth constant (3.1 deg one-way)
M = pi/(1.125*slres); % range point spread function constant
Ni = 16;                % number of azimuth elements about peak to interpolate
Nr = 21;                % number of range cells (must be odd!)
Ir = 16;                % interpolation factor for peak analysis
NNi = Ni*Ir;            % interpolation length
beta = 0;               % beta used for matched filter kaiser window
div_zero = 1E-11;       % avoids divides by zero in sinc(x)
k = 2*pi/wave;          % wave number
interp_size = 16;       % interpolate in RCMC to 1/interp_size of a sample
Nk = 8;                 % length of RCMC kernel
Wn = 1/interp_size;     % Cutoff for RCMC kernel =1 ~ Fr/2
betai = 3.5;            % RCMC kernel kaiser beta
%
%%%%%%%%%%%%%%%%%%%%%%%%%%%%%%%%%%%%%%%%%%%%%%%%%%%%%%%%%%%%%%%%%%%%%%%%%%%%
% generate motion compensation data
%%%%%%%%%%%%%%%%%%%%%%%%%%%%%%%%%%%%%%%%%%%%%%%%%%%%%%%%%%%%%%%%%%%%%%%%%%%%
%
h = 1000;                % elevation of target above reference level (m)
offset = 0;              % offset for extracting azimuth peak
Bc =1;                   % distance from antenna a to reference track
thetaBc = 50*pi/180;     % off horizontal angle of antenna a to ref. track
delhc = Bc*cos(thetaBc); % horizontal offset of channel a from reference
delvc = Bc*sin(thetaBc); % vertical offset of channel a from reference
dabh = 1.812;            % offset between antenna a and b horizontal
dabv = 2.141;            % offset between antenna a and b vertical
b = sqrt(dabh^2+dabv^2); % antenna baseline distance
alphart = atan2(dabh,dabv); % antenna baseline angle
brt = b;                 % reference track baseline distance
Mh = 5;                  % flight motion horizontal amplitude
Mv = 5;                  % flight motion vertical amplitude
Mr = 0.15*(pi/180);      % roll variation (rad)
eta = -(Na-1)/(2*PRF) : 1/PRF : (Na-1)/(2*PRF); % azimuth slow time
prd = 3;                 % period of sinusoid in seconds
```

```
pphase = 0.25 ;          % phase offset of motion in seconds
delva = zeros(size(eta));
delvb = zeros(size(eta));
delha = zeros(size(eta));
delhb = zeros(size(eta));
%
% linear flight motion (+/- M/2 peak)
%
%delva = (Mv*PRF*(Na/Nmf)/(Na-1)).*eta + delvc;
%delha = (Mh*PRF*(Na/Nmf)/(Na-1)).*eta + delhc;
%delvb = (Mv*PRF*(Na/Nmf)/(Na-1)).*eta + delvc;
%delhb = (Mh*PRF*(Na/Nmf)/(Na-1)).*eta + delhc;
%
% quadratic flight motion ( 0 to +M peak)
%
%Av = Mv*4*PRF^2*(Na/Nmf)^2/(Na-1)^2;
%Ah = Mh*4*PRF^2*(Na/Nmf)^2/(Na-1)^2;
%delva = Av*(eta-pphase).^2 + delvc;
%delha = Ah*(eta-pphase).^2 + delhc;
%delvb = Av*(eta-pphase).^2 + delvc;
%delhb = Ah*(eta-pphase).^2 + delhc;
%
% sinusoidal flight motion (+/- M peak)
%
%delva = Mv*sin((2*pi/prd).*(eta-pphase)) + delvc;
%delha = Mh*sin((2*pi/prd).*(eta-pphase)) + delhc;
%delvb = Mv*sin((2*pi/prd).*(eta-pphase)) + delvc;
%delhb = Mh*sin((2*pi/prd).*(eta-pphase)) + delhc;
%
% roll motion
%
%  linear roll (+/- Mr/2)
%
%roll = (Mr*PRF*(Na/Nmf)/(Na-1)).*eta + alphart;
%
%  quadratic roll (0 to +Mr peak)
%
%Ar = Mr*4*PRF^2*(Na/Nmf)^2/(Na-1)^2;
%roll = Ar*(eta).^2 + alphart;
%
%  sinusoidal roll (+/- Mr)
roll = Mr*sin((2*pi/prd).*(eta-pphase)) + alphart;
%
%  roll
%
delva = delvc*ones(size(eta));
delha = delhc*ones(size(eta));
delvb = b*cos(roll) - dabv + delvc;
delhb = b*sin(roll) - dabh + delhc;
%
% mocomp displacements at center of aperture
%
delvac = delva(Na/2);
delhac = delha(Na/2);
delvbc = delvb(Na/2);
delhbc = delhb(Na/2);
%
% Calculate registered channel b range to h=0 target for middle of aperture
%
delv = dabv + delvb - delva;
delh = dabh + delhb - delha;
alphaab = atan2(delh,delv);
alphaabc = alphaab(Na/2);
thetaaco = acos((H+delvac)/Rao);
Rbo = sqrt(Rao^2 + b^2 +2*Rao*b*cos(alphaabc+thetaaco));
%
% Calculate antenna to reference track geometry along aperture
%
alpha1a = atan2(delha,delva);
```

```
alpha1b = atan2(delhb,delvb);
l1a = sqrt(delha.^2+delva.^2);
l1as = l1a.*l1a;
l1b = sqrt(delhb.^2+delvb.^2);
l1bs = l1b.*l1b;
%
% mocomp displacements
%
%%%%%%%%%%%%%%%%%%%%%%%%%%%%%%%%%%%%%%%%%%%%%%%%%%%%%%%%%%%%%%%%%%%%%%%%%%%%%%%
% Generate range varying matched filters for each channel
%%%%%%%%%%%%%%%%%%%%%%%%%%%%%%%%%%%%%%%%%%%%%%%%%%%%%%%%%%%%%%%%%%%%%%%%%%%%%%%
%
rg = 0;
etamf = -(Nmf-1)/(2*PRF) : 1/PRF : (Nmf-1)/(2*PRF);
for Ras = Rao-(Nr-1)*slpix/2+div_zero : slpix : Rao+(Nr)*slpix/2+div_zero
   rg = rg + 1;
   theta1as = acos((H+delvac)/Ras);
   Rbs = sqrt(Ras^2 + b^2 + 2*Ras*b*cos(theta1as+alphaabc));
   Ka = 2*V^2/(wave*Ras);
   mfa = exp(j*pi*Ka*(etac-etamf).^2-(j*pi*V^4*(etac-etamf).^4)
                  /(wave*2*Ras^3));
   MFA(rg,:) = fft(mfa,Na);
   Kb = 2*V^2/(wave*(Ras+Rbs)/2);
   mfb = exp(j*pi*Kb*(etac-etamf).^2-(j*pi*V^4*(etac-etamf).^4)
       /(wave*2*((Ras+Rbs)/2)^3));
   MFB(rg,:) = fft(mfb,Na);
end
%
% Assume that delva,delha,delvb,delhb are measured from individual ref. tks
%
% calculate deviation of antenna from center of aperture position
%
l3a = sqrt((delva-delvac).^2+(delha-delhac).^2);
l3as = l3a.*l3a;
alpha3a = atan2(delha-delhac,delva-delvac);
l3b = sqrt((delvb-delvbc).^2+(delhb-delhbc).^2);
l3bs = l3b.*l3b;
alpha3b = atan2(delhb-delhbc,delvb-delvbc);
%
% calculate actual range from center of aperture to target for channel b
%
thetaah = acos((H+delvac-h)/Rao);
Rbh = sqrt(Rao^2+b^2+2*Rao*b*cos(alphaabc+thetaah));
thetabh = acos((H+brt*cos(alphart)+delvbc-h)/Rbh);
%
%%%%%%%%%%%%%%%%%%%%%%%%%%%%%%%%%%%%%%%%%%%%%%%%%%%%%%%%%%%%%%%%%%%%%%%%%%%%%%%
% generate signal data then mocomp it using flat earth for each channel
%%%%%%%%%%%%%%%%%%%%%%%%%%%%%%%%%%%%%%%%%%%%%%%%%%%%%%%%%%%%%%%%%%%%%%%%%%%%%%%
%
fprintf('raw data generation in progress\n');
az = 0;
for eta = -(Na-1)/(2*PRF)+div_zero : 1/PRF : (Na-1)/(2*PRF)+div_zero
   az = az + 1;
   if (rem(az,64) == 0)
      fprintf('line %d \n',az);
   end
%
%  calculate Ra in range-elevation plane from antenna a to target: assuming
%  that range to target from "nominal" track is always Ras independent
%  of h (this is for simplicity of equations for changing h)
%
   R1a = sqrt(Rao^2+l3as(az) +2*Rao*l3a(az)*cos(thetaah+alpha3a(az)));
%
%  calculate Rb in range-elevation plane from antenna b to target
%
   R1b = sqrt(Rbh^2+l3bs(az) +2*Rbh*l3b(az)*cos(thetabh+alpha3b(az)));
%
%  calculate instantaneous range from antenna a to target
%     (RCM included)
```

```
   Ra = sqrt(R1a^2+V^2*(eta-etac)^2);
   Aa = (sin(K*V*eta/Ra)/(K*V*eta/Ra))^2;  % antenna a beam pattern
%
%  calculate instantaneous range from antenna b to target
%     (RCM included)
%
   Rb = sqrt(R1b^2+V^2*(eta-etac)^2);
   Ab = (sin(K*V*eta/Rb)/(K*V*eta/Rb))^2;  % antenna b beam pattern
%
%  Generate range compressed data in range
%
   rg = 0;
   for Ras = Rao-(Nr-1)*slpix/2+div_zero : slpix : Rao+(Nr)*slpix/2+div_zero
      rg = rg + 1;
      theta1as = acos((H+delva(az))/Ras);
      Rbs = sqrt(Ras^2 + b^2 + 2*Ras*b*cos(theta1as+alphaab(az)));
      theta1bs = acos((H+brt*cos(alphart)+delvb(az))/Rbs);
      data_a(rg,az) = Aa*exp(-j*2*k*Ra) * sin(M*(Ras-Ra))/(M*(Ras-Ra));
      data_b(rg,az) = Ab*exp(-j*k*(Ra+Rb))*
                      sin(M*((Ra+Rb)/2-(Ras+Rbs)/2))/(M*((Ra+Rb)/2-(Ras+Rbs)/2));
%
%     Calculate required motion phase correction, dual track
%
      Rtao = sqrt(Ras^2 + l1as(az)- 2*Ras*l1a(az)*cos(theta1as+alpha1a(az)));
      delra = Rtao - Ras;
      Rtbo = sqrt(Rbs^2 + l1bs(az)- 2*Rbs*l1b(az)*cos(theta1bs+alpha1b(az)));
      delra = Rtao - Ras;
      delrb = Rtbo - Rbs;
%
%     now mocomp it to reference paths using flat earth assumption
%
      data_a(rg,az) = data_a(rg,az)*exp(-j*k*2*delra);
      data_b(rg,az) = data_b(rg,az)*exp(-j*k*(delra+delrb));
   end
end
fprintf('raw data generation complete\n');
%
% Calculate expected differential phase from center of aperture positions
%
theta1as = acos((H+delvac)/Rao);
theta1bs = acos((H+brt*cos(alphart)+delvbc)/Rbo);
Rtao = sqrt(Rao^2 + l1as(Na/2)- 2*Rao*l1a(Na/2)*cos(theta1as+alpha1a(Na/2)));
Rtbo = sqrt(Rbo^2 + l1bs(Na/2)- 2*Rbo*l1b(Na/2)*cos(theta1bs+alpha1b(Na/2)));
DPP = k*(Rtbo - Rtao + Rbh - Rbo);
DPe = atan2(sin(DPP),cos(DPP));
%
%
% generate interpolation kernel for RCMC
%
kernel = interp_size*fir1(interp_size*Nk,Wn,kaiser(interp_size*Nk+1,betai));
%
% extract every 8th value to generate 16 different filters
% - one for interpolating to the ith/16 sample interval
%
for l=1:interp_size;
   for m=1:Nk;
      filt(l,m) = kernel((m-1)*interp_size+l+1);
   end
end
tt = 1:Na;
cdata = zeros(size(data_a));
fftdata = zeros(size(tt));
cfftdata = zeros(size(tt));
Fa = 0 : PRF/Na : (Na-1)*PRF/Na;
phaser = exp(j*2*pi*(Nmf/(2*PRF)).*Fa);
%
%%%%%%%%%%%%%%%%%%%%%%%%%%%%%%%%%%%%%%%%%%%%%%%%%%%%%%%%%%%%%%%%%%%%%%%%%%%%%%%
% perform RCMC on channel A
%%%%%%%%%%%%%%%%%%%%%%%%%%%%%%%%%%%%%%%%%%%%%%%%%%%%%%%%%%%%%%%%%%%%%%%%%%%%%%%
```

```
%
for rg = 1:Nr;
   fftdata(rg,:) = fft(data_a(rg,:));
end
for az = 1:Na;
   if (rem(az,64) == 0)
      fprintf('line %d \n',az);
   end
   if (az <= Na/2+1)
      shift = (2*Fr/c)*0.5*V^2*((az-1)*PRF/Na)^2/(Ka^2*Rao); % in samples
   else
      shift = (2*Fr/c)*0.5*V^2*((Na+1-az)*PRF/Na)^2/(Ka^2*Rao); % in samples
   end
%
%  determine integer shift part
%
   int_shift = floor(shift + 1/(2*interp_size));
%
%  determine fractional shift
%
   frs = round(interp_size*(shift - int_shift));
%
%  perform integer shift on data
%
   fftrcmcdata(1:Nr-int_shift,az) = fftdata(int_shift+1:Nr,az);
%
%  perform fractional interpolation and discard Nk/2 points at start
%   leaving them zero and leave last Nk/2+1 points zero, note also
%   that the last int_shift non-zero values are throwaway
%
   filt_no = interp_size - frs;
   for rg = 1:Nr-Nk+1;
      fftrcmcdata(rg+Nk/2-1,az) = sum(fftrcmcdata(rg:rg+Nk-1,az).*
          filt(filt_no,:).');
   end
end
%
%%%%%%%%%%%%%%%%%%%%%%%%%%%%%%%%%%%%%%%%%%%%%%%%%%%%%%%%%%%%%%%%%%%%%%%%%%%%%%%
% compress channel A
%%%%%%%%%%%%%%%%%%%%%%%%%%%%%%%%%%%%%%%%%%%%%%%%%%%%%%%%%%%%%%%%%%%%%%%%%%%%%%%
%
for rg = 1:Nr;
   MF = MFA(rg,:);
   cfftdata =  fftrcmcdata(rg,:).*MF.*phaser;
   cdata_a(rg,:) = ifft(cfftdata);
end
%
%%%%%%%%%%%%%%%%%%%%%%%%%%%%%%%%%%%%%%%%%%%%%%%%%%%%%%%%%%%%%%%%%%%%%%%%%%%%%%%
% perform RCMC on channel B
%%%%%%%%%%%%%%%%%%%%%%%%%%%%%%%%%%%%%%%%%%%%%%%%%%%%%%%%%%%%%%%%%%%%%%%%%%%%%%%
%
for rg = 1:Nr;
   fftdata(rg,:) = fft(data_b(rg,:));
end
for az = 1:Na;
   if (rem(az,64) == 0)
      fprintf('line %d \n',az);
   end
   if (az <= Na/2+1)
      shift = (2*Fr/c)*0.5*V^2*((az-1)*PRF/Na)^2/(Ka^2*Rao); % in samples
   else
      shift = (2*Fr/c)*0.5*V^2*((Na+1-az)*PRF/Na)^2/(Ka^2*Rao); % in samples
   end
%
%  determine integer shift part
%
   int_shift = floor(shift + 1/(2*interp_size));
%
%  determine fractional shift
```

```
%
   frs = round(interp_size*(shift - int_shift));
%
%  perform integer shift on data
%
   fftrcmcdata(1:Nr-int_shift,az) = fftdata(int_shift+1:Nr,az);
%
%  perform fractional interpolation and discard Nk/2 points at start
%   leaving them zero and leave last Nk/2+1 points zero, note also
%   that the last int_shift non-zero values are throwaway
%
   filt_no = interp_size - frs;
   for rg = 1:Nr-Nk+1;
      fftrcmcdata(rg+Nk/2-1,az) = sum(fftrcmcdata(rg:rg+Nk-1,az).*
          filt(filt_no,:).');
   end
end
%
%%%%%%%%%%%%%%%%%%%%%%%%%%%%%%%%%%%%%%%%%%%%%%%%%%%%%%%%%%%%%%%%%%%%%%%%%%%%%%%
% compress channel B
%%%%%%%%%%%%%%%%%%%%%%%%%%%%%%%%%%%%%%%%%%%%%%%%%%%%%%%%%%%%%%%%%%%%%%%%%%%%%%%
%
for rg = 1:Nr;
   MF = MFB(rg,:);
   cfftdata =  fftrcmcdata(rg,:).*MF.*phaser;
   cdata_b(rg,:) = ifft(cfftdata);
end
fprintf('data compressed\n')
%
%%%%%%%%%%%%%%%%%%%%%%%%%%%%%%%%%%%%%%%%%%%%%%%%%%%%%%%%%%%%%%%%%%%%%%%%%%%%%%%
% interpolate channels A and B by 2 to prepare for i'gram generation
%%%%%%%%%%%%%%%%%%%%%%%%%%%%%%%%%%%%%%%%%%%%%%%%%%%%%%%%%%%%%%%%%%%%%%%%%%%%%%%
%
for rg = 1:Nr;
   cdata_ar(rg,:) =
       interp(cdata_a(rg,offset+Na/2-(Ni-1)/2:Na/2+(Ni-1)/2+offset),2);
   cdata_br(rg,:) =
       interp(cdata_b(rg,offset+Na/2-(Ni-1)/2:Na/2+(Ni-1)/2+offset),2);
end
for az = 1:2*Ni;
   cdata_arr(:,az) = interp(cdata_ar(:,az),2);
   cdata_brr(:,az) = interp(cdata_br(:,az),2);
end
inter = cdata_arr .* conj(cdata_brr);
cd = inter(Nr/2:3*Nr/2-1,Ni/2:3*Ni/2-1);
%
%%%%%%%%%%%%%%%%%%%%%%%%%%%%%%%%%%%%%%%%%%%%%%%%%%%%%%%%%%%%%%%%%%%%%%%%%%%%%%%
% perform point target analysis of interferogram
%%%%%%%%%%%%%%%%%%%%%%%%%%%%%%%%%%%%%%%%%%%%%%%%%%%%%%%%%%%%%%%%%%%%%%%%%%%%%%%
%
% interpolate in range
%
cdf = fft(cd);      % fft columns (each of length Nr)
Nri = Ir*Nr;
cdfi = zeros(Nri,Ni);
cdfi(1:(Nr-1)/2+1,:) = cdf(1:(Nr-1)/2+1,:);
cdfi(Nri-(Nr-1)/2+1:Nri,:) = cdf((Nr-1)/2+2:Nr,:);
cdi = ifft(cdfi);
%
% interpolate in azimuth
%
cdff = fft(cdi.');      % fft columns (each of length Ni)
Nai = Ir*Ni;
cdfii = zeros(Nai,Nri);
cdfii(1:Ni/2+1,:) = cdff(1:Ni/2+1,:);
cdfii(Nai-Ni/2+2:Nai,:) = cdff(Ni/2+2:Ni,:);
cdii = ifft(cdfii).';
%
% find peak and plot results
```

```
%
[Val,Row] = max(abs(cdii));
[val,midxc] = max(Val);
midxr = Row(midxc);
mid = Nai/2;
[w3a,sla] = widlobe(cdii(midxr,:));
[w3r,slr] = widlobe(cdii(:,midxc));
peakphase = angle(cdii(midxr,midxc));
%
% calculate estimated elevation
%
abs_phase = peakphase + ((DPP-rem(DPP,2*pi))/(2*pi)-1)*2*pi;
h_est = H+delvac-Rao*cos(-alphaabc+acos(((wave*abs_phase/(2*pi))+
    Rtao-Rtbo+Rbo)^2 - b^2-Rao^2)/(2*b*Rao)));
n = 1:Nai;
axis([1 Nai -val val]);
plot(n,abs(cdii(midxr,:)),n,angle(cdii(midxr,:))*.3183*val);
title('Azimuth Cross-section through point target');
xlabel('Azimuth samples');
ylabel('Magnitude and phase');
text(mid,.9*val,sprintf('Error in estimated elevation %2.3f m',h-h_est));
text(mid,.8*val,sprintf('Measured Peak phase %2.3f rad.', peakphase))
text(mid,.6*val,sprintf('Expected Peak phase %2.3f rad.', DPe))
text(mid,.4*val,sprintf('Peak phase error %2.0f mrad.',
    1000*(peakphase-DPe)))
text(mid,.2*val,sprintf('Az. 3dB width %2.3f m', V*w3a/(PRF*2*Ir)))
text(mid,0,sprintf('Az. First side lobe %2.2f dB', sla))
text(mid,-.2*val,sprintf('Rg. 3dB width %2.2f m', slpix*w3r/(2*Ir)))
text(mid,-.4*val,sprintf('Rg. First side lobe %2.2f dB', slr))
text(mid,-.6*val,sprintf('Peak at %2.0f/%2.0f range',midxr,Nri));
text(mid,-.8*val,sprintf('Peak at %2.0f/%2.0f azimuth',midxc,Nai));
grid
%meta plot
pause
n = 1:Nri;
mid = Nri/2;
axis([1 Nri -val val]);
plot(n,abs(cdii(:,midxc)),n,angle(cdii(:,midxc))*.3183*val);
title('Range Cross-section through point target');
xlabel('Range samples');
ylabel('Magnitude and phase');
text(mid,.8*val,sprintf('Measured Peak phase %2.3f rad.', peakphase))
text(mid,.6*val,sprintf('Expected Peak phase %2.3f rad.', DPe))
text(mid,.4*val,sprintf('Peak phase error %2.0f mrad.',
    1000*(peakphase-DPe)))
text(mid,.2*val,sprintf('Az. 3dB width %2.3f m', V*w3a/(PRF*2*Ir)))
text(mid,0,sprintf('Az. First side lobe %2.2f dB', sla))
text(mid,-.2*val,sprintf('Rg. 3dB width %2.2f m', slpix*w3r/(2*Ir)))
text(mid,-.4*val,sprintf('Rg. First side lobe %2.2f dB', slr))
text(mid,-.6*val,sprintf('Peak at %2.0f/%2.0f range',midxr,Nri));
text(mid,-.8*val,sprintf('Peak at %2.0f/%2.0f azimuth',midxc,Nai));
grid
pause
%
%%%%%%%%%%%%%%%%%%%%%%%%%%%%%%%%%%%%%%%%%%%%%%%%%%%%%%%%%%%%%%%%%%%%%%%%%%%%%%%
% extract peak area and do 2D interpolation of channel A
%%%%%%%%%%%%%%%%%%%%%%%%%%%%%%%%%%%%%%%%%%%%%%%%%%%%%%%%%%%%%%%%%%%%%%%%%%%%%%%
%
cd = cdata_a(1:Nr,offset+Na/2-(Ni-1)/2-1:Na/2+(Ni-1)/2+offset-1);
%
% interpolate in range
%
cdf = fft(cd);      % fft columns (each of length Nr)
Nri = Ir*Nr;
cdfi = zeros(Nri,Ni);
cdfi(1:(Nr-1)/2+1,:) = cdf(1:(Nr-1)/2+1,:);
cdfi(Nri-(Nr-1)/2+1:Nri,:) = cdf((Nr-1)/2+2:Nr,:);
cdi = ifft(cdfi);
%
```

```
% interpolate in azimuth
%
cdff = fft(cdi.');      % fft columns (each of length Ni)
Nai = Ir*Ni;
cdfii = zeros(Nai,Nri);
cdfii(1:Ni/2+1,:) = cdff(1:Ni/2+1,:);
cdfii(Nai-Ni/2+2:Nai,:) = cdff(Ni/2+2:Ni,:);
cdii = ifft(cdfii).';
%
% find peak and plot results
%
[Val,Row] = max(abs(cdii));
[val,midxc] = max(Val);
midxr = Row(midxc);
mid = Nai/2;
[w3a,sla] = widlobe(cdii(midxr,:));
[w3r,slr] = widlobe(cdii(:,midxc));
peakphase = angle(cdii(midxr,midxc));
Pae = angle(exp(-j*4*pi*Rtao/wave));
n = 1:Nai;
axis([1 Nai -val val]);
plot(n,abs(cdii(midxr,:)),n,angle(cdii(midxr,:))*.3183*val);
title('Azimuth Cross-section through point target Ch A');
xlabel('Azimuth samples');
ylabel('Magnitude and phase');
text(mid,.8*val,sprintf('Measured Peak phase %2.3f rad.', peakphase))
text(mid,.6*val,sprintf('Expected Peak phase %2.3f rad.', Pae))
text(mid,.4*val,sprintf('Peak phase error %2.0f mrad.',
    1000*(peakphase-Pae)))
text(mid,.2*val,sprintf('Az. 3dB width %2.3f m', V*w3a/(PRF*Ir)))
text(mid,0,sprintf('Az. First side lobe %2.2f dB', sla))
text(mid,-.2*val,sprintf('Rg. 3dB width %2.2f m', slpix*w3r/Ir))
text(mid,-.4*val,sprintf('Rg. First side lobe %2.2f dB', slr))
text(mid,-.6*val,sprintf('Peak at %2.0f/%2.0f range',midxr,Nri));
text(mid,-.8*val,sprintf('Peak at %2.0f/%2.0f azimuth',midxc,Nai));
grid
%meta plot
pause
n = 1:Nri;
mid = Nri/2;
axis([1 Nri -val val]);
plot(n,abs(cdii(:,midxc)),n,angle(cdii(:,midxc))*.3183*val);
title('Range Cross-section through point target Ch A');
xlabel('Range samples');
ylabel('Magnitude and phase');
text(mid,.8*val,sprintf('Measured Peak phase %2.3f rad.', peakphase))
text(mid,.6*val,sprintf('Expected Peak phase %2.3f rad.', Pae))
text(mid,.4*val,sprintf('Peak phase error %2.0f mrad.',
    1000*(peakphase-Pae)))
text(mid,.2*val,sprintf('Az. 3dB width %2.3f m', V*w3a/(PRF*Ir)))
text(mid,0,sprintf('Az. First side lobe %2.2f dB', sla))
text(mid,-.2*val,sprintf('Rg. 3dB width %2.2f m', slpix*w3r/Ir))
text(mid,-.4*val,sprintf('Rg. First side lobe %2.2f dB', slr))
text(mid,-.6*val,sprintf('Peak at %2.0f/%2.0f range',midxr,Nri));
text(mid,-.8*val,sprintf('Peak at %2.0f/%2.0f azimuth',midxc,Nai));
grid
pause
%
%%%%%%%%%%%%%%%%%%%%%%%%%%%%%%%%%%%%%%%%%%%%%%%%%%%%%%%%%%%%%%%%%%%%%%%%%%%%%%%
% extract peak area and do 2D interpolation of channel B
%%%%%%%%%%%%%%%%%%%%%%%%%%%%%%%%%%%%%%%%%%%%%%%%%%%%%%%%%%%%%%%%%%%%%%%%%%%%%%%
%
cd = cdata_b(1:Nr,offset+Na/2-(Ni-1)/2-1:Na/2+(Ni-1)/2+offset-1);
%
% interpolate in range
%
cdf = fft(cd);      % fft columns (each of length Nr)
Nri = Ir*Nr;
cdfi = zeros(Nri,Ni);
```

```
cdfi(1:(Nr-1)/2+1,:) = cdf(1:(Nr-1)/2+1,:);
cdfi(Nri-(Nr-1)/2+1:Nri,:) = cdf((Nr-1)/2+2:Nr,:);
cdi = ifft(cdfi);
%
% interpolate in azimuth
%
cdff = fft(cdi.');      % fft columns (each of length Ni)
Nai = Ir*Ni;
cdfii = zeros(Nai,Nri);
cdfii(1:Ni/2+1,:) = cdff(1:Ni/2+1,:);
cdfii(Nai-Ni/2+2:Nai,:) = cdff(Ni/2+2:Ni,:);
cdii = ifft(cdfii).';
%
% find peak and plot results
%
[Val,Row] = max(abs(cdii));
[val,midxc] = max(Val);
midxr = Row(midxc);
mid = Nai/2;
[w3a,sla] = widlobe(cdii(midxr,:));
[w3r,slr] = widlobe(cdii(:,midxc));
peakphase = angle(cdii(midxr,midxc));
Pbe = angle(exp(-j*2*pi*(Rtao+Rtbo)/wave));
n = 1:Nai;
axis([1 Nai -val val]);
%psf1000 = abs(cdii(midxr,:));
%save psf1000_1024.mat psf1000
plot(n,abs(cdii(midxr,:)),n,angle(cdii(midxr,:))*.3183*val);
title('Azimuth Cross-section through point target Ch B');
xlabel('Azimuth samples');
ylabel('Magnitude and phase');
text(mid,.8*val,sprintf('Measured Peak phase %2.3f rad.', peakphase))
text(mid,.6*val,sprintf('Expected Peak phase %2.3f rad.', Pbe))
text(mid,.4*val,sprintf('Peak phase error %2.0f mrad.',
    1000*(peakphase-Pbe)))
text(mid,.2*val,sprintf('Az. 3dB width %2.3f m', V*w3a/(PRF*Ir)))
text(mid,0,sprintf('Az. First side lobe %2.2f dB', sla))
text(mid,-.2*val,sprintf('Rg. 3dB width %2.2f m', slpix*w3r/Ir))
text(mid,-.4*val,sprintf('Rg. First side lobe %2.2f dB', slr))
text(mid,-.6*val,sprintf('Peak at %2.0f/%2.0f range',midxr,Nri));
text(mid,-.8*val,sprintf('Peak at %2.0f/%2.0f azimuth',midxc,Nai));
grid
%meta plot
pause
n = 1:Nri;
mid = Nri/2;
axis([1 Nri -val val]);
plot(n,abs(cdii(:,midxc)),n,angle(cdii(:,midxc))*.3183*val);
title('Range Cross-section through point target Ch B');
xlabel('Range samples');
ylabel('Magnitude and phase');
text(mid,.8*val,sprintf('Measured Peak phase %2.3f rad.', peakphase))
text(mid,.6*val,sprintf('Expected Peak phase %2.3f rad.', Pbe))
text(mid,.4*val,sprintf('Peak phase error %2.0f mrad.',
    1000*(peakphase-Pbe)))
text(mid,.2*val,sprintf('Az. 3dB width %2.3f m', V*w3a/(PRF*Ir)))
text(mid,0,sprintf('Az. First side lobe %2.2f dB', sla))
text(mid,-.2*val,sprintf('Rg. 3dB width %2.2f m', slpix*w3r/Ir))
text(mid,-.4*val,sprintf('Rg. First side lobe %2.2f dB', slr))
text(mid,-.6*val,sprintf('Peak at %2.0f/%2.0f range',midxr,Nri));
text(mid,-.8*val,sprintf('Peak at %2.0f/%2.0f azimuth',midxc,Nai));
grid
```

```
%%%%%%%%%%%%%%%%%%%%%%%%%%%%%%%%%%%%%%%%%%%%%%%%%%%%%%%%%%%%%%%%%%%%%%%%%%%%%%%
% widlobe.m
%
%    1 D point target analysis
%
% [width,slobe] = WIDLOBE (input_array)
%         - input_array must be amplitude units
%         - Calculate 3dB width, first side lobe level
%         Note: Peak and sidelobes must not be at an edge
%
% change control
%  feb 92 - initial release
%  nov 12/92 - fixed up index checking
%%%%%%%%%%%%%%%%%%%%%%%%%%%%%%%%%%%%%%%%%%%%%%%%%%%%%%%%%%%%%%%%%%%%%%%%%%%%%%%
%
function [width,slobe] = widlobe (x)
%
% Convert to power units
pow = 20*log10(abs(x));
[maxval,maxidx] = max(pow);
pow = pow - maxval;
%
% locate 3dB width (to sample spacing accuracy only)
%
k = maxidx-1;
threshold = -3.0;
l = length(x);
while ((k>1) & (pow(k) > threshold))
   k = k - 1;
end
if (pow(k) > threshold)
   sprintf('could not find left 3dB point');
end
left = k + (-3.0 - pow(k))/(pow(k+1)-pow(k));
k = maxidx+1;
while ((k<l) & (pow(k) > threshold))
   k = k + 1;
end
if (pow(k) > threshold)
   sprintf('could not find right 3dB point');
end
right = k  - (-3.0 - pow(k))/(pow(k-1)-pow(k));
width = right - left;
%
% Locate first sidelobe
%
k = maxidx-1;
while ((k > 2) & (pow(k-1) < pow(k)))
   k = k - 1;
end
if (pow(k-1) < pow(k))
    sprintf('could not find left sidelobe');
end
leftlobe = max(pow(1:k-1));
k = maxidx+1;
while ( (k < (l-1)) & (pow(k+1) < pow(k)))
   k = k + 1;
end
if (pow(k+1) < pow(k))
   sprintf('could not find right sidelobe');
end
rightlobe = max(pow(k+1:length(pow)));
slobe = max(leftlobe,rightlobe);
```

```
%%%%%%%%%%%%%%%%%%%%%%%%%%%%%%%%%%%%%%%%%%%%%%%%%%%%%%%%%%%%%%%%%%%%%%%%%%%%%%%
% reg1.m
%
%    Register Channel B to Channel A at reference level
%
% Change control
% Jan 18/94 Initial release
% Jan 20/94 modified for multi-segments
%
%%%%%%%%%%%%%%%%%%%%%%%%%%%%%%%%%%%%%%%%%%%%%%%%%%%%%%%%%%%%%%%%%%%%%%%%%%%%%%%
% Initialize Parameters
%%%%%%%%%%%%%%%%%%%%%%%%%%%%%%%%%%%%%%%%%%%%%%%%%%%%%%%%%%%%%%%%%%%%%%%%%%%%%%%
%
atodfreq=37.5;                          % Range sampling rate (MHz)
delay=[13.289, 13.2737];                % SAW delay (usec) A,B
wave=0.0565646;              % wavelength
c=299.79;                 % speed of light in m/microsec
delsr=c/(2*atodfreq);            % slant range pixel spacing (4 m)
rgd=51.99;                              % range gate delay in microsec.
rbase=(rgd-delay(1))*c/2;        % base range, only ch A used
H=6059;                                 % elevation of reference track
K=2*pi/wave;                            % wavenumber
D = 1;                                  % antenna length (m)
%
segment = 6;        % segment number
interp_size = 16;   % interpolate to 1/interp_size of a sample
Nk = 8;             % length of kernel
Wn = 1/interp_size;% Cutoff for kernel =1 ~ Fr/2
betai = 3.5;        % kernel kaiser beta
%
%%%%%%%%%%%%%%%%%%%%%%%%%%%%%%%%%%%%%%%%%%%%%%%%%%%%%%%%%%%%%%%%%%%%%%%%%%%%%%%
% generate interpolation kernel
%%%%%%%%%%%%%%%%%%%%%%%%%%%%%%%%%%%%%%%%%%%%%%%%%%%%%%%%%%%%%%%%%%%%%%%%%%%%%%%
%
kernel = interp_size*fir1(interp_size*Nk,Wn,kaiser(interp_size*Nk+1,betai));
%
% extract every 8th value to generate 16 different filters
% - one for interpolating to the ith/16 sample interval
%
for l=1:interp_size;
   for m=1:Nk;
      filt(l,m) = kernel((m-1)*interp_size+l+1);
   end
end
%
load kp10_prf               % load in motion data
ddelh = delh(:,2)-delh(:,1);
ddelv = delv(:,2)-delv(:,1);
b = sqrt(ddelh.^2 + ddelv.^2);
alphaab = atan2(ddelh,ddelv);
n_range= 12000;             % # of range lines no. available to process
srange= 1;                  % first range line no. to process
erange=srange+n_range-1;    % last range line no. to process
n_azimuth= 180;             % # of azimuth lines to process
pstart= 1;                  % starting azimuth line
pend = pstart+n_azimuth-1;% last azimuth line
uniend=(segment-1)*(n_azimuth-10)+n_azimuth; % unimat last pixel #
unistart= uniend-n_azimuth + 1;  % unimat file start range pixel no.
%
%%%%%%%%%%%%%%%%%%%%%%%%%%%%%%%%%%%%%%%%%%%%%%%%%%%%%%%%%%%%%%%%%%%%%%%%%%%%%%%
% Load in the data
%%%%%%%%%%%%%%%%%%%%%%%%%%%%%%%%%%%%%%%%%%%%%%%%%%%%%%%%%%%%%%%%%%%%%%%%%%%%%%%
%
load p10bs
k=pstart:pend;
Ra=(delsr*(k+unistart-2))+rbase;
%
%%%%%%%%%%%%%%%%%%%%%%%%%%%%%%%%%%%%%%%%%%%%%%%%%%%%%%%%%%%%%%%%%%%%%%%%%%%%%%%
% Perform the resampling
```

```
%%%%%%%%%%%%%%%%%%%%%%%%%%%%%%%%%%%%%%%%%%%%%%%%%%%%%%%%%%%%%%%%%%%%%%%%%%%%%%%%
%
rdata = zeros(size(data));
for l=srange:erange
   temp=(H+delv(1,1))./Ra;
   temp2=find(temp>1);
   temp(temp2)=ones(size(temp2));
   theta_a=acos(temp);
   Rb = sqrt(Ra.^2 + b(1)^2 + 2*Ra*b(1).*cos(theta_a+alphaab(1)));
%
%  chB pixel # - chA pixel # = deln for coincident scene patches
%
   deln = -(Ra-Rb-c*(delay(2)-delay(1)))./(2*delsr);
   int_shift = floor(deln + 1/(2*interp_size));  % integer sample shift
   frs = round(interp_size*(deln - int_shift));  % fractional sample shift
   fprintf(' Processing range line %4.0f\n', l);
   %
   % process integer and fractional shifts
   %
   index = 1;
   for k=pstart:pend
      istart = k + int_shift(index) - Nk/2 + 1;
      iend = istart + Nk - 1;
      if ((istart >= pstart) & (iend <= pend))
     filt_no = interp_size - frs(index);
     rdata(k,l) = sum(data(istart:iend,l).*filt(filt_no,:).');
      else
     rdata(k,l) = 0;
      end
   end
end
data = rdata;
save p10brs data
```

```
%%%%%%%%%%%%%%%%%%%%%%%%%%%%%%%%%%%%%%%%%%%%%%%%%%%%%%%%%%%%%%%%%%%%%%%%%%%%%%%
% igram1.m
%
%   Single channel motion compensation and azimuth compression
%
% Change control
% Jan 17/94 Initial Release
% Jan 18/94 modified for dual reference tracks
% Jan 20/94 corrected transpose problem, modified for segment processing
% Jan 21/94 modified for dual track
%
%%%%%%%%%%%%%%%%%%%%%%%%%%%%%%%%%%%%%%%%%%%%%%%%%%%%%%%%%%%%%%%%%%%%%%%%%%%%%%%
% Initialize Parameters
%%%%%%%%%%%%%%%%%%%%%%%%%%%%%%%%%%%%%%%%%%%%%%%%%%%%%%%%%%%%%%%%%%%%%%%%%%%%%%%
%
atodfreq=37.5;                          % Range sampling rate (MHz)
delay=[13.289, 13.2737];                % SAW delay (usec)
wave=0.0565646;              % wavelength
c=299.79;                 % speed of light in m/microsec
delsr=c/(2*atodfreq);           % slant range pixel spacing (4 m)
rgd=51.99;
rbase=(rgd-delay(1))*c/2;       % base range, only ch A used
H=6059;                                 % elevation of reference track
K=2*pi/wave;                            % wavenumber
D = 1;                                  % antenna length (m)
%
%%%%%%%%%%%%%%%%%%%%%%%%%%%%%%%%%%%%%%%%%%%%%%%%%%%%%%%%%%%%%%%%%%%%%%%%%%%%%%%
% Obtain processing instructions
%%%%%%%%%%%%%%%%%%%%%%%%%%%%%%%%%%%%%%%%%%%%%%%%%%%%%%%%%%%%%%%%%%%%%%%%%%%%%%%
%
segment = 6;              % image segment number across range
channelsw=2;              % processing channel A (1) or B (2)
%
n_range= 12000;           % # of range lines no. available to process
srange= 1;                % first range line no. to process
erange=srange+n_range-1;  % last range line no. to process
n_azimuth= 180;           % # of azimuth lines to process
pstart= 1;                % starting azimuth line
uniend=(segment-1)*(n_azimuth-10)+n_azimuth; % unimat last pixel#
unistart= uniend-n_azimuth + 1;  % unimat file start range pixel no.
swathend = 2048;          % last range pixel no. in swath to process
%
%%%%%%%%%%%%%%%%%%%%%%%%%%%%%%%%%%%%%%%%%%%%%%%%%%%%%%%%%%%%%%%%%%%%%%%%%%%%%%%
% load in the motion compensation file and extract relevant data
%%%%%%%%%%%%%%%%%%%%%%%%%%%%%%%%%%%%%%%%%%%%%%%%%%%%%%%%%%%%%%%%%%%%%%%%%%%%%%%
%
load kp10_prf             % mocomp file name for single reference track
delha=delh(srange:erange,1);
delva=delv(srange:erange,1);
brt=2.8013;               % reference tk baseline length (0 for single track)
alphart=40.22*(pi/180);   % reference track baseline angle
%
% transform insar channel to its own reference track
%
delhb=delh(srange:erange,2)-brt*sin(alphart);
delvb=delv(srange:erange,2)-brt*cos(alphart);
delv = brt*cos(alphart) + delvb - delva;
delh = brt*sin(alphart) + delhb - delha;
b = sqrt(delv.^2+delh.^2);      % antenna baseline length
alphaab = atan2(delh,delv);     % antenna baseline angle
alpha1a = atan2(delha,delva);  % channel A angle to reference track
alpha1b = atan2(delhb,delvb);  % channel B angle to reference track
l1a = sqrt(delha.^2+delva.^2);
l1as = l1a.*l1a;
l1b = sqrt(delhb.^2+delvb.^2);
l1bs = l1b.*l1b;
%
% calculate azimuth processing parameters
%
```

```
mspacing=mean(spacing(srange:erange));
maxr=rbase+delsr*(swathend-1);       % maximum range, channel A
proc_phi = 2.23*(pi/180);              % azimuth beamwidth to process
nfft = 13824;                           % forward FFT length
maxrefsize = proc_phi*maxr/mspacing;    % maximum matched filter length
%
%%%%%%%%%%%%%%%%%%%%%%%%%%%%%%%%%%%%%%%%%%%%%%%%%%%%%%%%%%%%%%%%%%%%%%%%%%%%%%%
% load in registered raw data
%%%%%%%%%%%%%%%%%%%%%%%%%%%%%%%%%%%%%%%%%%%%%%%%%%%%%%%%%%%%%%%%%%%%%%%%%%%%%%%
%
if ( channelsw == 1 );
  load p10as;
else
  load p10brs;
end
%
%%%%%%%%%%%%%%%%%%%%%%%%%%%%%%%%%%%%%%%%%%%%%%%%%%%%%%%%%%%%%%%%%%%%%%%%%%%%%%%
% phase correct the raw data based on the navigation data
%%%%%%%%%%%%%%%%%%%%%%%%%%%%%%%%%%%%%%%%%%%%%%%%%%%%%%%%%%%%%%%%%%%%%%%%%%%%%%%
%
index = 1;
for k=pstart:pstart+n_azimuth-1;
   Ra=(delsr*(k+unistart-2))+rbase;
   temp=(H+delva)/Ra;
   temp2=find(temp>1);
   temp(temp2)=ones(size(temp2));
   theta_a=acos(temp);
   Rtao = sqrt(Ra^2 + l1as - 2*Ra*l1a.*cos(theta_a+alpha1a));
   delra = Rtao - Ra;
   if channelsw==1;
      delr=2*delra;
   else
      Rb = sqrt(Ra^2 + b.^2 + 2*Ra.*b.*cos(theta_a+alphaab));
      temp=(H+delvb+brt*cos(alphart))./Rb;
      temp2=find(temp>1);
      temp(temp2)=ones(size(temp2));
      theta_b=acos(temp);
      Rtbo = sqrt(Rb.^2 + l1bs - 2*Rb.*l1b.*cos(theta_b+alpha1b));
      delrb = Rtbo - Rb;
      delr = delra+delrb;
      Rbmf(index) = Rb(n_range/2);
   end % of if channelsw ==1 ..
   fprintf(' Phase correcting azimuth line %4.0f, range=%8.1f\n', k,Ra);
   phc=exp(-sqrt(-1)*K*delr);
   data(k,1:n_range)=data(k,1:n_range).*phc(1:n_range).';
   index = index + 1;
end;        % end of for k= loop
%
%%%%%%%%%%%%%%%%%%%%%%%%%%%%%%%%%%%%%%%%%%%%%%%%%%%%%%%%%%%%%%%%%%%%%%%%%%%%%%%
% Loop to azimuth process the data
%%%%%%%%%%%%%%%%%%%%%%%%%%%%%%%%%%%%%%%%%%%%%%%%%%%%%%%%%%%%%%%%%%%%%%%%%%%%%%%
%
out1 = zeros(n_azimuth,n_range-maxrefsize);
index=1;
for k=pstart:pstart+n_azimuth-1;
   if channelsw==1;
     r=(delsr*(k+unistart-2))+rbase;
   else
     r=Rbmf(index);
   end
   fprintf(' Processing azimuth line %4.0f, range=%8.1f\n', k,r);
   temp=fft(data(k,1:n_range), nfft);
   ref=refgen(r, mspacing, wave, proc_phi);
   nref=length(ref);
   temp=ifft(fft(ref, nfft).*temp);
   startindex=(nref+maxrefsize)/2;
   endindex=n_range-(maxrefsize-nref)/2;
   out1(index,1:endindex-startindex+1)=temp(startindex:endindex);
   index=index+1;
```

```
end
if channelsw==1;
   save sega.mat out1
else
   save segb.mat out1
end

%%%%% Generate azimuth matched filter %%%%%%%%%%%%%%%%%%%%%

function [ref]=refgen(r, spacing, wave, proc_phi)
Nref=1+2*round(r*proc_phi/2/spacing);
for j=1:Nref
ref(j)=exp(i*2*pi*(spacing)^2*(j-Nref/2)^2/r/wave);
end
```

```
%%%%%%%%%%%%%%%%%%%%%%%%%%%%%%%%%%%%%%%%%%%%%%%%%%%%%%%%%%%%%%%%%%%%%%%%%%%%%%%
% elev1.m
%
%    Estimate terrain height from interferogram
%
% Change control
% Feb 1/94 Initial release
%
%%%%%%%%%%%%%%%%%%%%%%%%%%%%%%%%%%%%%%%%%%%%%%%%%%%%%%%%%%%%%%%%%%%%%%%%%%%%%%%
% Initialize Parameters
%%%%%%%%%%%%%%%%%%%%%%%%%%%%%%%%%%%%%%%%%%%%%%%%%%%%%%%%%%%%%%%%%%%%%%%%%%%%%%%
%
atodfreq=37.5;                              % Range sampling rate (MHz)
delay=[13.289, 13.2737];                    % SAW delay (usec) A,B
wave=0.0565646;                 % wavelength
c=299.79;                  % speed of light in m/microsec
delsr=c/(2*atodfreq);              % slant range pixel spacing (4 m)
rgd=51.99;                                  % range gate delay in microsec.
rbase=(rgd-delay(1))*c/2;          % base range, only ch A used
H=6059;                                     % elevation of reference track
K=2*pi/wave;                                % wavenumber
D = 1;                                      % antenna length (m)
%
%%%%%%%%%%%%%%%%%%%%%%%%%%%%%%%%%%%%%%%%%%%%%%%%%%%%%%%%%%%%%%%%%%%%%%%%%%%%%%%
% load in igram
%%%%%%%%%%%%%%%%%%%%%%%%%%%%%%%%%%%%%%%%%%%%%%%%%%%%%%%%%%%%%%%%%%%%%%%%%%%%%%%
%
load cigrams
%
%
% load in the motion compensation file and extract relevant data
%
load kp10_prf           % mocomp file name for single reference track
n_range= 1024;           % # of range lines no. available to process
n_azimuth= 2045;         % # of azimuth lines to process
delha=delh(1:10:10*n_range,1);
delva=delv(1:10:10*n_range,1);
%brt=2.8013;              % reference track baseline length
brt=0;              % reference track baseline length
n = 1:512;
alphart = zeros(size(delha));
alphart(1:512)=40.22*(pi/180)*ones(size(n)); % reference track baseline angle
alphart(513:1024)=40.8*(pi/180)*ones(size(n)); % reference tk baseline angle
%
% transform insar channel to its own reference track
%
delhb=delh(1:10:10*n_range,2)-brt.*sin(alphart);
delvb=delv(1:10:10*n_range,2)-brt.*cos(alphart);
delv = brt*cos(alphart) + delvb - delva;
delh = brt*sin(alphart) + delhb - delha;
b = sqrt(delv.^2+delh.^2);      % antenna baseline length
alphaab = atan2(delh,delv);     % antenna baseline angle
alpha1a = atan2(delha,delva);  % channel A angle to reference track
alpha1b = atan2(delhb,delvb);  % channel B angle to reference track
l1a = sqrt(delha.^2+delva.^2);
l1as = l1a.*l1a;
l1b = sqrt(delhb.^2+delvb.^2);
l1bs = l1b.*l1b;
%
%%%%%%%%%%%%%%%%%%%%%%%%%%%%%%%%%%%%%%%%%%%%%%%%%%%%%%%%%%%%%%%%%%%%%%%%%%%%%%%
% perform further phase smoothing
%%%%%%%%%%%%%%%%%%%%%%%%%%%%%%%%%%%%%%%%%%%%%%%%%%%%%%%%%%%%%%%%%%%%%%%%%%%%%%%
%
filtnr = 6;     % filter size range
filtna = 6;     % filter size azimuth
for i=1:filtnr
   for j=1:filtna
      filt(i,j) = 1/(filtnr*filtna);
   end
```

```
end
cigramsf = conv2(cigrams,filt,'same');
cigramsf = rot90(cigramsf);
a = angle(cigramsf);
for i=1:80
   a(:,i) = zeros(size(l1a));
end
%
%%%%%%%%%%%%%%%%%%%%%%%%%%%%%%%%%%%%%%%%%%%%%%%%%%%%%%%%%%%%%%%%%%%%%%%%%%%%%%%%
% phase unwrap assuming no residues!
%%%%%%%%%%%%%%%%%%%%%%%%%%%%%%%%%%%%%%%%%%%%%%%%%%%%%%%%%%%%%%%%%%%%%%%%%%%%%%%%
%
aa(1,:) = unwrap(a(1,:));
for i=1:n_azimuth
   for j=2:n_range
      diff = a(j,i) - a(j-1,i);
      if (abs(diff) < pi)
     aa(j,i) = aa(j-1,i) + diff;
      else
     if (diff < 0)
        aa(j,i) = aa(j-1,i) + 2*pi + diff;
     else
        aa(j,i) = aa(j-1,i) - 2*pi + diff;
     end
      end
   end
end
%
%%%%%%%%%%%%%%%%%%%%%%%%%%%%%%%%%%%%%%%%%%%%%%%%%%%%%%%%%%%%%%%%%%%%%%%%%%%%%%%%
% Calculate motion compensation data and height estimate
%%%%%%%%%%%%%%%%%%%%%%%%%%%%%%%%%%%%%%%%%%%%%%%%%%%%%%%%%%%%%%%%%%%%%%%%%%%%%%%%
%
h=zeros(size(aa));
for k=1:n_azimuth
   Ra=(delsr*(k-1))+rbase;
   temp=(H+delva)/Ra;
   temp2=find(temp>1);
   temp(temp2)=ones(size(temp2));
   theta_a=acos(temp);
   Rtao = sqrt(Ra^2 + l1as - 2*Ra*l1a.*cos(theta_a+alpha1a));
   Rbo = sqrt(Ra^2 + b.^2 + 2*Ra.*b.*cos(theta_a+alphaab));
   temp=(H+delvb+brt*cos(alphart))./Rbo;
   temp2=find(temp>1);
   temp(temp2)=ones(size(temp2));
   theta_b=acos(temp);
   Rtbo = sqrt(Rbo.^2 + l1bs - 2*Rbo.*l1b.*cos(theta_b+alpha1b));
%
%  calculate height estimate
%
   temp0 =  (wave* (aa(:,k)-2*pi)/(2*pi));
   temp00 = (temp0 +Rbo).^2;
   temp1 = acos((temp00 - b.^2-Ra^2)./(2*b.*Ra));
   h(:,k) = (H+delva-Ra.*cos(-alphaab+ temp1));
   fprintf('processed azimuth line %d\n',k);
end
save h.mat h
h_disp=rem((64*3.28/100)*(h+40),64);
index = 0;
for i=1:16:1024
   temp(1:16,1:80) = index*ones(16,80);
   h_disp(i:i+15,1:80) = temp(1:16,1:80);
   index = index + 1;
end
image(h_disp)
title('3 Hills, Alberta:  Elevation')
xlabel('Slant Range Samples')
ylabel('Azimuth Samples')
```